CHAPTER IV

ROCK QUALITY INDEX TESTS

Some simple laboratory tests or quick field measurements provide the adequate quantitative indices of rock quality and degree of weathering. The indices are the basic components of the applied classification systems. The importance and usefulness of the index properties has been demonstrated in the field of soil mechanics. The properties are as well important when being applied to the rock mechanics problems of the most construction projects.

Pomeroy (1957) and Deere (1963) stated that a useful index property must have to following characteristics.

1. It must be an index of a material property which is used by an engineer to solve the design problems.

2. The test to determine the property must be simple, inexpensive, and easy to perform.

3. The test results must be reproducible within the certain limits by different operators and in the different locations using the standardized equipments and procedures.

Aufmuth (1974) added the fourth requirement to fullfill the objective of his study as:

4. The test to determine the property should be performable in the field at the project site.

Table 4.1 Index rock properties of significance in tunneling (after Cording and Mahar, 1978)

Index Property	Method of Determination: Core Logging	Method of Determination: Lab Index Test	Method of Determination: In-Hole Tests	Method of Determination: Field Mapping, Regional Geology, Remote Sensing, Geophysical, In Situ Tests	Method of Determination: Tunnel Exposures	Application of the Index Property
1. *Average Rock Mass Quality*						
a. RQD, core recovery	Log core				Log wall of tunnel	Estimate field deformation modulus to evaluate rock displacement measurements and lining-rock interaction. Large scale plate load tests are sometimes used to evaluate modulus; not usually warranted for tunnels. Estimate tunnel support requirements
b. Fracture frequency (fractures/foot)	Log core		Water pressure tests		Log wall of tunnel	
c. Seismic ratio $\left(\frac{V_{p\ field}}{V_{p\ lab}}\right)^2$		Lab sonic velocity ($V_{p\ lab}$)	Sonic logging ($V_{p\ field}$)	Field seismic ($V_{p\ field}$)		
d. Degree of weathering	Log core: evaluate joint weathering as well as general weathering	Evaluate strength, porosity, hardness of sample				
2. *Properties of Major Joint Sets and Shear Zones*						
a. Spacing	Log core			Observe in exposures	Observe in tunnel	Estimate tunnel support requirements
b. Filling and roughness	Evidence of slickensides, clay. Smoothness of joints. (Evidence may be limited.)	Direct shear tests of joint surface or of filling. Determination of plasticity indices.	Indications of soft materials from geophysical logging.	Large scale direct shear tests not usually warranted for tunnels.	Sampling and observation of gouge, evidence of slickensides, joint surfaces.	
c. Waviness (inclination, "i" and wavelength)				Observe in exposures	Observe in tunnel	
d. Continuity (length)				Observe extent of joints in outcrops	Observe extent of joints in tunnel	
e. Attitude (dip and strike with respect to tunnel)	Oriented core		Borehole camera	Map orientations in exposures	Map orientations in tunnels	
f. Combinations of joint sets	Oriented core		Borehole camera	Map orientations in exposures	Map orientations in tunnels	
3. *Properties of the Rock Sample*						
a. Modulus, E_{lab}		Unconfined compression test with strain measurements				Use lab modulus as base for estimating the field modulus (see also 1)
b. Unconfined compressive strength, σ_c		Unconfined compression test				Estimate effect of high stresses on slabbing and popping of rock
c. Creep properties	Evidence of sheared, weathered and low quality rock	Constant load triaxial creep tests and plasticity indices		Evaluate extent of shear zones	Observations of squeezing	Estimate pressures and deformations on linings in squeezing ground
d. Swelling properties	Deterioration of core	Measure swell pressure on samples, evaluate plasticity			Observations of swelling and heave in tunnel	Estimate pressures and deformation in swelling ground
e. Slake durability	Deterioration of core	Slake-durability test and plasticity indices			Observations of slaking in tunnel	Evaluate tendency for slaking (time dependent deterioration due to moisture changes)
f. Boreability (for tunnel boring machines)	Presence of hard minerals	Abrasion hardness tests, impact hardness tests, micro-bits	Observe field drill rates	Determine extent of rock types		Evaluate feasibility of machine tunneling
g. Plasticity of shales, altered rock or filling materials		Atterberg limits (liquid, plastic)				Correlate with residual shear strength, slaking, swelling, and creep properties
4. *In-Situ Permeability*	Fracturing, open zones in drilling	Sample permeability tests for porous materials	Borehole water pressure tests, pumping tests	Evidence of fault zones, cavities, other high permeability zones		Water problems in tunnel

Geological Society Engineering Group Work Partly (1977), Goodman (1980), Price (1981), and ISRM (1981) designated the similar index properties for a rock specimen to constitute the porosity, density, sonic velocity, durability, hardness, and strength. These properties help describe the classification of the intact rocks and may relate primarily to their behavior and the natural stability of rock mass in the field (Goodman, 1980). Cording et al. (1975) summaried the significant index rock propetties for a tunnel design and construction in Table 4.1.

In general, the index properties characteristics are separated into three main groups, namely, petrological, physical, and mechanical properties. The determination of the quality indices of the rock specimens from the study area, according to the groups of characteristics, is listed below.

4.1 Description of Samples

Some of the fresh diamond-drilled core samples available along the diversion tunnel length and at the main dam foundation were randomly selected. The description of the samples to determine the physiomechanical and mineralogical properties in the laboratory are listed in Appendix A-2.

Some specimens, in a form of rock chumps of pebbly graywackes, subarkosic sandstones and mudshales were collected along the diversion tunnel, at the portal slopes, and at the open excavation quarry. These specimens are determined for the properties similar to those of the core samples. The determination for the rock chumps was especially performed in the field laboratory.

4.2 Petrographic and Mineralogical Examinations

Forty-nine thinsections were prepared from the rock-cores and chumps for a petrographic analysis. The surface area of the thinsections was as suggested by Hutchison (1974), i.e. half of the cross-sectional area of the core samples, 22.90 cm^2, and 1.50 x 4.00 cm^2 for the chumps samples, as the mineral contents and the alteration product in these thinsections were considered as the representative of the whole rock.

The average fracture intensity (number of fractures per unit length) and the average size of the fracture opening in the rocks were also obtained by counting the fractures number and measuring the width of the fracture openings along several traverse lines in each thinsection.

The results of the petrography study of these samples were summarized in Table 4.2. The results were further used as the parameters for the rock mass classification, the analyses of slope stability condition, and the assessment of rock masses for the maindam foundation.

4.3 The Basic Physical Property Tests

The following physical properties of the intact rocks in the study area were determined to supplement the mechanical properties of rocks.

Table 4.2 Summary of petrographic and mineral examination of the Chiew Larn rock types

Rock Type	No. of Thin Sections	Mineral Content, %					Fracture Intensity	Fracture Opening mm.
		Quartz	Feldspar	Rock Fragments	Clay Minerals	Other		
Feldspatic Greywacke	16	28.86 ± 11.46	20.93 ± 10.81	4.73 ± 3.33	44.96 ± 7.79	0.63 ± 1.20	7.93 ± 8.30	0.26 ± 0.32
Lithic Greywacke	6	27.65 ± 15.36	8.03 ± 4.72	24.42 ± 20.62	39.90 ± 6.11	-	4.33 ± 4.23	0.23 ± 0.23
Arkosic Sandstone	4	55.73 ± 9.29	24.78 ± 6.21	11.90 ± 8.52	8.38 ± 5.21	1.50 ± 2.38	2.00 ± 3.37	0.38 ± 0.62
Subarkosic Sandstone	4	78.48 ± 3.53	13.68 ± 3.38	1.55 ± 1.82	4.05 ± 4.72	-	2.75 ± 3.20	0.46 ± 0.05
Pebbly Mudstone	13	18.12 ± 8.95	9.40 ± 6.25	1.21 ± 1.23	71.67 ± 10.42	-	3.17 ± 5.06	0.16 ± 0.32
Mudshale	2	11.45 ± 4.03	-	-	88.55 ± 4.03	-	-	-

Note : Classification after Pettijohn (1954)

4.3.1 Water Content

The water content or moisture content of a rock is defined as the quantity of water in the rock voids expressed as a percentage of the water weight to that of the completely dry rock specimen (Duncan, 1969; Lama & Vutukuri, 1978; Mclean and Gribble, 1979; Junikis, 1979; ISRM, 1972, 1981).

ISRM (1972, 1981) suggested a method to determine the water content by using at least ten rock lumps, each mass at least 50 gm, or a minimum dimension of ten times of the maximum grain size. The moist rock is weighted, then brought to constant dry weight by heating it to $105° \pm 3°$ C for at least 24 hours. The difference in weight is recorded as a percentage of water content to the dry weight of the sample.

$$w = Mv/Ms = (B - C)/(C - A) \times 100\% \quad \ldots\ldots\ldots\ldots(4.1)$$

where
- w = water content in %
- Mv = pore water mass
- Ms = grain mass
- A = mass of container with lid
- B = mass of naturally moist sample plus container with lid
- C = mass of dried sample-plus container with lid

The procedure adopted for the present test was to weight the samples to an accuracy of 0.01 gm, then dry them to a constant weight in an oven ($105° \pm 3°$ C) for 24 hours. The oven-dried samples was again weighted to an accuracy of 0.01 gm. The water content of the samples was thus calculated, using the following the equation

$$w = (Wi - Wd)/Wd \times 100\% \quad \ldots\ldots\ldots\ldots\ldots\ldots (4.2)$$

where w = water content in %

Wi = initial weight in gm

Wd = dried weight in gm

The results of the water content determination are summarized in the Table 4.3.

4.3.2 Water Absorption

The ASTM Standards Designation: C - 97 - 47 (Reapproved 1970) stated that the water absorption or free saturation is the capacity of the rock to take up, assimilate, incorporate, or absorb water when soaked for a comparatively long time at atmospheric pressure and room temperature. This practical method is to dry the samples at 105° C for 24 hours, then to weight them. The specimens are soaked in distilled water at 20° C for 48 hours then are weighted again. The percentage of water absorption, by weight, is

$$Sr = \frac{(W_{wet} - W_d)}{W_d} \times 100\% \quad \ldots\ldots\ldots\ldots\ldots (4.3)$$

where W_{wet} = weight of the specimen after immersion

W_d = weight of the dried specimen

Sr = water absorption

The results of the water absorption determination using the above method are summarized in Table 4.3.

4.3.3 Bulk Density and Unit Weight

The mass of a unit volume of rock is its bulk density or simply "density". The Committee on Definitions and Standards of the Geotechnical Engineering Division (1983) explained that the density (ρ) is an inherent measure of the denseness of a material including its void space, and that the unit weight (γ) is a function of gravity. They stated that the term "unit weight" was commonly and erronously used interchangeably for the term (mass) "density", e.g., in the unit weight of a compared fill. The unit weight can be calculated (Lama & Vutukuri, 1978; ISRM, 1981) using the following relationship

$$\gamma = \rho g \qquad \text{.................. (4.4)}$$

wher γ = unit weight

ρ = density

g = acceleration due to gravity

ISRM (1972, 1981) suggested four laboratory methods to determine the density of a rock. Only 2 will be mentioned here since they are the methods employed in the present study. They are the saturation and caliper technique and saturation and buoyancy technique.

4.3.3.1 Saturation and Caliper Technique

ISRM (1981) suggested that at least three specimens from a representative sample of rock are to be tested. The bulk density is to obtain the mass of specimen to an accuracy of

0.01% then divide that value by the bulk volume (V) calculated from the average of several caliper readings obtained for each dimension of a sample block with an accuracy of 0.1 mm.

Similarly Lama & Vutukuri (1978) suggested a measurement of the dimensions of a cylindrical specimen, by averaging the diameter measurements taken at both ends, and the height measured at the right angle to each other on both flat ends. There measurements are to be an accuracy of 0.05 mm. The bulk density is then calculated in the following equation.

$$\rho_b = (M_s + M_w)/V \qquad \text{.................(4.5)}$$

where ρ_b = bulk density

M_s = mass of grains

M_w = mass of pore water

V = bulk sample volume

4.3.3.2 Saturation and Buoyancy Technique

ISRM (1981) suggested to use the representative samples comprising a minimum of ten rock lumps, each with a mass of at least 50 gm. According to ISRM (1981) and Lama & Vutukuri (1978), the procedure is to weight the rock sample in air, dry it to a constant mass of the sample, saturate it in the water in a vacuum of less than 800 N/m^2 for at least one hour. The saturated sample whose surface is wipe-dried with a moist cloth, to be called the "surface-dry sample", is weighted in air. The measurement should be done with a accuracy of 0.01% of the sample mass. The bulk density of the rock sample is determined using the equation

$$\rho_b = (M_s + M_w) \times \rho_w/(M_{sat} - M_{sub}) \quad \ldots\ldots\ldots\ldots\ldots(4.6)$$

where ρ_b = bulk density

M_{sat} = saturated surface-dry mass

M_{sub} = saturated submerged mass

ρ_w = density of water

Various types of density and specific gravity can also be calculated using the following relationships.

Bulk density $\rho = M/V = (M_s + M_v)/V$ ......(4.7)

Dry density $\rho_d = M_s/V$ ......(4.8)

Saturated density $\rho_{sat} = (M_{sat} + V_v \cdot \rho_w)/V$......(4.9)

Grain density $\rho_g = M_s/V_s$ ......(4.10)

Bulk specific gravity $d = \rho/\rho_w$ ......(4.11)

Dry specific gravity $d_d = \rho_d/\rho_w$ ......(4.12)

Saturated specific gravity $d_{sat} = \rho_{sat}/\rho_w$ ......(4.13)

Grain specific gravity $d_g = \rho_g/\rho_w$ ......(4.14)

The results of the density determination done in the present study are summarized in Table 4.3.

4.3.4 Porosity

The porosity of a rock or other substance is the ratio of the volume of voids to the total volume of the rock (Lama and Vutukuri, 1978; Duncan, 1969; McLean & Gribble, 1979; Jumikis, 1979; Goodman, 1980). Goodman (1980) and ISRM (1981) suggested that the porosity, like the density, could be measured using a variety of techniques. The procedure to determine the porosity of Chiew Larn rocks was done during the determination of the bulk density using the technique of ISRM (1981). The porosity is thus calculated using the following relationship.

$$n = \frac{w.d}{1 + w.d} \% \qquad \ldots\ldots\ldots\ldots\ldots (4.15)$$

where n = porosity in %

w = water content in %

d = specific gravity

The results of porosity determination are summarized in Table 4.3.

4.3.5 Void Index

ISRM (1981) defined that the void index is the percentage of the mass of water contained in a rock sample after a one-hour immersion of the initially desicator-dried mass.

ISRM (1981) suggested a method to determine the void index of rock by selecting a minimum of ten rock lumps, each having a mass of at least 50 gm (0.1 lb) to obtain a total sample mass of at least 500 gm (1 lb). The samples, in their air-dry condition, are packed into a container, each lump separated from one another by crystals of dehydrated silica gel. The container is left to stand for a period of 24 hours. After then, the sample are removed from the container, brushed clean of loose rock and silica gel crystals, and their mass are measured to a 0.5 gm (0.001 lb) accuracy. The samples are further placed in the container and water is added until the samples are fully immersed. The container is agitated to remove the air bubbles and is left to stand for a period of one hour. The samples are removed from the container again. The surfaces of the samples are wipe-dried using a moist cloth to carefully remove only the water on the surfaces and to ensure that no fragments are lost. The mass B of the surface-dried samples is measured to a 0.5 - gm (.0001 lb) accuracy. The void index, I_v, is calculated from the relationship

$$I_v = \frac{(B - A) \times 100\%}{A} \quad \text{................}(4.16)$$

where I_v = void index in %

A = mass of dried sample

B = mass of surface-dried sample

The results of the determination from the said relationship are summarized in Table 4.3.

4.3.6 Slake Durability Index

According to ISRM (1972, 1981) and Lama and Vutukuri (1978), the slake durability test can be used to assess the resistance to the weakening and disintegration of a rock sample which is subjected to two cycles of drying and wetting.

Gamble (1971) reported that the durability increases linearly with density and varies inversely with the natural water content. Basead on his study results, Gamble (1971) proposed a classification of the slake durability as shown in Table 4.4.

Table 4.3 Summary of physical properties results in Chiew Larn dam site area

Rock Type	No. of Tests	Ranging Value	W	Sr	ρ_s	ρ_d	ρ_n	ρ_b	γ_b	n	I_v
			%		gm/cc				gm/cm^2.sec^2		
Sark	5	minimum	0.11	0.24	2.59	2.56	2.52	2.53	2.48	0.34	1.16
		average	0.33 ± 0.23	1.02 ± 0.61	2.68 ± 0.07	2.63 ± 0.07	2.65 ± 0.06	2.61 ± 0.07	2.56 ± 0.07	1.25 - 0.84	1.54 ± 0.54
		maximum	1.92	1.92	2.73	2.72	2.77	2.72	2.66	2.53	1.92
Gwke	88	minimum	0.10	0.10	2.53	2.53	2.52	2.51	2.51	0.26	0.18
		average	0.48 ± 0.24	0.64 ± 0.37	2.71 ± 0.06	2.68 ± 0.08	2.70 ± 0.03	2.67 ± 0.06	2.62 ± 0.06	0.97 ± 0.45	0.83 ± 0.57
		maximum	1.22	1.72	2.78	2.77	2.77	2.77	2.71	2.32	3.41
Gwke WIV-V	5	minimum	0.45	0.56	2.59	2.42	2.61	2.64	2.22	0.56	
		average	0.52 ± 0.10	2.37 ± 2.56	2.65 ± 0.04	2.56 ± 0.08	2.63 ± 0.04	2.51 ± 0.14	2.46 ± 0.14	2.58 ± 2.50	-
		maximum	0.59	6.87	2.69	2.64	2,66	2.61	2.56	6.87	
Msh	1	-	0.76	2.69	2.70	2.59	2.67	2.52	2.47	-	-

The test procedure followed in this study was the method given in ISRM (1972). The rock lumps of each sample were grinded to a roughly spherical shape. The lumps were then placed in the cleaned test drum and dried to a constant weight in the oven at a temperature of 105°± 3° C. The weight of the drum with the sample (W_{s_o}) was measured to an accuracy of 0.01 gm. Immediately after this, the drum was mounted in the trough filled with water at 20 ° C to a level of 20 mm below the drum axis. The drum was then rotated at a rate of 20 rpm for 10 minutes. After that it was removed from the trough and the drum with the retained portion of the sample was dried to a constant weight in the oven at 105°± 3° C. The weight (W_{s_1}) was measured to an accuracy of 0.01 gm.

This process was repeated for five cycles. The dry weight (W_{s_1}, W_{s_2},....W_{s_5}) of the drum plus the retained sample after each cycle and the weight (W_o) of the brush-cleaned drum alone were measured to an accuracy of 0.01 gm. The slake durability index after the second cycle was calculated according to the equation

$$I_{d_2} = \frac{W_{s_2} - W_o}{W_{s_o} - W_o} \times 100\% \qquad \text{................(4.17)}$$

where I_{d_2} = slake durability index (after second cycle) of the rock material.

The results of the slake durability tests are shown in Table 4.5. The slake durability values seem to indicate a linear decrease with the number of cycle as illustrated in Figure 4.1.

Table 4.4 Gamble's slake durability classification (after Gamble, 1971)

Group name	% retained after one 10 - minute cycle (dry weight basis)	% retained after two 10 - minute cycles (dry weight basis)
Very high durability	>99	>98
High durability	98 - 99	95 - 98
Medium high durability	95 - 98	85 - 95
Medium durability	85 - 95	60 - 85
Low durability	60 - 85	30 - 60
Very low durability	<60	<30

4.3.7 Results and Discussion of Physical Properties

The total physical properties test results of the Chiew larn rocks are summarized in Table 4.3 and only those of the subarkosic sandastones and pebbly graywackes to pebbly mudstones are listed in Table 4.26 and 4.27. In general, the water content, density and unit weight of both rock groups are nearly of the same value, even though the percentage of the porosity and water absorption of subarkosic sandstones is a little higher than that of the pebbly graywackes. This may be because of influence the difference in mineral composition, degree of alteration, aperture and veinlets intensity of the rock types.

Table 4.5 Summary of slake durability tests results.

Rock type	No. of tests	Ranging value	Slake durability index, I_d, %				
			No of cycle				
			1	2	3	4	5
Gwke	8	minimum	98.80	97.70	97.00	95.90	95.20
		average	99.31 ± 0.35	98.88 ± 0.60	98.49 ± 0.78	98.08 ± 1.11	97.68 ± 1.29
		maximum	99.60	99.40	99.30	99.00	98.80

Note : Gwke = pebbly graywackes to pebbly mudstones

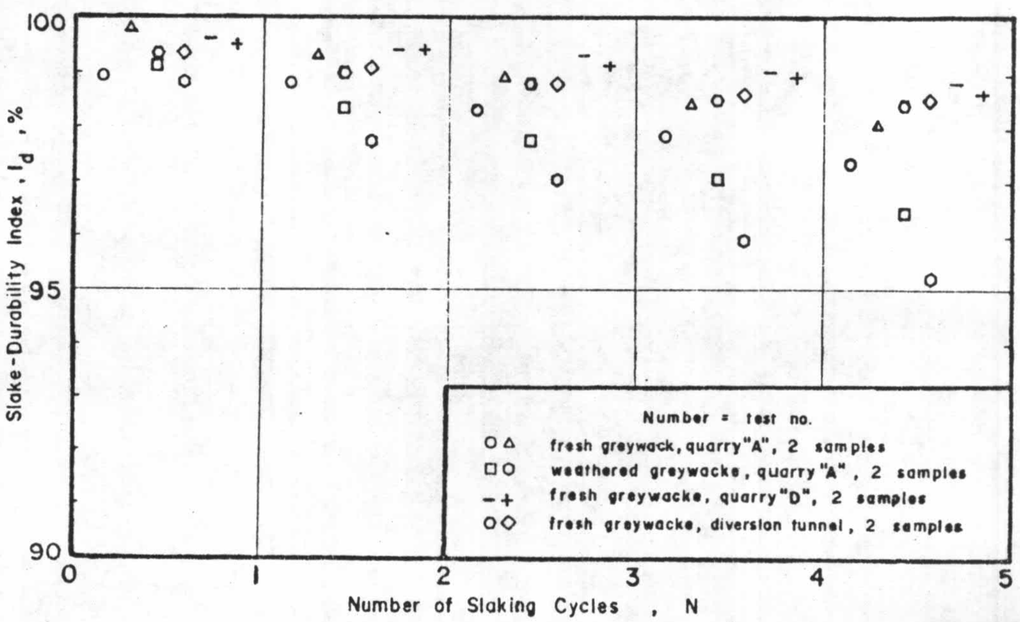

Figure 4.1 Slake-durability index vs. number of slaking cycles for slake-durability tests, graywacke of quarry areas and the diversion tunnel

Table 4.6 Summary of pulse velocity tests results in oven-dry condition*

Core Specimen		Ranging Values	Pulse Velocity		ρ_b	ν_d	E_d	Y_d	G_d	K_d	λ_d
Rock Type	No. of Tests		m/sec		m/sec	-	$x10^4$ MPa				
			V_p	V_s							
Gwke	37	minimum	3675	2075	2.61	0.19	2.88	3.73	1.13	1.89	0.79
		average	4420 ± 367	2510 ± 163	2.69 ± 0.01	0.26 ± 0.03	4.19 ± 0.57	5.22 ± 0.89	1.66 ± 0.22	2.96 ± 0.64	1.85 ± 0.54
		maximum	5044	2766	2.71	0.34	5.38	7.32	2.19	4.37	3.17
Sark	2	minimum	3965	2408	2.61	0.16	3.58	4.09	1.49	1.89	0.79
		average	4112 ± 210	2464 ± 80	2.63 ± 0.03	0.21 ± 0.07	3.63 ± 0.05	4.37 ± 0.40	1.57 ± 0.12	2.28 ± 0.55	1.23 ± 0.63
		maximum	4260	2520	2.65	2.27	3.68	4.65	1.65	2.67	1.58

Note : * = density determined by buoyancy method

Gwke = pebbly graywackes to pebbly mudstones; Sark = subarkosic sandstones

Table 4.7 Sumary of pulse velocity tests results in air-dry condition*

Core Specimen		Ranging Values	Pulse Velocity		ρ_a	ν_a	E_a	Y_a	G_a	K_a	λ_a
Rock Type	No. of Tests		m/sec		gm/cc	-	$\times 10^4$ Mpa				
			V_p	V_s							
Gwke	36	minimum	3427	2133	2.70	0.32	3.19	3.15	1.22	1.52	0.71
		average	4529 $\pm$ 410	2525 $\pm$ 160	2.72 $\pm$ 0.01	0.27 $\pm$ 0.03	4.33 $\pm$ 0.58	5.55 $\pm$ 0.95	1.71 $\pm$ 0.21	3.29 $\pm$ 0.68	2.11 $\pm$ 0.62
		maximum	5160	2774	2.73	0.31	5.21	7.11	2.04	4.59	3.33
Sark	2	minimum	4395	2429	2.72	0.27	3.45	5.18	1.58	3.07	2.01
		average	4487 $\pm$ 130	2504 $\pm$ 110	2.73 $\pm$ 0.01	0.27 $\pm$ 0.01	3.75 $\pm$ 0.43	5.51 $\pm$ 0.47	1.72 $\pm$ 0.19	3.22 $\pm$ 0.21	2.07 $\pm$ 0.08
		maximum	4579	2580	2.73	0.28	4.05	5.84	1.85	3.36	0.13

Note : * = density determined by buoyancy method

Gwke = pebbly graywackes to pebbly mudstones; Sark = subarkosic sandstones

Table 4.8 Summary of pulse velocity tests results in saturated condition*

Core Specimen		Ranging Values	Pulse Velocity		ρ_s	ν_s	E_s	Y_s	G_s	K_s	λ_s
Rock Type	No. of Tests		m/sec		gm/cc	-	$\times 10^4$ MPa				
			V_p	V_s							
Gwke	37	minimum	3315	2213	2.65	0.21	2.69	2.91	1.29	1.39	0.63
		average	4539 $\pm$ 320	2483 $\pm$ 280	2.69 $\pm$ 0.08	0.28 $\pm$ 0.02	4.18 $\pm$ 0.85	5.49 $\pm$ 0.78	1.64 $\pm$ 0.36	3.31 $\pm$ 0.31	2.21 $\pm$ 0.07
		maximum	5194	2705	2.71	0.36	4.98	7.17	1.94	4.70	3.53
Sark	2	minimum	4260	2233	2.65	0.28	3.39	4.71	1.29	2.99	2.12
		average	4486 $\pm$ 320	2428 $\pm$ 280	2.66 $\pm$ 0.02	0.29 $\pm$ 0.02	3.99 $\pm$ 0.85	5.26 $\pm$ 0.78	1.55 $\pm$ 0.36	3.20 $\pm$ 0.31	2.17 $\pm$ 0.07
		maximum	4712	2622	2.67	0.31	4.60	5.82	1.80	3.42	2.21

Note : * = density determined by buoyancy method

Gwke = pebbly graywackes to pebbly mustones; Sark = subarkosic sandstones

Table 4.9 Summary of pulse velocity tests results in oven-dry condition**

Core Specimen		Ranging Values	Pulse Velocity		ρ_d	ν_d	E_d	Y_d	G_d	K_d	λ_d
Rock Type	No. of Tests		m/sec		gm/cc	-	$\times 10^4$ MPa				
			V_p	V_s							
Gwke	37	minimum	3675	2075	2.62	0.19	2.84	3.52	1.12	1.89	0.10
		average	4420 ± 367	2510 ± 163	2.67 ± 0.02	0.26 ± 0.03	4.18 ± 0.58	5.16 ± 0.92	1.65 ± 0.22	2.94 ± 0.64	1.84 ± 0.54
		maximum	5044	2766	2.70	0.34	5.35	7.34	2.18	4.36	3.16
Sark	2	minimum	3965	2408	2.48	0.16	3.58	4.56	1.41	1.81	0.75
		average	4112 ± 210	2464 ± 80	2.52 ± 0.04	0.21 ± 0.07	3.63 ± 0.08	4.17 ± 0.35	1.50 ± 0.12	2.18 ± 0.51	1.18 ± 0.60
		minimum	4260	2520	2.55	0.27	3.68	4.42	1.59	2.54	1.60

Note : ** = density determined by geometry method

Gwke = pebbly graywackes to pebbly mudstones; Sark = subarkosic sandstones

Table 4.10 Summary of pulse velocity tests results in air-dry condition**

Core Specimen		Ranging Values	Pulse Velocity		ρ_a	ν_a	E_a	Y_a	G_a	K_a	λ_a
Rock Type	No. of Tests		m/sec		gm/cc	-	$\times 10^4$ MPa				
			V_p	V_s							
Gwke	36	minimum	3427	2133	2.61	0.03	3.05	3.04	1.18	1.47	0.69
		average	4529 $\pm$ 410	2525 $\pm$ 160	2.66 $\pm$ 0.02	0.27 $\pm$ 0.03	4.24 $\pm$ 0.60	5.40 $\pm$ 0.10	1.67 $\pm$ 0.22	3.17 $\pm$ 0.72	2.05 $\pm$ 0.61
		maximum	5160	2774	2.70	0.31	5.16	6.97	2.04	4.44	3.22
Sark	2	minimum	4395	2429	2.47	0.27	3.08	4.68	1.43	2.77	1.82
		average	4487 $\pm$ 130	2504 $\pm$ 110	2.50 $\pm$ 0.05	0.27 $\pm$ 0.10	3.37 $\pm$ 0.41	4.94 $\pm$ 0.38	1.54 $\pm$ 0.16	2.89 $\pm$ 0.16	1.86 $\pm$ 0.06
		maximum	4579	2580	2.54	0.28	3.66	5.21	1.66	3.01	1.90

Note : ** = density determined by geometry method

Gwke = pebbly graywackes to pebbly mudstones; Sark = subarkosic sandstones

Table 4.11 Summary of pulse velocity tests results in saturated condition**

Core Specimen		Ranging	Pulse Velocity		ρ_s	ν_s	E_s	Y_s	G_s	K_s	λ_s
Rock Type	No. of Tests	Values	m/sec		gm/cc	-	x10^4 MPa				
			V_p	V_s							
Gwke	37	minimum	3315	2213	2.63	0.21	2.65	2.87	1.12	1.37	0.62
		average	4539 ± 320	2483 ± 280	2.67 ± 0.02	0.28 ± 0.02	4.15 ± 0.62	5.45 ± 1.02	1.62 ± 0.21	3.28 ± 0.80	2.20 ± 0.69
		maximum	5194	2705	2.71	0.36	4.10	7.15	1.94	4.69	3.48
Sark	2	minimum	4260	2233	2.52	0.28	3.23	4.48	1.23	2.84	2.02
		average	4486 ± 320	2428 ± 280	2.54 ± 0.03	0.29 ± 0.02	3.82 ± 0.84	5.03 ± 0.78	1.48 ± 0.35	3.06 ± 0.31	2.07 ± 0.08
		maximum	4712	2622	2.56	0.31	4.41	5.58	1.73	3.28	2.13

Note : ** = density determined by geometry method

Gwke = pebbly graywackes to pebbly mudstones; Sark = subarkosic sandstones

4.3.8 Correlations of Various Physical Properties

In order to see if any significant correlationship existed of various physical properties of Chiew Larn sandstones, a number of correlations, were performed, are shown in Table 4.25. Since the amount of the correlation results by means of the chi-square test. The correlation between the bulk density and porosity of the Chiew Larn sandstones is not as good as was expected. This presumably can be explained by the fact that the two parameters take account of the grain arrangement without referring to the cementing or the secondary-filled materials occupying the intervening voids, which, of course, reduces the porosity. The best correlation coefficient was obtained between the bulk denstity and porosity, it being -0.65 (Figure 4.2 a).

The results of both water absorption and void index were compared with those of bulk density by mean of the chi-square test. It follows that there is a good relationship between the buld density and water absorption, in this case the correlation coefficient is -0.77 (Figure 4.2 b), indication that as the porosity decreases, the bulk density increases. The correlation between the void index and the bulk density is also good, the coefficient being -0.83 (Figure 4.2 c). The correlation coefficient between the dry density and saturated density is 0.95 (Figure 4.2 d). The influence of water content on the bulk density was surprisingly poor, as the correlation coefficient between the two being -0.63 (Figure 4.2 c). Thus, the relationship is insignificant. This suggests that the amount of water contained is not the most important factor in this

Figure 4.2 Correlations of various physical properties of Chiew Larn pebbly graywackes to pebbly mudstones.

a) relationship between porosity and the bulk density.

b) relationship between the bulk density and water absorption.

c) relationship between porosity and the void index.

d) relationship between the dry density and saturated density

e) relationship between the water content and bulk density.

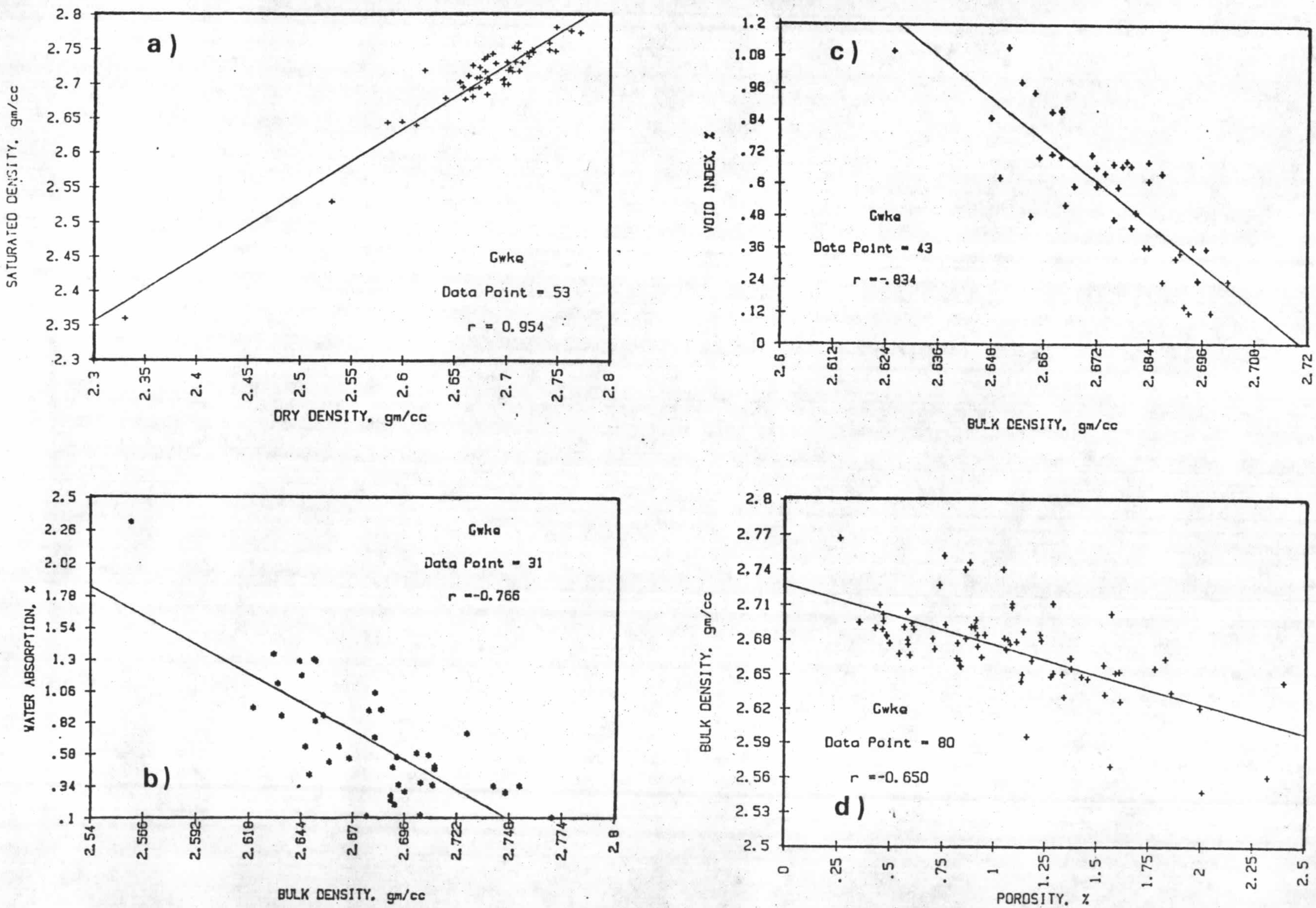
a)
SATURATED DENSITY, gm/cc
DRY DENSITY, gm/cc
Gwke
Data Point = 53
r = 0.954
b)
WATER ABSORPTION, %
BULK DENSITY, gm/cc
Gwke
Data Point = 31
r =-0.766
c)
VOID INDEX, %
BULK DENSITY, gm/cc
Gwke
Data Point = 43
r =-.834
d)
BULK DENSITY, gm/cc
POROSITY, %
Gwke
Data Point = 80
r =-0.650

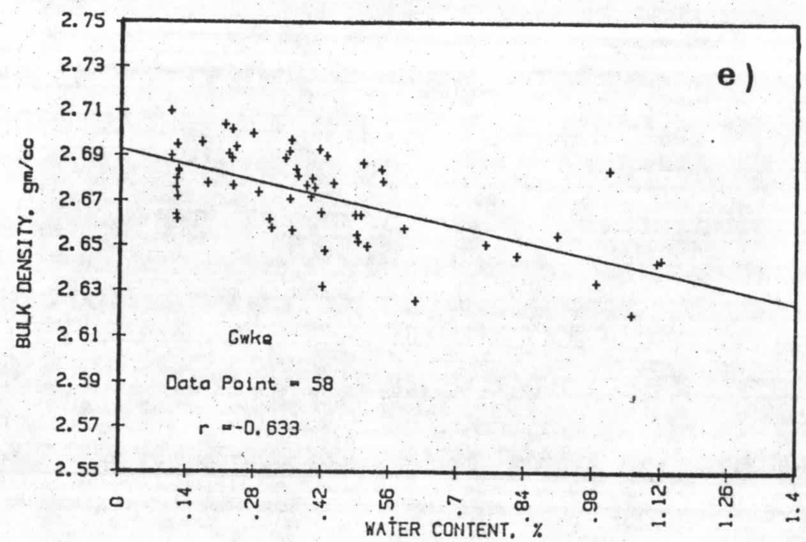

Figure 4.2 cont.

respect. The relationship among these physical properties can be derived in the empirical equations which are summarized in Table 4.25.

4.4 The Mechanical Property Tests

The mechanical properties determined include the unconfined compressive strength, modulus of deformation, Poisson's ratio, tensile strength, shear strength, point-load strength index, and sonic velocity. The other properties determined include the Los Angeles abrasion hardness and Schmidt rebound hardness.

4.4.1 Determination of Sonic Velocity

Numerous papers have dealt with the various laboratory techniques to measure the sound waves velocity in the rocks as a function of pressure. The method most applicable to the rocks is that of simply pulsing one end of a specimen and measuring the time taken for the pulse to reach the opposite end (Goodman, 1980; Bonner and Schock, 1981)

ISRM (1981) recommended to use a rectangular block, cylindrical cores or sphere-shaped specimens, all having a minimum lateral dimension not less than 10 times the wave length and the height or the travel distance of the pulse through the specimen not less than to times the average grain size. However, in order to determine the first arrival of the shear wave accurately and conveniently, ISRM (1981) recommended a height-to-width ratio of 2 to be used.

The compression and shear wave velocities, Vp and Vs are calculated from the equations (ASTM-D-2845-69, 1979; ISRM, 1981)

$$Vp = L/t_p \quad \ldots\ldots\ldots\ldots\ldots\ldots\ldots\ldots\ldots(4.18)$$

$$Vs = L/t_s \quad \ldots\ldots\ldots\ldots\ldots\ldots\ldots\ldots\ldots(4.19)$$

where Vp = compressional velocity (P-wave velocity)

Vs = shear velocity (S-wave velocity)

L = pulse travel distance

t_p = time taken by compressional wave total the distance L

t_s = time taken by shear wave total the distance L

The elastic constants are obtained from density and the velocities as follow.

Modulus of elasticity $E = \dfrac{\rho Vs^2.(3Vp^2 - 4Vs^2)}{Vp^2 - Vs^2}$ ......(4.20)

Stiffness modulus $Y = \rho Vp^2$ ......(4.21)

Rigidity modulus $G = \rho Vs^2$ ......(4.22)

Bulk modulus $K = \dfrac{\rho(3Vp^2 - 4Vs^2)}{3}$ ......(4.23)

Lame's constant $\lambda = \rho(Vp^2 - 2Vs^2)$ ......(4.24)

Poisson's ratio $\nu = \dfrac{(Vs^2 - Vp^2)}{2(Vp^2 - Vs^2)}$ ......(4.25)

where ρ = density

The test was performed according to the method described by ISRM (1981). The height (h) of the core samples was obtained by averaging four measurements taken to the nearest 0.1 mm at the opposite corners of two orthogonal diametrical planes. A vernier caliper was used for these measurements. The ultrasonic material tester (OYO-model 5217A Sonic Viewer with pulse generator) was used to transmit the compression (P) and shear (S) waves and the zero-time was adjusted first by placing the transducer and reciever in a direct contact with each other, and by shifting the first arrival of the pulse frequency used was 500 cycles per second. The core sample was placed in between the transducer and reciever and the travel time (t) of the pulse through the axial direction of the core specimen was measured by adjusting the time-delay circuit. While measuring the travel time of the compression wave through the sample, a thin film of vacuum grease was applied at the both ends of the specimen whereas no such medium was used with the transmission of shear waves.

This procedure was repeated for other core samples prepared for the uniaxial compression test and the pulse velocities (V_p and V_s) were calculated according to the equations 4.18 and 4.19 given above. The histograms illustrating the range and distribution of the sonic velocities are shown in Figure 4.3 a, b and 4.4.

The dynamic moduli such as dynamic Young's modulus (E), Poisson's ratio (ν), modulus of rigidity (G), Lame's constant (λ), and bulk modulus (K) are given in the equations 4.20 to 4.25. The moduli obtained in the present study are summarized in Table 4.6 to 4.11.

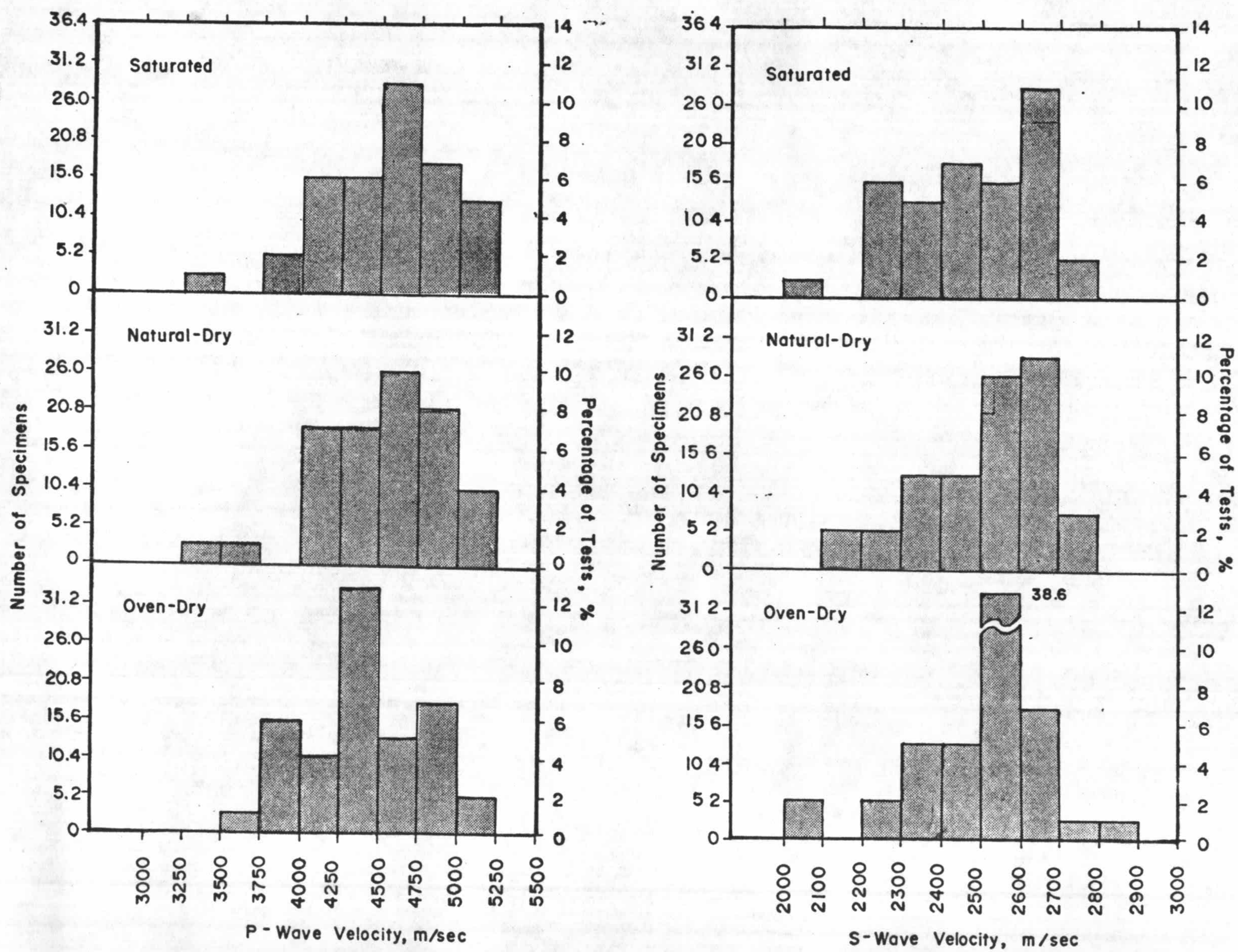

Figure 4.3 Histogram illustrating range and distribution of a) mean velocity (Vp)

b) mean velocity (Vs).

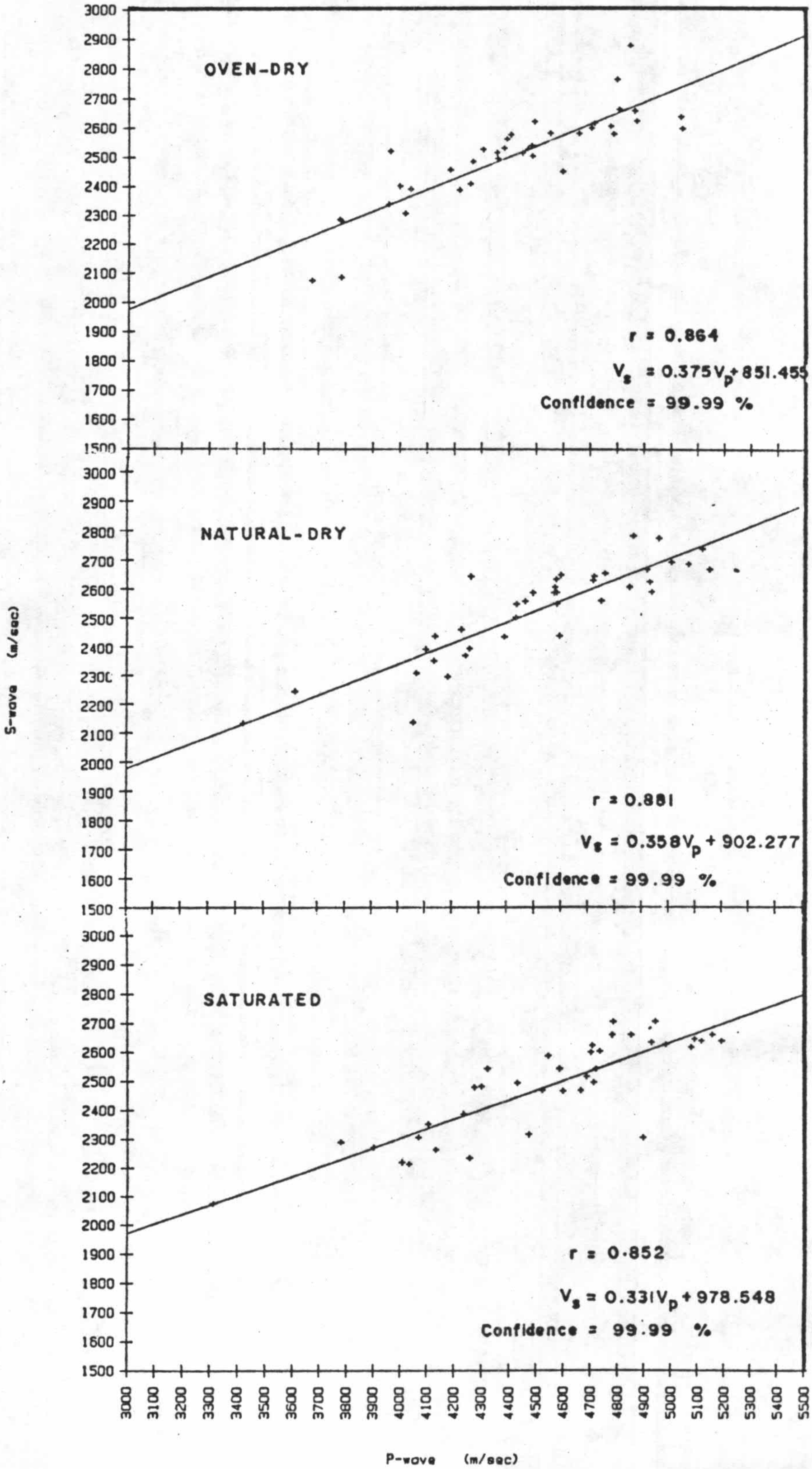

Figure 4.4 Relationship between P-wave vs. S-wave in core specimens in oven-dry, air-dry and saturaed condition.

4.4.2 Determination of Strength

The strength of a rock is its ultimate ability to resist the stress without any failure. It can be categorized into compression strength, tensile strength, and shear strength.

4.4.2.1 Uniaxial Compressive Strength

The uniaxial compressive strength is defined as the compressive stress applied in only one direction which causes the failure of a rock specimen. The uniaxial compression test is widely used for the strength classification and characterization of intact rock. It is calculated as the ratio of the breaking load, which causes fracture, to the cross-sectional area of the specimen.

$$\sigma_c = F/A \qquad \text{.............(4.26)}$$

where σ_c = uniaxial compressive strength of the specimen

F = applied force at failure, and

A = initial cross-sectional area transverse to the direction of force

Gyenge and Herget (1980) and ISRM (1972, 1981) suggested the similar methods to determine the uniaxial compressive strength of an intact rock core specimen within some specific tolerances. The right circular cylinder specimen should have a length-to-diameter ratio of 2.5 to 3.0 and a diameter of not less than the NX core size approximately $2\frac{1}{8}$ in (54 mm). Both ends of the specimen should be parallel to each other and at the right angle to the lower bearing block. The load is applied and increased continuously, without any pulse, to produce an approximately constant rate of load and/or deformation within the limit of 0.5 - 1.0 MPa/sec such that failure will occur within 5 to 15 minutes of loading.

According to Gaddy (1958), Brown and Pomeroy (1958), Griggs et al. (1960), Price (1960, 1979, 1981), Brace (1961), Mogi (1962, 1966), Brosvenor (1963), Hobbs (1964 b), Holland (1964), Colback and Wild (1965), Meikle and Holland (1965), Zaruba (1965), Fairhurst and Cook (1966), McLamore (1966), Paul and Gangal (1966), Bieniawski (1968 a, 1968 b, 1971), Evans and Pomeroy (1968), Alekseev et al. (1970), Kartashov et al. (1970), Hodgson and Cook (1970), Hawkes & Mellor (1970), Houpert (1970), Hudson et al. (1970), Vutukuri et al. (1974), Roberts (1977), Jeager and Cook (1979), Hoek and Brown (1980), Singh (1981), and numerous other investigators who conducted experiments extensively the influence of the parameters on the uniaxial compressive strength. It has been found that the parameters are generally the size and shape of rock specimen, height to diameter ratio (h/d ratio), friction between the end-surfaces and platens, rate of loading, grain size of the mineral constituents, moisture content, pores and porosity, temperature, number of sample tested, mode of failure of specimens, failure mechanism of specimens, testing machine stiffness, stress-strain curve behaviors and anisotropy of strength, etc.

The preparation of the cylindrical specimens for the test is as follows. The specimen was laid down on its side. Two lines were marked on the specimen, one along the axial direction and the other line along the circumference at its mid-height. The specimen surfaces were cleaned around two lines by using carbon tetrachloride and the strain-gage adhesive (CY - 10) was applied on the cleaned surface and then two electrical resistance strain gages (type-S160, Shinkoh, Japan) mounted at the mid-height of the specimen by placing them along the lines drawn. The lead wires were connected to the strain gages and fixed them in position by covering them with cellophane tapes.

Two sets of convex-concave spherical seat assemblages having the cross sectional area equal to that of specimen were placed on both ends of the test specimen. The whole set up was then inserted in between the loading platens of the compression machine. The purpose of using these spherical seats was to minimize the lateral pressure acting on the edges of the specimen during loading. The centre of the strain gages system was then set to align with the centre of the loading platens and the compression machine (ELE - Engineering Laboratory Equipment, England) was set to have a stress rate of 0.5 MPa/sec on the specimen.

The axial and circumferential strains of the specimen were obtained by observing the change of electric resistance of the strain gages using a wheatstone bridge in a digital strain indicator (model PSD-701, Shrinkoh, Japan). The lead-wires from the strain gages were connected to the digital strain indicator. To compensate for the variations in electric resistance caused by temperature and humidity changes in the surrounding environment the same type of strain gages were mounted on a dummy specimen of the same material, with the lead wires connected to the arms of the wheatstone bridge opposite to the corresponding arms connected to the active gages. The required gages factor was selected from the digital strain indicator and the whole circuit was checked for a proper functioning.

The load was then applied and increased continously without any pulse while the axial and circumferential strain readings were recorded with the increase of axial load to the selected load values. The ultimate load born by the specimen at failure was recorded to the nearest 0.01 N. The mode of failure was also observed and sketched. The procedure was repeated for all other core specimens.

The Equation 4.26 given on above was used to calculate for the uniaxial compressive strength of the rock core specimes. The graphs of axial stress versus axial strain and axial stress versus lateral strain were plotted and the Poisson's ratio of the specimen was calculated at the certain stress-strain curve levels.

The unconfined compressive strength, modul deformations, and Poisson's ratio are summarized and plotted in Tables 4.12 to 4.15 and Figure 4.5 respectively.

It can be seen from the stress-strain curves of the specimens in Figure 4.5 and distributed uniaxial compressive strength in Figure 4.6 that the stress-strain relationship of Chiew Larn pebbly graywackes to pebbly mudstones from various borehole locations can be divided into four categories.

(a) Type A (straight line)

The stress/strain relationship of this type is characterized by a linearly elastic behavior indicating a constant value of the modulus of elasticity till the point of failure. These

Table 4.12 Summary of uniaxial compression tests results

Core Specimen: Rock Type	Core Specimen: No. of Tests	Ranging Values	W %	A	B	C	D	E	F
Sark	4	minimum	0.08	-	40	75.72	4.08	3.41	4.21
		average	0.11 ± 0.03	-	50.75 ± 8.69	144.32 ± 42.89	9.31 ± 5.36	5.78 ± 2.01	6.79 ± 2.06
		maximum	0.16	-	60	193.61	14.50	8.33	8.64
Gwke	37	minimum	0.10	3	7	24.45	1.68	1.18	2.20
		average	0.53 ± 0.32	22.00 ± 20.59	28.78 ± 13.51	54.51 ± 24.00	6.50 ± 4.87	5.43 ± 2.87	7.88 ± 6.33
		maximum	1.31	50	58	150.03	27.08	14.58	30.61

Table 4.13 Summary of uniaxial compression tests results

Core Specimen: Rock Type	Core Specimen: No. of Tests	Ranging Values	G	H	I	J	K	L	M
Sark	4	minimum	0.13	0.05	0.11	1.74	1.44	1.84	-334
		average	0.17 ± 0.03	0.16 ± 0.02	0.15 ± 0.03	3.93 ± 2.19	2.48 ± 0.85	2.95 ± 0.85	907.25 ± 742.84
		maximum	0.22	0.43	0.17	5.97	3.53	3.72	1925
Gwke	37	minimum	0.06	0.14	0.04	0.81	0.57	1.05	53
		average	0.16 ± 0.06	0.16 ± 0.07	0.17 ± 0.09	2.75 ± 2.03	2.28 ± 1.21	3.36 ± 2.62	735.75 ± 596.72
		maximum	0.25	0.18	0.36	10.83	6.25	11.48	2187

Table 4.14 Summary of uniaxial compression tests results

Core Specimen		Ranging	N	O	P	Q	R	S
Rock Type	No. of Tests	Values			$\times 10^4$ MPa			
Sark	4	minimum	2.09	1.79	1.98	0.83	0.83	0.76
		average	4.97 ± 3.12	2.81 ± 1.11	3.50 ± 1.06	2.35 ± 1.79	1.23 ± 0.54	1.29 ± 0.62
		maximum	8.48	4.37	4.25	4.50	2.02	1.87
Gwke	29	minimum	0.60	0.41	0.80	0.06	0.03	0.09
		average	3.58 ± 3.56	2.88 ± 1.74	4.46 ± 5.42	1.74 ± 2.24	1.39 ± 1.20	2.44 ± 4.21
		maximum	18.06	8.33	30.55	10.83	5.00	22.89

Table 4.15 Summary of uniaxial compression tests results

Core Specimen		Ranging Values	T	U	V	W	X	Y	Z
Rock Type	No. of Tests			$\times 10^{4}$ MPa		$\times 10^{4}$	$\times 10^{4}$ MPa		$\times 10^{-4}$ MPa
Sark	4	minimum	23.05	10.42	13.19	227.69	1.57	2.65	29.94
		average	29.73 ± 8.00	20.61 ± 10.59	25.91 ± 12.68	443.88 ± 227.93	2.66 ± 0.93	19.52 ± 12.56	994.95 ± 747.38
		maximum	40.18	34.40	38.12	761.89	3.84	30.99	1773.72
Gwke	99	minimum	3.57	3.33	3.84	334.79	0.59	0.28	31.92
		average	17.99 ± 9.46	15.80 ± 9.17	22.34 ± 17.07	997.01 ± 770.08	2.54 ± 1.32	5.06 ± 4.58	344.02 ± 306.22
		maximum	35.27	34.24	37.46	3403.21	6.70	18.65	1228.02

Note of Tables Uniaxial compression test results symbols

Sark = Subarkosic to arkosic sandstones

Gwke = pebbly greywackes to pebbly mudstones

A = inclination of discontinuity to axial stress

B = inclination of fracture failure to axial stress

C = ultimate uniaxial compressive strength, MPa

D = average Young's modulus of axial stress-strain curves, $x10^4$ MPa

E = tangent Young's modulus at 50 % of ultimate strength, $x10^4$ MPa

F = secant Young's modulus at 50 % of ultimate strength, $x10^4$ MPa

G = average Poisson's ratio

H = tangent Poisson's ratio

I = secant Poisson's ratio

J = average shear modulus, $x10^4$ MPa

K = tangent shear modulus, $x10^4$ MPa

L = secant modulus, $x10^4$ MPa

M = volumetric strain, $x10^{-6}$

N = average bulk modulus or compressibility, $x10^4$ MPa

O = tangent bulk modulus, $x10^4$ MPa

P = sectant bulk modulus, $x10^4$ MPa

Q = average Lame's constant, $x10^4$ MPa

R = tangent Lame's constant, $x10^4$ MPa

S = secant Lame's constant, $x10^4$ MPa

T = average hydrostatic pressure, $x10^4$ MPa

U = tangent hydrostatic pressure, $x10^4$ MPa

V = secant hydrostatic pressure, $x10^4$ MPa

W = tangent modulus ratio, $x10^4$ MPa

X = constrained modulus, $x10^4$ MPa

Y = toughness modulus, $x10^4$ MPa

Z = resilience modulus, $x10^{-4}$ MPa

Figure 4.5 Axial and diametrical stress -strain curves for uniaxial compression test.

Rock sample no. 1, borehole DH 1 with depth 23.53 - 23.68 m.

Rock sample no. 2, borehole DH 1 with depth 42.25 - 42.40 m.

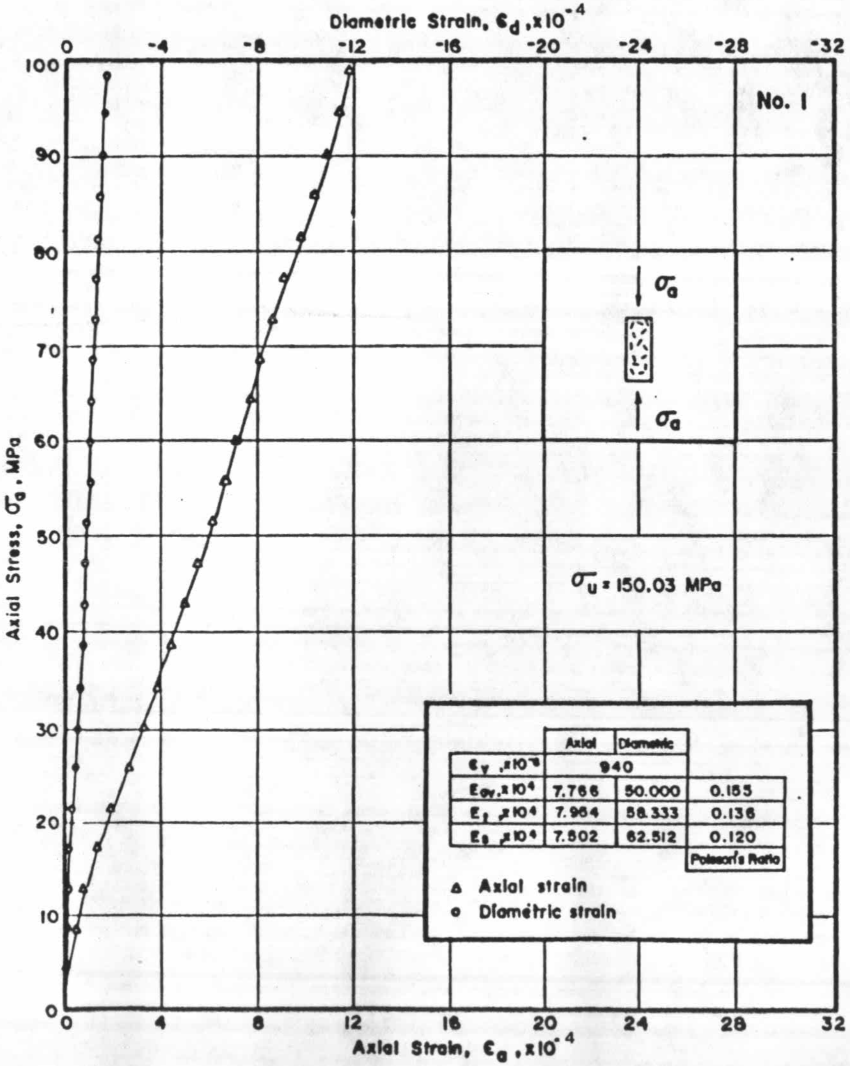
Diametric Strain, ϵ_d, x10^{-4}
0
-4
-8
-12
-16
-20
-24
-28
-32
No. 1
σ_a
σ_a
σ_u = 150.03 MPa
Axial Stress, σ_a, MPa
100
90
80
70
60
50
40
30
20
10
0
Axial
Diametric
ϵ_v, x10^{-6} 940
E_{av}, x10^4 7.766 50.000 0.155
E_t, x10^4 7.964 58.333 0.136
E_s, x10^4 7.502 62.512 0.120
Poisson's Ratio
Axial strain
Diametric strain
0
4
8
12
16
20
24
28
32
Axial Strain, ϵ_a, x10^{-4}

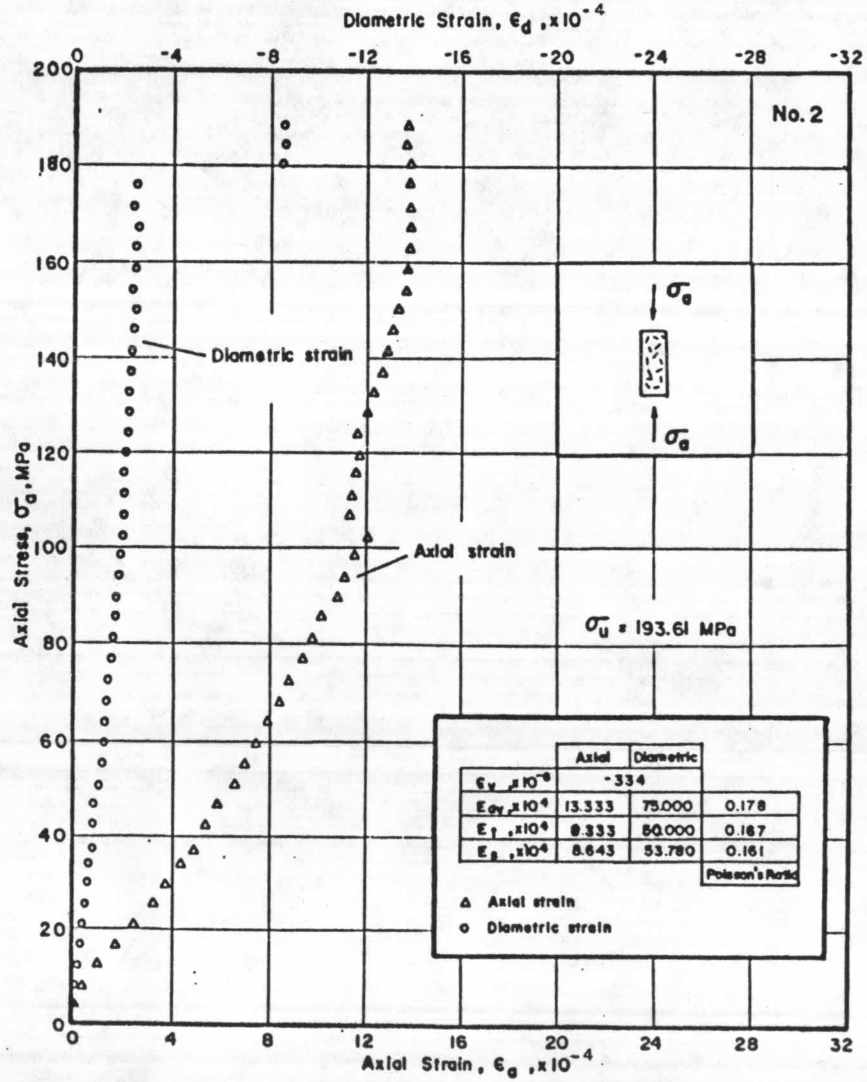
Diametric Strain, ϵ_d, x10^{-4}
0
-4
-8
-12
-16
-20
-24
-28
-32
No. 2
σ_a
σ_a
Diametric strain
Axial strain
σ_u = 193.61 MPa
Axial Stress, σ_a, MPa
200
180
160
140
120
100
80
60
40
20
0
Axial
Diametric
ϵ_v, x10^{-6} -334
E_{av}, x10^4 13.333 75.000 0.178
E_t, x10^4 8.333 50.000 0.167
E_s, x10^4 8.643 53.780 0.161
Poisson's Ratio
Axial strain
Diametric strain
0
4
8
12
16
20
24
28
32
Axial Strain, ϵ_a, x10^{-4}

Figure 4.5 cont.

Rock sample no. 3, borehole DH 2 with depth 1.10 -1030 m.

Rock sample no. 4, borehole DH 2 with depth 54.20 - 54.50 m.

Rock sample no. 5, borehole DH 3 with depth 30.20 - 30.40 m.

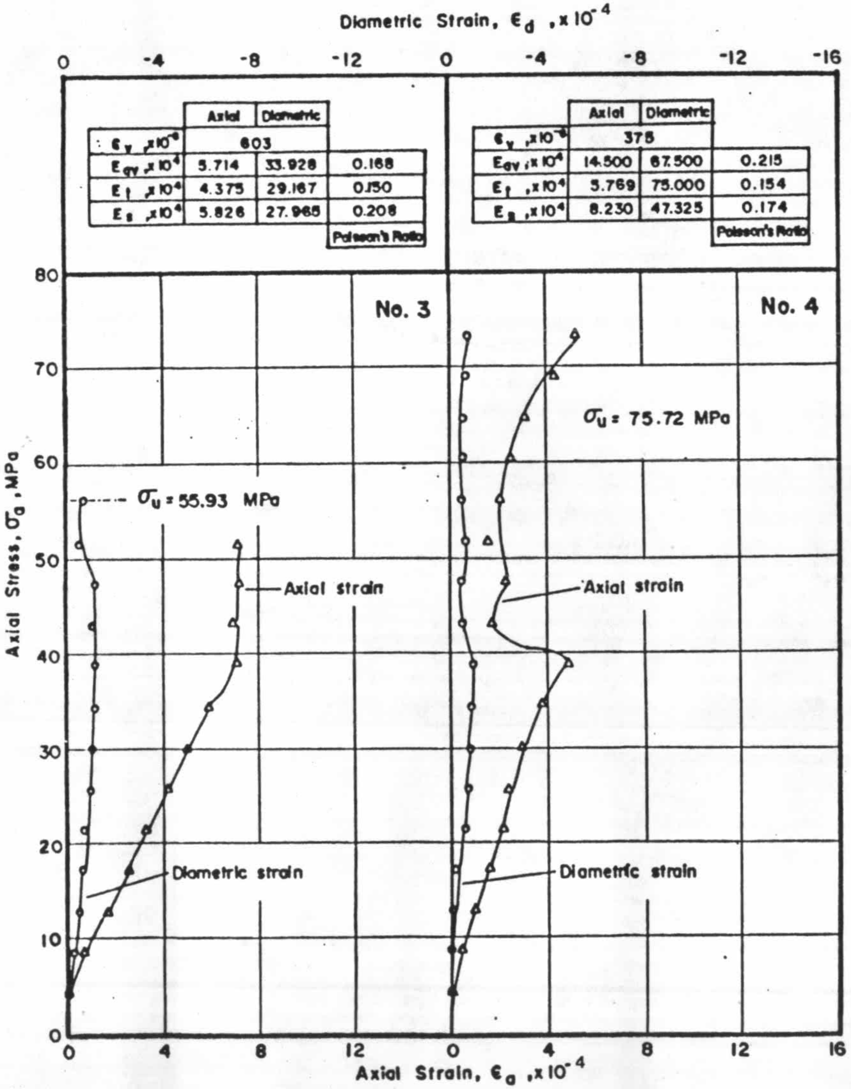

Diametric Strain, ε_d, x 10^-4
Axial | Diametric
ε_v, x10^-6 | 603
E_av, x10^4 | 5.714 | 33.928 | 0.168
E_t, x10^4 | 4.375 | 29.167 | 0.150
E_s, x10^4 | 5.826 | 27.965 | 0.208
Poisson's Ratio
Axial | Diametric
ε_v, x10^-6 | 375
E_av, x10^4 | 14.500 | 67.500 | 0.215
E_t, x10^4 | 5.769 | 75.000 | 0.154
E_s, x10^4 | 8.230 | 47.325 | 0.174
Poisson's Ratio
No. 3
No. 4
σ_u = 55.93 MPa
σ_u = 75.72 MPa
Axial strain
Axial strain
Diametric strain
Diametric strain
Axial Stress, σ_a, MPa
Axial Strain, ε_a, x 10^-4

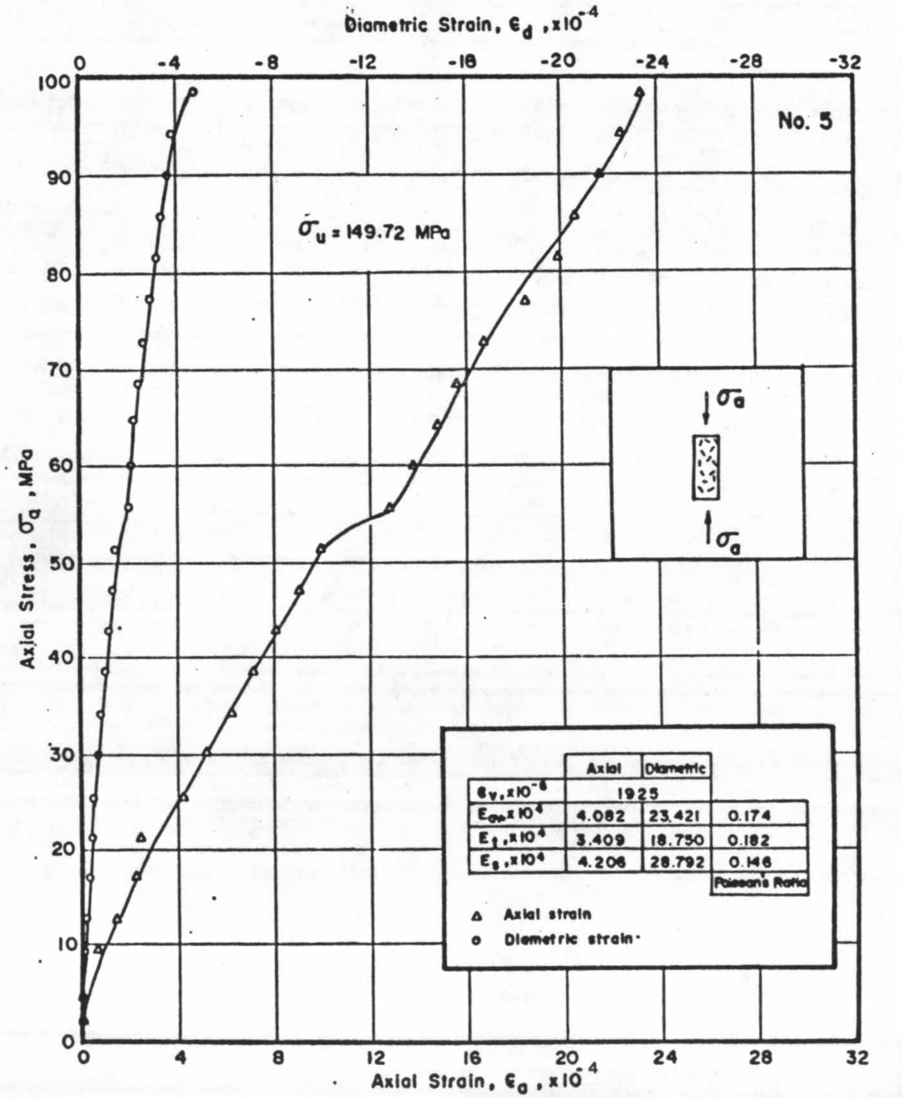

Diametric Strain, ε_d, x10^-4
No. 5
σ_u = 149.72 MPa
σ_a
σ_a
Axial | Diametric
ε_v, x10^-6 | 1925
E_av, x10^4 | 4.082 | 23.421 | 0.174
E_t, x10^4 | 3.409 | 18.750 | 0.182
E_s, x10^4 | 4.206 | 28.792 | 0.146
Poisson's Ratio
Δ Axial strain
o Diametric strain
Axial Stress, σ_a, MPa
Axial Strain, ε_a, x10^-4

Figure 4.5 cont.

Rock sample no. 6, borehole DH 3 with depth 59.00 - 59.13 m.

Rock sample no. 7, borehole DH 3 with depth 59.13 - 59.30 m.

Rock sample no. 8, borehole DH 4 with depth 66.22 - 66.24 m.

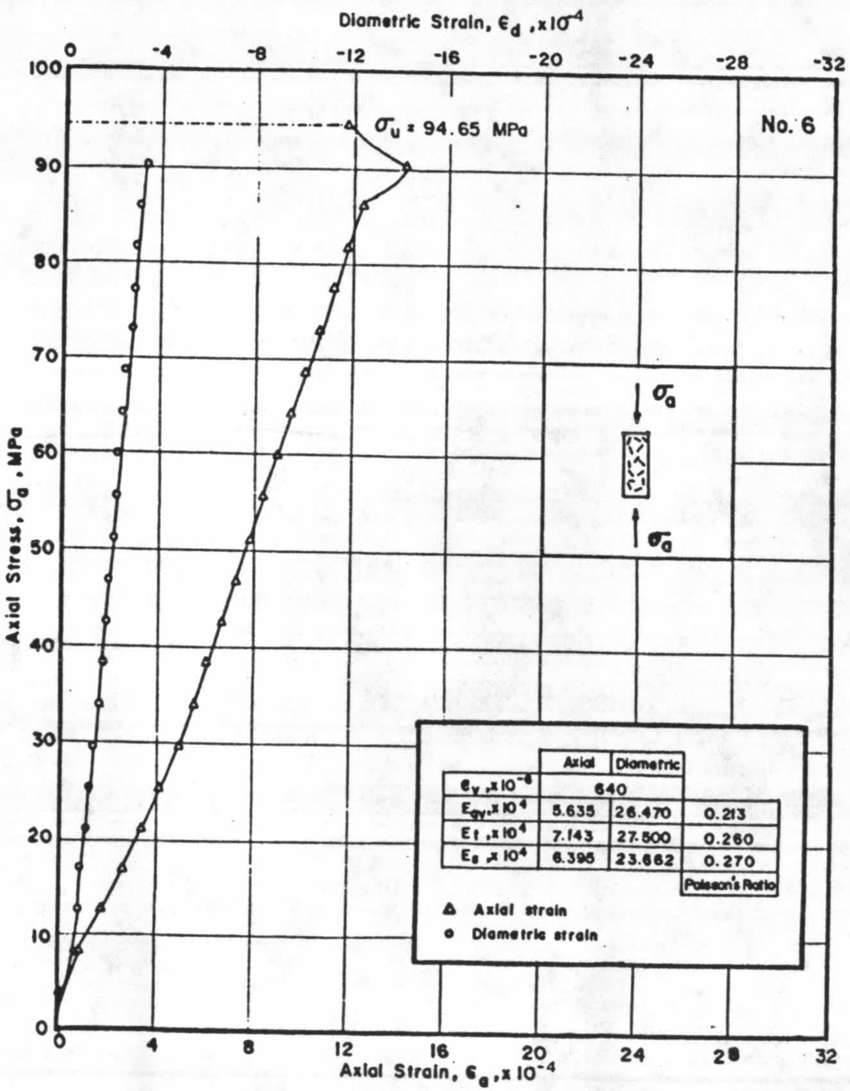

Diametric Strain, ϵ_d, x10^{-4}
Axial Stress, σ_a, MPa
Axial Strain, ϵ_a, x 10^{-4}
σ_u = 94.65 MPa
No. 6
σ_a
σ_a
	Axial	Diametric	
ϵ_y, x10^{-6}	640		
E_{av}, x10^{4}	5.635	26.470	0.213
E_t, x10^{4}	7.143	27.500	0.260
E_s, x10^{4}	6.395	23.662	0.270
			Poisson's Ratio
Axial strain
Diametric strain

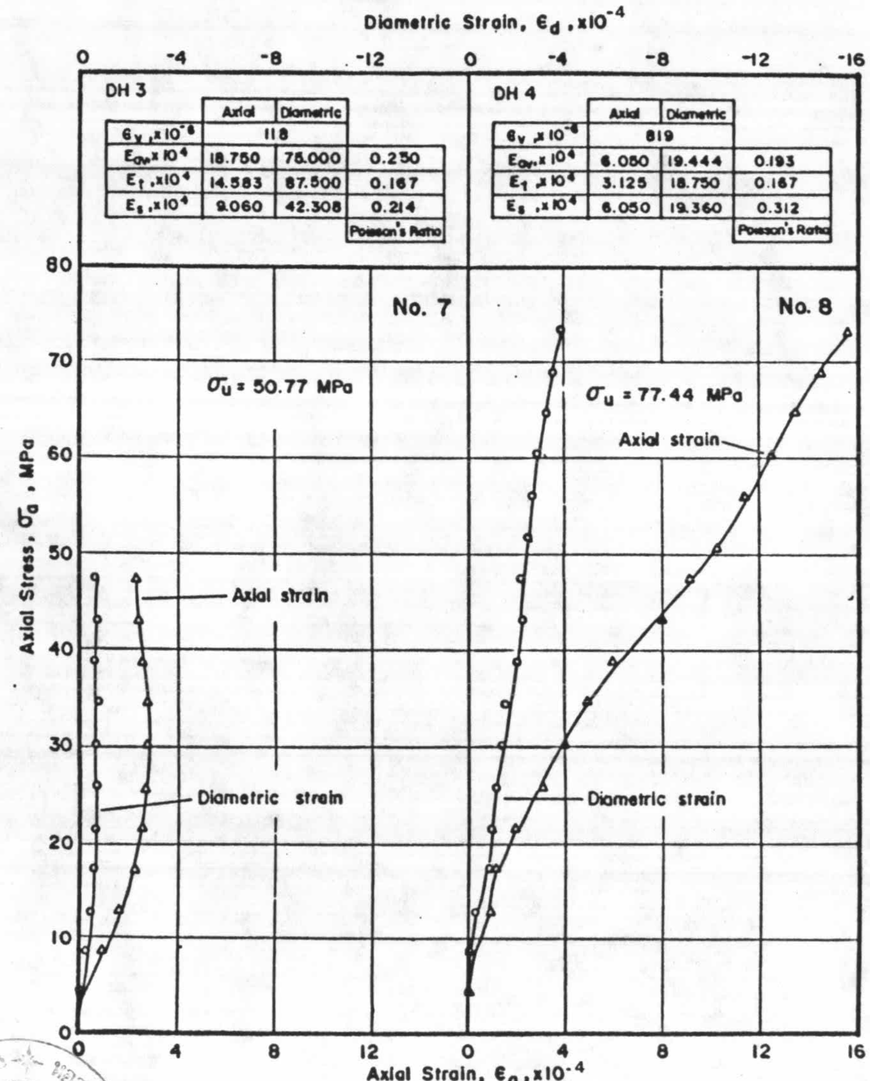

Diametric Strain, ϵ_d, x10^{-4}
Axial Stress, σ_a, MPa
Axial Strain, ϵ_a, x10^{-4}
DH 3
	Axial	Diametric	
ϵ_y, x10^{-6}	118		
E_{av}, x10^{4}	18.750	75.000	0.250
E_t, x10^{4}	14.583	87.500	0.167
E_s, x10^{4}	9.060	42.308	0.214
			Poisson's Ratio
DH 4
	Axial	Diametric	
ϵ_y, x10^{-6}	819		
E_{av}, x10^{4}	6.050	19.444	0.193
E_t, x10^{4}	3.125	18.750	0.167
E_s, x10^{4}	6.050	19.360	0.312
			Poisson's Ratio
No. 7
No. 8
σ_u = 50.77 MPa
σ_u = 77.44 MPa
Axial strain
Diametric strain
Axial strain
Diametric strain

Figure 4.5 cont.

Rock sample no. 9, borehole DH 4 with depth 21.71 - 22.13 m.

Rock sample no. 10, borehole DH 11 with depth 60.65 - 61.05 m.

Rock sample no. 11, borehole DH 5 with depth 14.90 - 15.40 m.

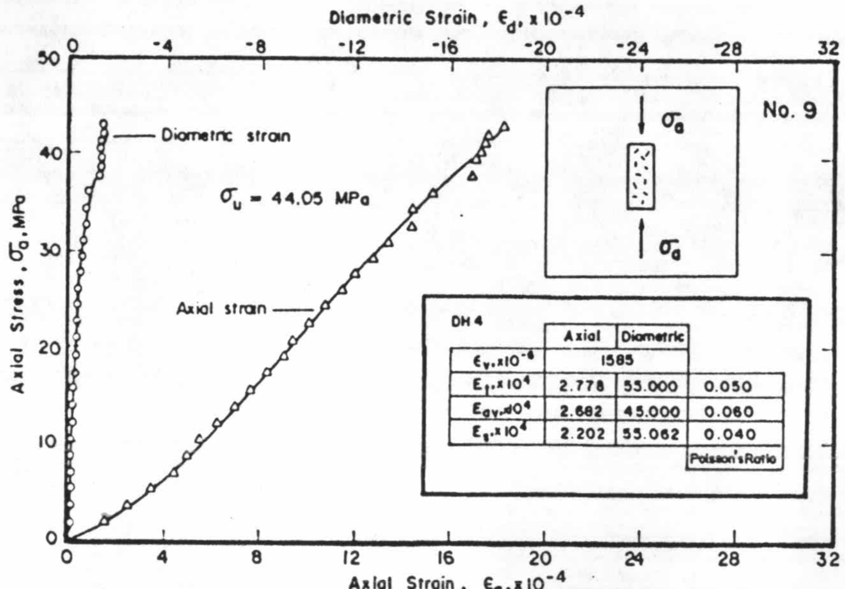
Diametric Strain, ϵ_d, x 10^{-4}
Axial Stress, σ_a, MPa
Axial Strain, ϵ_a, x 10^{-4}
No. 9
Diametric strain
Axial strain
σ_u = 44.05 MPa
σ_a
DH 4
Axial | Diametric
ϵ_v, x10^{-6} 1585
E_t, x10^4 2.778 55.000 0.050
E_{av}, x10^4 2.682 45.000 0.060
E_s, x10^4 2.202 55.062 0.040
Poisson's Ratio

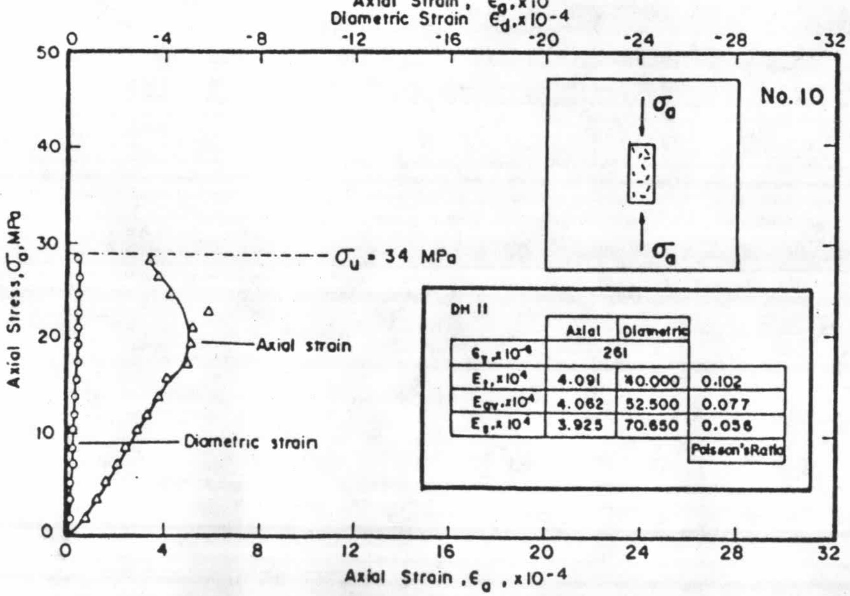
Diametric Strain, ϵ_d, x 10^{-4}
Axial Stress, σ_a, MPa
Axial Strain, ϵ_a, x 10^{-4}
No. 10
σ_u = 34 MPa
Axial strain
Diametric strain
σ_a
DH 11
Axial | Diametric
ϵ_v, x10^{-6} 261
E_t, x10^4 4.091 40.000 0.102
E_{av}, x10^4 4.062 52.500 0.077
E_s, x10^4 3.925 70.650 0.056
Poisson's Ratio

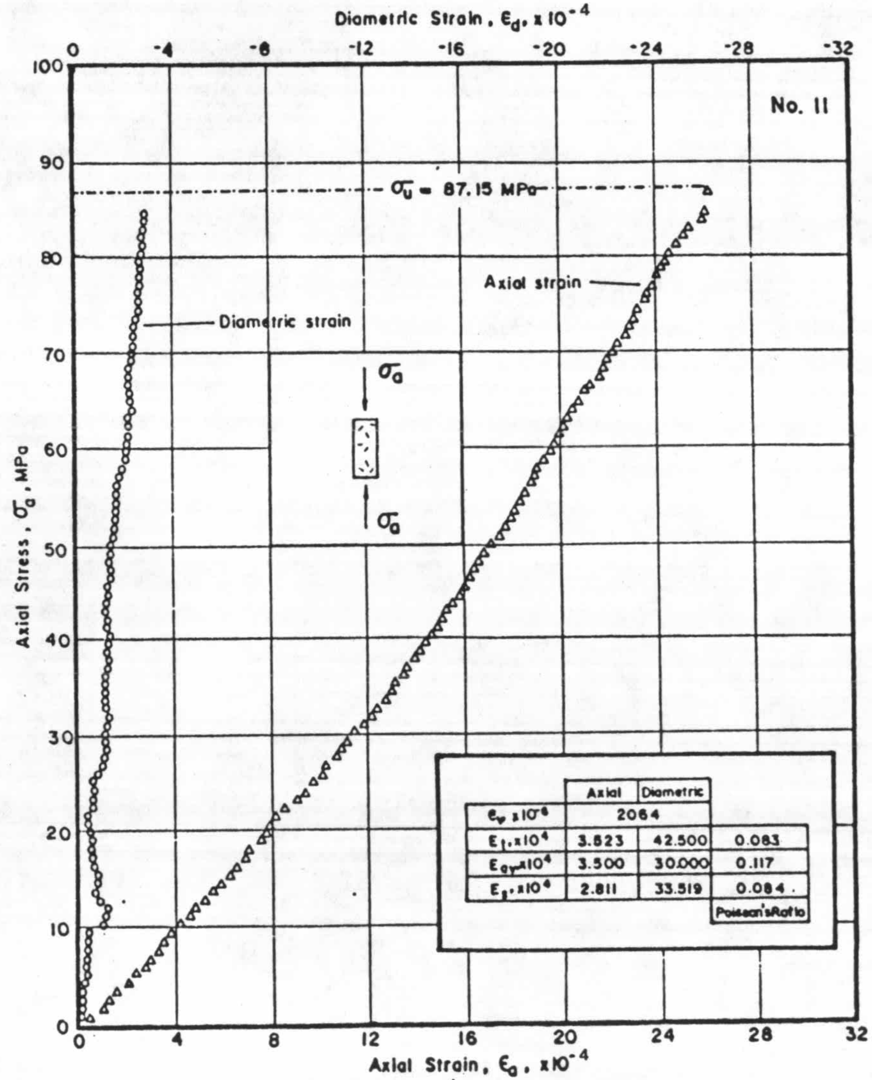
Diametric Strain, ϵ_d, x 10^{-4}
Axial Stress, σ_a, MPa
Axial Strain, ϵ_a, x10^{-4}
No. 11
σ_u = 87.15 MPa
Axial strain
Diametric strain
σ_a
Axial | Diametric
ϵ_v x10^{-6} 2064
E_t, x10^4 3.823 42.500 0.083
E_{av}, x10^4 3.500 30.000 0.117
E_s, x10^4 2.811 33.519 0.084
Poisson's Ratio

Figure 4.5 cont.

Rock sample no. 12, borehole DH 5 with depth 39.00 - 39.20 m.

Rock sample no. 13, borehole DH 5 with depth 58.40 - 58.63 m.

Rock sample no. 14, borehole DH 6 with depth 40.00 - 40.15 m.

Rock sample no. 15, borehole DH 7 with depth 43.64 - 43.78 m.

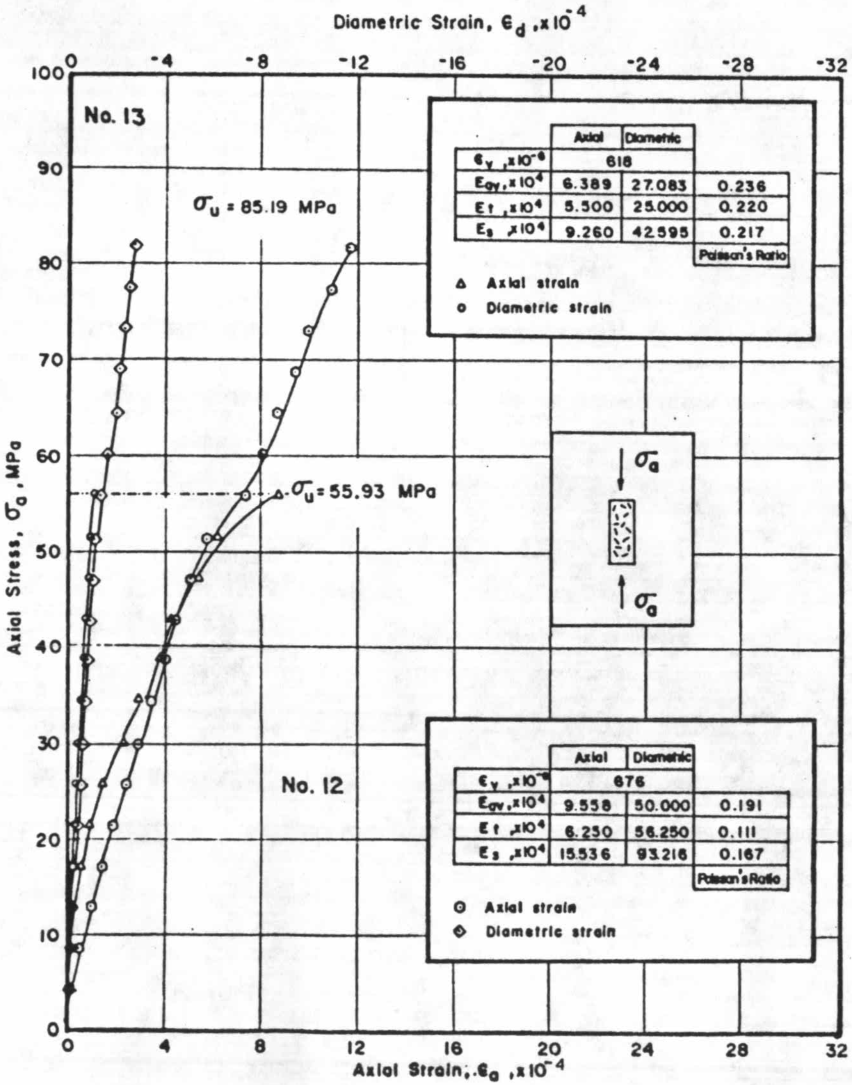
Diametric Strain, ϵ_d, x10^{-4}
Axial Stress, σ_a, MPa
Axial Strain, ϵ_a, x10^{-4}
No. 13
σ_u = 85.19 MPa
Axial | Diametric
ϵ_v, x10^{-6} | 618
E_{av}, x10^4 | 6.389 | 27.083 | 0.236
E_t, x10^4 | 5.500 | 25.000 | 0.220
E_s, x10^4 | 9.260 | 42.595 | 0.217
Poisson's Ratio
Δ Axial strain
o Diametric strain
σ_a
σ_a
σ_u = 55.93 MPa
No. 12
Axial | Diametric
ϵ_v, x10^{-6} | 676
E_{av}, x10^4 | 9.558 | 50.000 | 0.191
E_t, x10^4 | 6.250 | 56.250 | 0.111
E_s, x10^4 | 15.536 | 93.216 | 0.167
Poisson's Ratio
Axial strain
Diametric strain

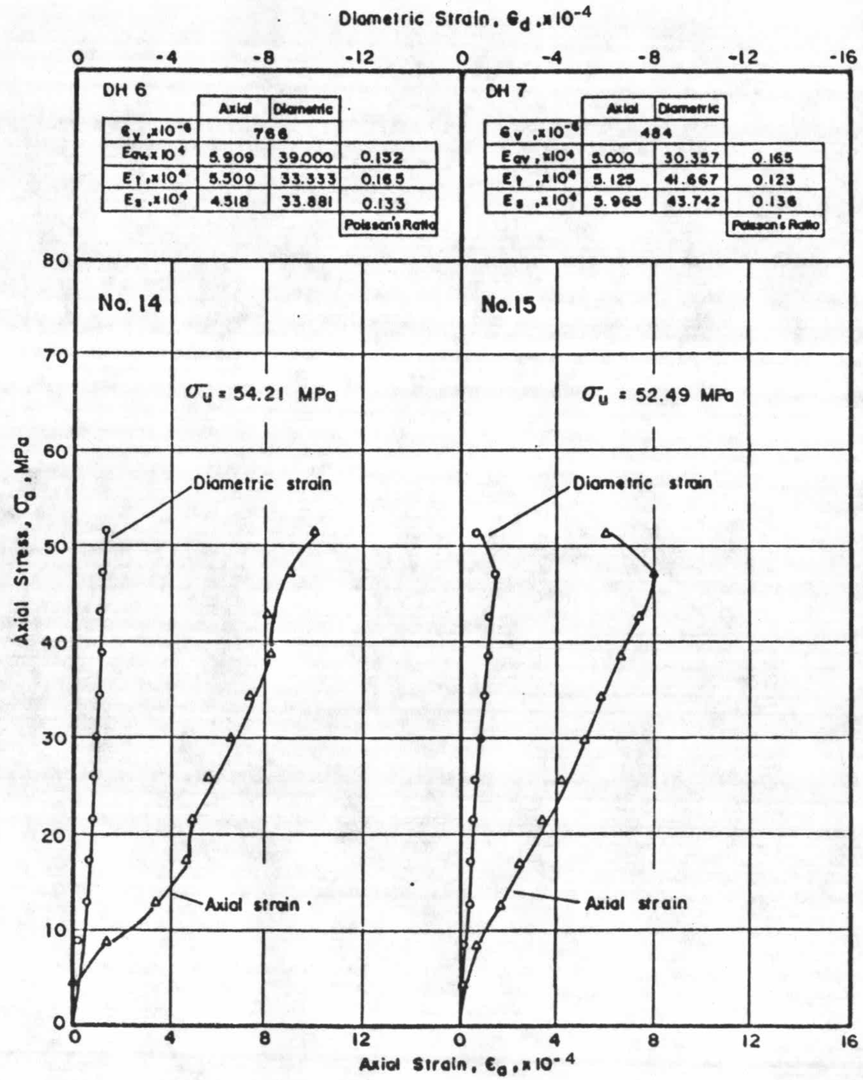
Diametric Strain, ϵ_d, x10^{-4}
Axial Stress, σ_a, MPa
Axial Strain, ϵ_a, x10^{-4}
DH 6
Axial | Diametric
ϵ_v, x10^{-6} | 766
E_{av}, x10^4 | 5.909 | 39.000 | 0.152
E_t, x10^4 | 5.500 | 33.333 | 0.165
E_s, x10^4 | 4.518 | 33.881 | 0.133
Poisson's Ratio
DH 7
Axial | Diametric
ϵ_v, x10^{-6} | 484
E_{av}, x10^4 | 5.000 | 30.357 | 0.165
E_t, x10^4 | 5.125 | 41.667 | 0.123
E_s, x10^4 | 5.965 | 43.742 | 0.136
Poisson's Ratio
No. 14
No. 15
σ_u = 54.21 MPa
σ_u = 52.49 MPa
Diametric strain
Diametric strain
Axial strain
Axial strain

Figure 4.5 cont.

Rock sample no. 16, borehole DH 7 with depth 42.00 - 42.34 m.

Rock sample no. 17, borehole DH 8 with depth 43.00 - 43.35 m.

(the first cyclic stress - strain).

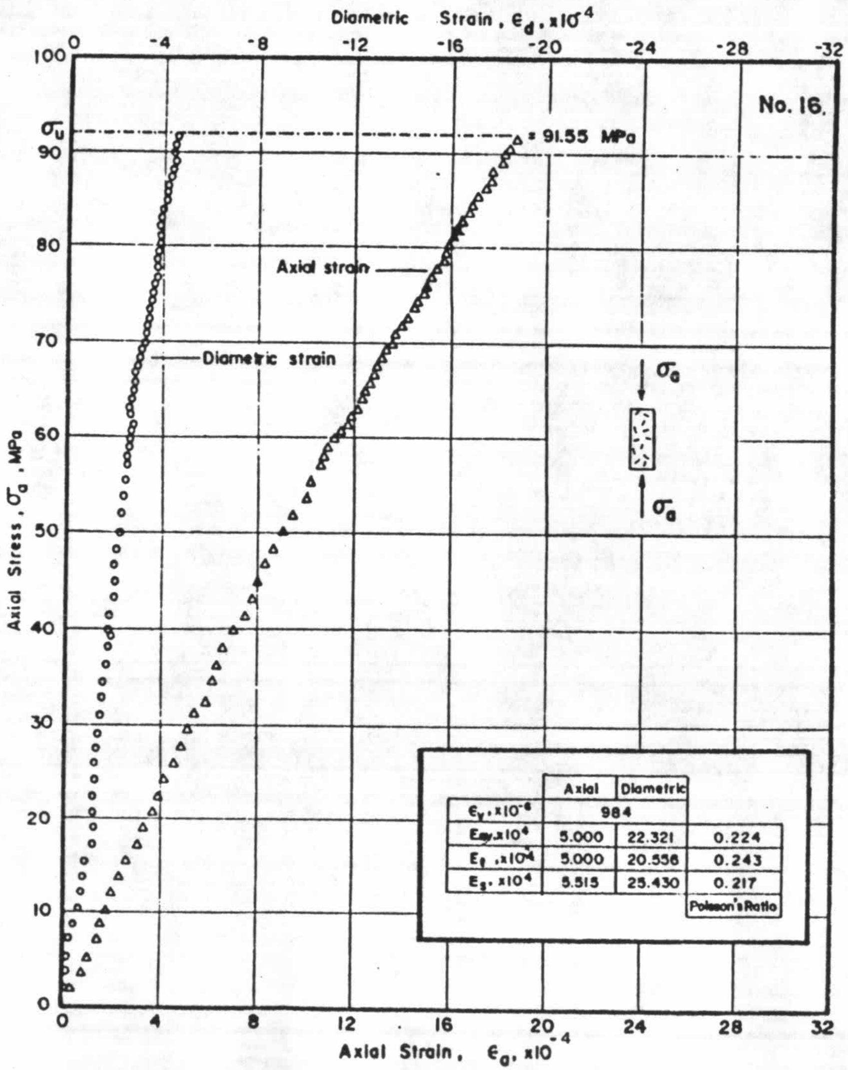
Diametric Strain, ϵ_d, x10^{-4}
No. 16.
σ_u = 91.55 MPa
Axial strain
Diametric strain
σ_a
Axial Stress, σ_a, MPa
Axial Strain, ϵ_a, x10^{-4}
Axial
Diametric
ϵ_v, x10^{-6} 984
E_{av}, x10^4 5.000 22.321 0.224
E_t, x10^4 5.000 20.556 0.243
E_s, x10^4 5.515 25.430 0.217
Poisson's Ratio

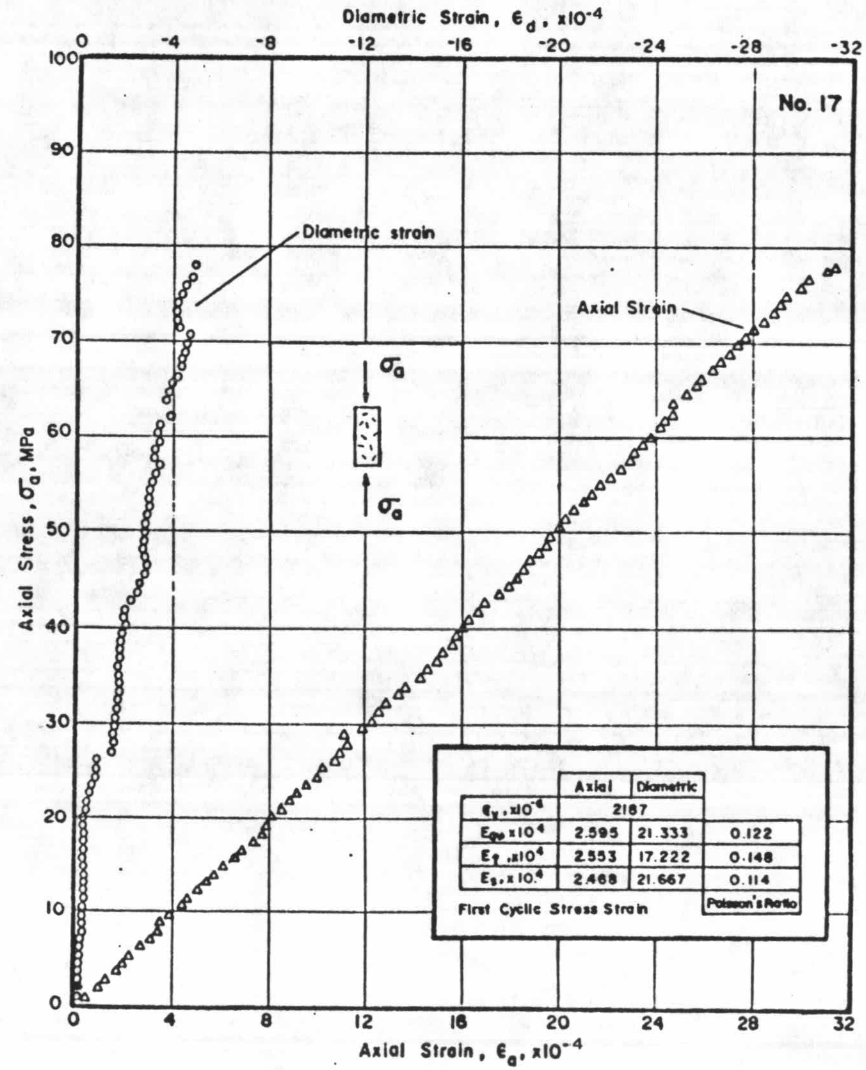
Diametric Strain, ϵ_d, x10^{-4}
No. 17
Diametric strain
Axial Strain
σ_a
Axial Stress, σ_a, MPa
Axial Strain, ϵ_a, x10^{-4}
Axial
Diametric
ϵ_v, x10^{-4} 2187
E_{av} x10^4 2.595 21.333 0.122
E_t, x10^4 2.553 17.222 0.148
E_s, x10^4 2.468 21.667 0.114
First Cyclic Stress Strain
Poisson's Ratio

Figure 4.5 cont.

Rock sample no. 17, borehole DH 8 with depth 43.00 - 43.35 (the second cyclic stress - strain).

Rock sample no. 18, borehole DH 9 with depth 49.65 - 49.80 m.

Rock sample no. 19, borehole DH 9 with depth 57.80 - 57.94 m.

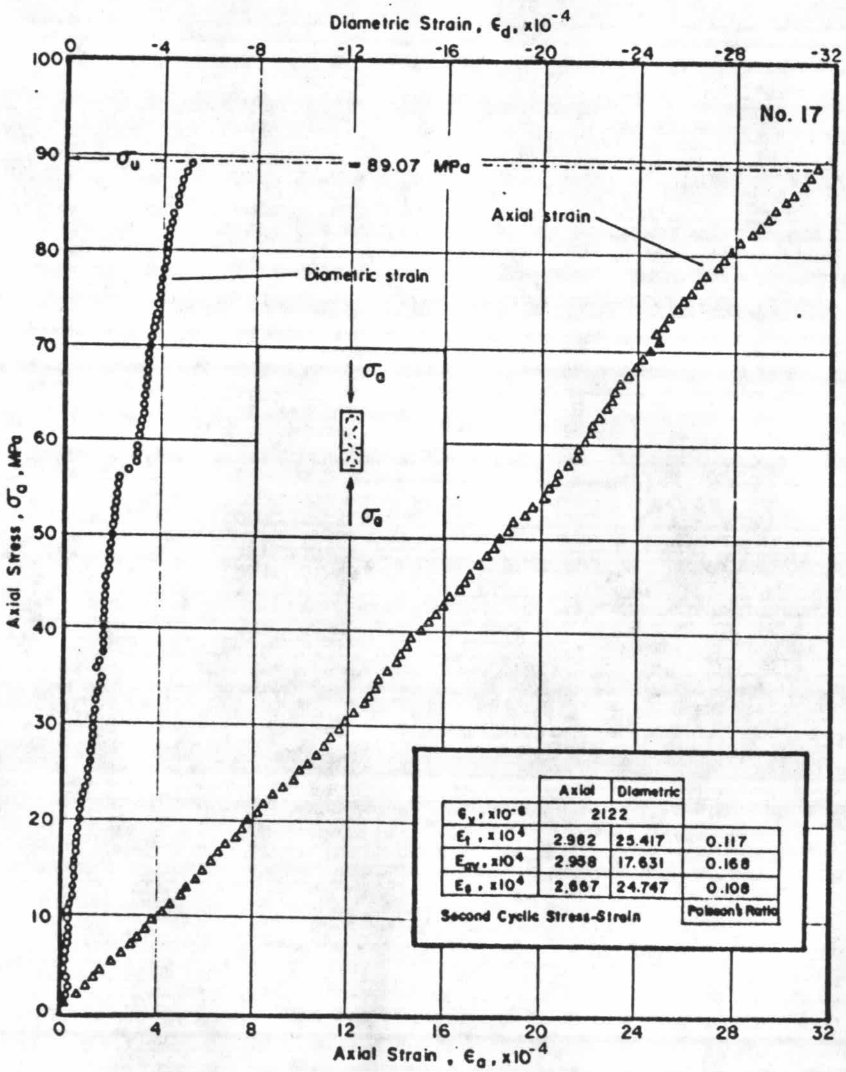
Diametric Strain, ϵ_d, x10^{-4}
Axial Strain, ϵ_a, x10^{-4}
Axial Stress, σ_a, MPa
No. 17
σ_u = 89.07 MPa
Axial strain
Diametric strain
σ_a
σ_a
	Axial	Diametric	
ϵ_v, x10^{-6}	2122		
E_t, x10^4	2.982	25.417	0.117
E_{av}, x10^4	2.958	17.631	0.168
E_s, x10^4	2.667	24.747	0.108
Second Cyclic Stress-Strain			Poisson's Ratio

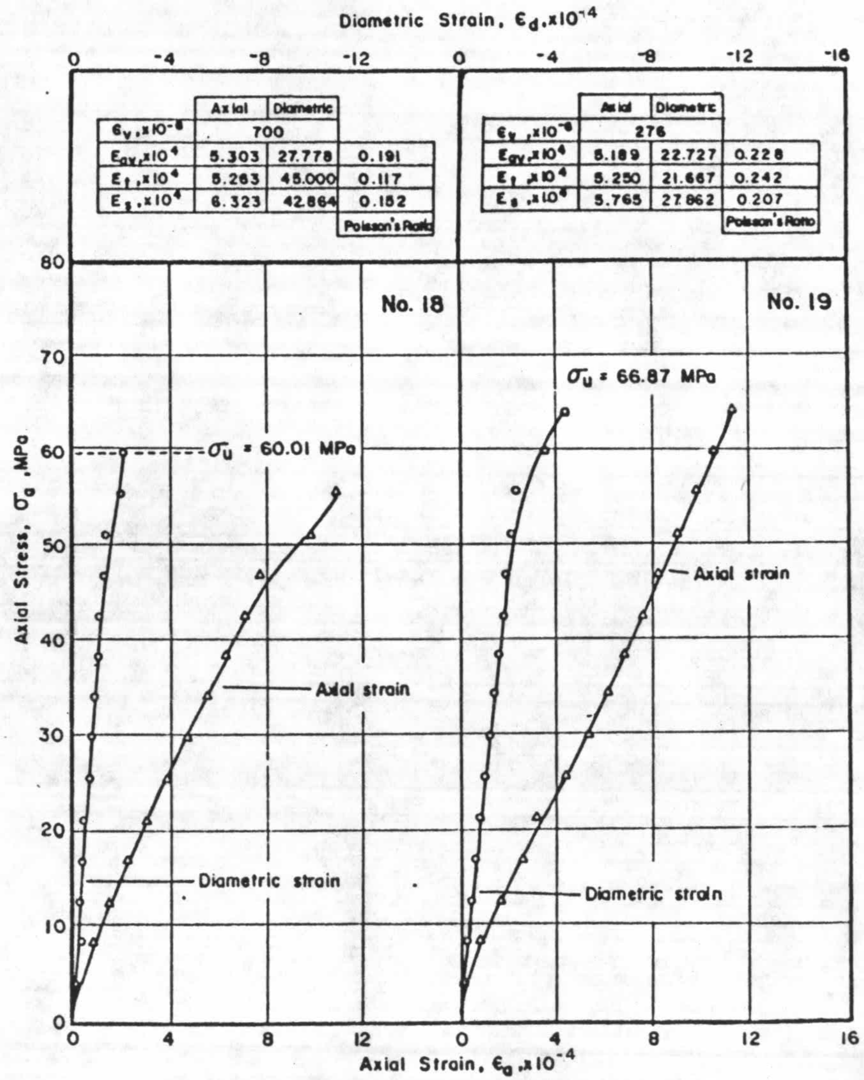
Diametric Strain, ϵ_d, x10^{-4}
Axial Strain, ϵ_a, x10^{-4}
Axial Stress, σ_a, MPa
	Axial	Diametric	
ϵ_v, x10^{-6}	700		
E_{av}, x10^4	5.303	27.778	0.191
E_t, x10^4	5.263	45.000	0.117
E_s, x10^4	6.323	42.864	0.152
			Poisson's Ratio

	Axial	Diametric	
ϵ_v, x10^{-6}	276		
E_{av}, x10^4	5.189	22.727	0.228
E_t, x10^4	5.250	21.667	0.242
E_s, x10^4	5.765	27.862	0.207
			Poisson's Ratio
No. 18
No. 19
σ_u = 60.01 MPa
σ_u = 66.87 MPa
Axial strain
Diametric strain
Axial strain
Diametric strain

Figure 4.5 cont.

Rock sample no. 20, borehole DH 9 with depth 25.50 - 25.88 m.

Rock sample no. 21, borehole DH 9 with depth 57.63 - 57.80 m.

Rock sample no. 22, borehole DH 13 with depth 59.05 - 59.53 m.

Rock sample no. 23, borehole DH 13 with depth 51.20 - 51.40 m.

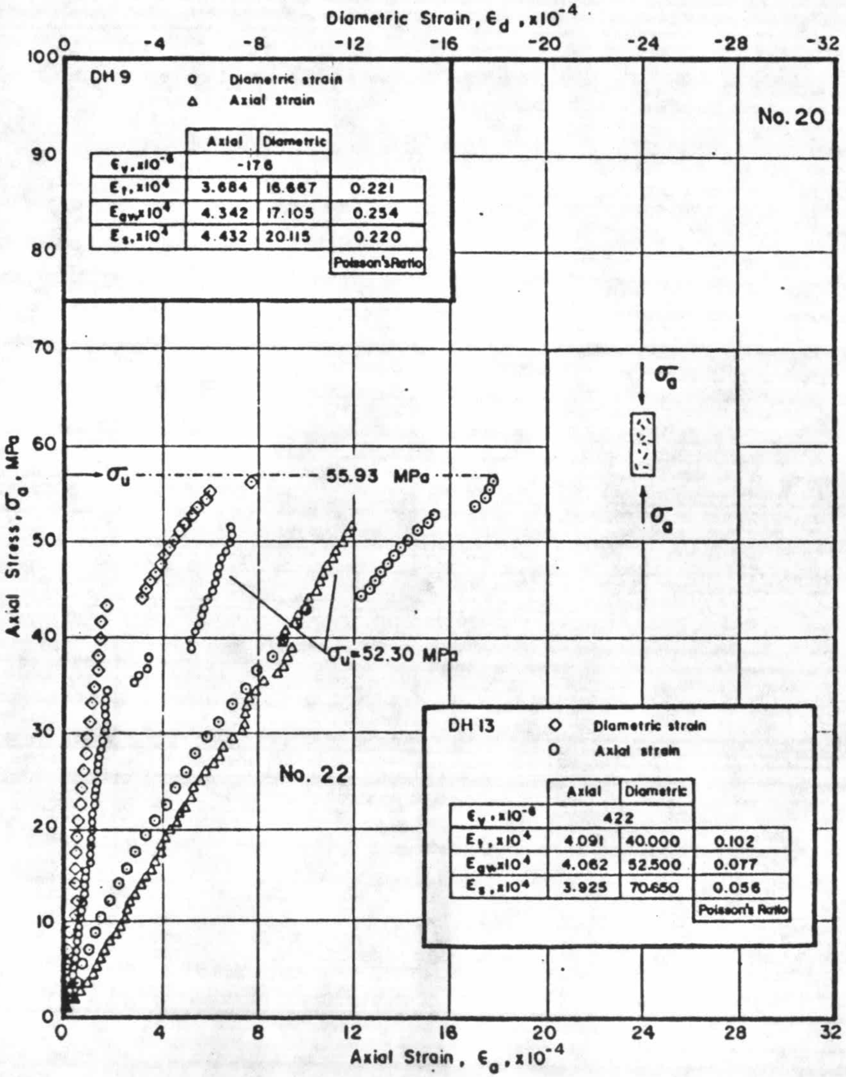
Diametric Strain, ϵ_d, x10^-4
DH 9
o Diametric strain
Δ Axial strain
Axial | Diametric
ϵ_v, x10^-6 | -176
E_t, x10^4 | 3.684 | 16.667 | 0.221
E_{av}, x10^4 | 4.342 | 17.105 | 0.254
E_s, x10^4 | 4.432 | 20.115 | 0.220
Poisson's Ratio
No. 20
σ_u — 55.93 MPa
σ_a
σ_u = 52.30 MPa
No. 22
DH 13
◇ Diametric strain
O Axial strain
Axial | Diametric
ϵ_v, x10^-6 | 422
E_t, x10^4 | 4.091 | 40.000 | 0.102
E_{av}, x10^4 | 4.062 | 52.500 | 0.077
E_s, x10^4 | 3.925 | 70.650 | 0.056
Poisson's Ratio
Axial Stress, σ_a, MPa
Axial Strain, ϵ_a, x10^-4

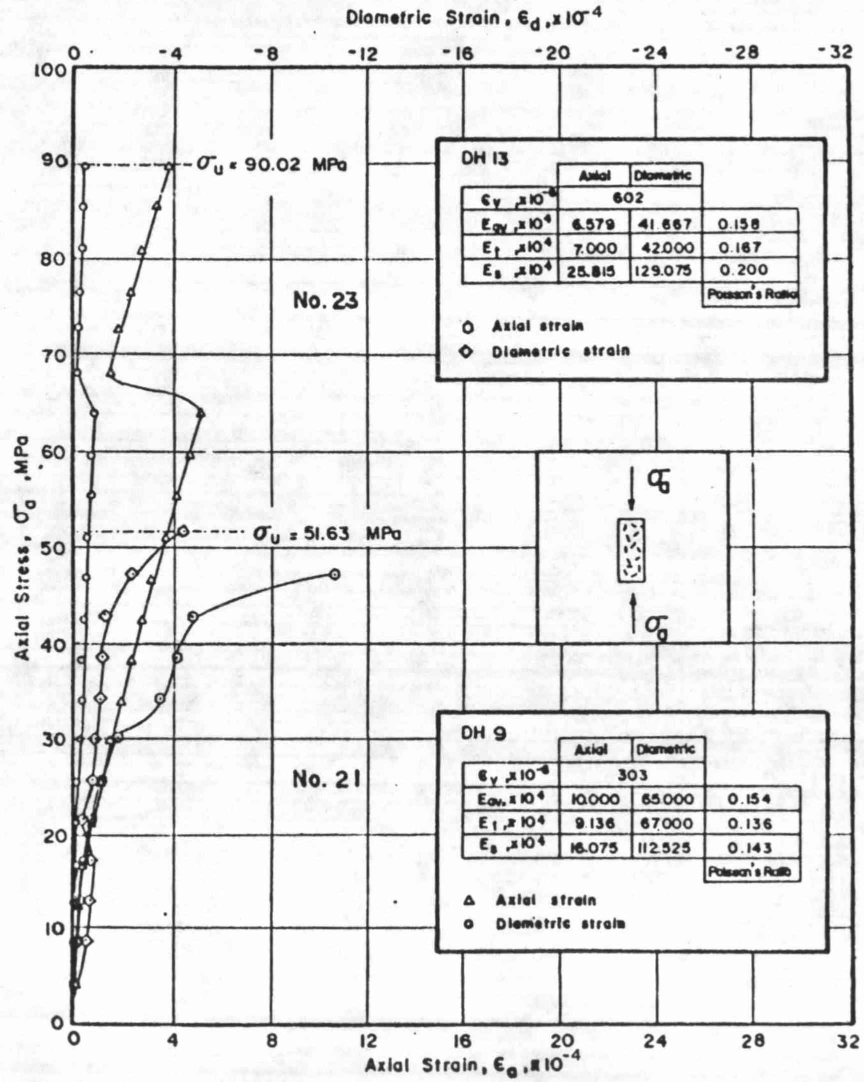
Diametric Strain, ϵ_d, x10^-4
σ_u = 90.02 MPa
DH 13
Axial | Diametric
ϵ_v, x10^-6 | 602
E_{av}, x10^4 | 6.579 | 41.667 | 0.158
E_t, x10^4 | 7.000 | 42.000 | 0.167
E_s, x10^4 | 25.815 | 129.075 | 0.200
Poisson's Ratio
O Axial strain
◇ Diametric strain
No. 23
σ_u = 51.63 MPa
σ_a
DH 9
Axial | Diametric
ϵ_v, x10^-6 | 303
E_{av}, x10^4 | 10.000 | 65.000 | 0.154
E_t, x10^4 | 9.136 | 67.000 | 0.136
E_s, x10^4 | 16.075 | 112.525 | 0.143
Poisson's Ratio
Δ Axial strain
o Diametric strain
No. 21
Axial Stress, σ_a, MPa
Axial Strain, ϵ_a, x10^-4

Figure 4.5 cont.

Rock sample no. 24, borehole NSP 1 with depth 4.540 - 45.80 m.

Rock sample no. 25, borehole NSP 2 with -epth 30.27 - 30.61 m.

Rock sample no. 26, borehole DD 2 with depth 32.00 - 32.20 m.

Rock sample no. 27, borehole DD 3 with depth 34.00 - 34.30 m.

Rock sample no. 34, borehole DD 25 with depth 15.43 - 15.73 m.

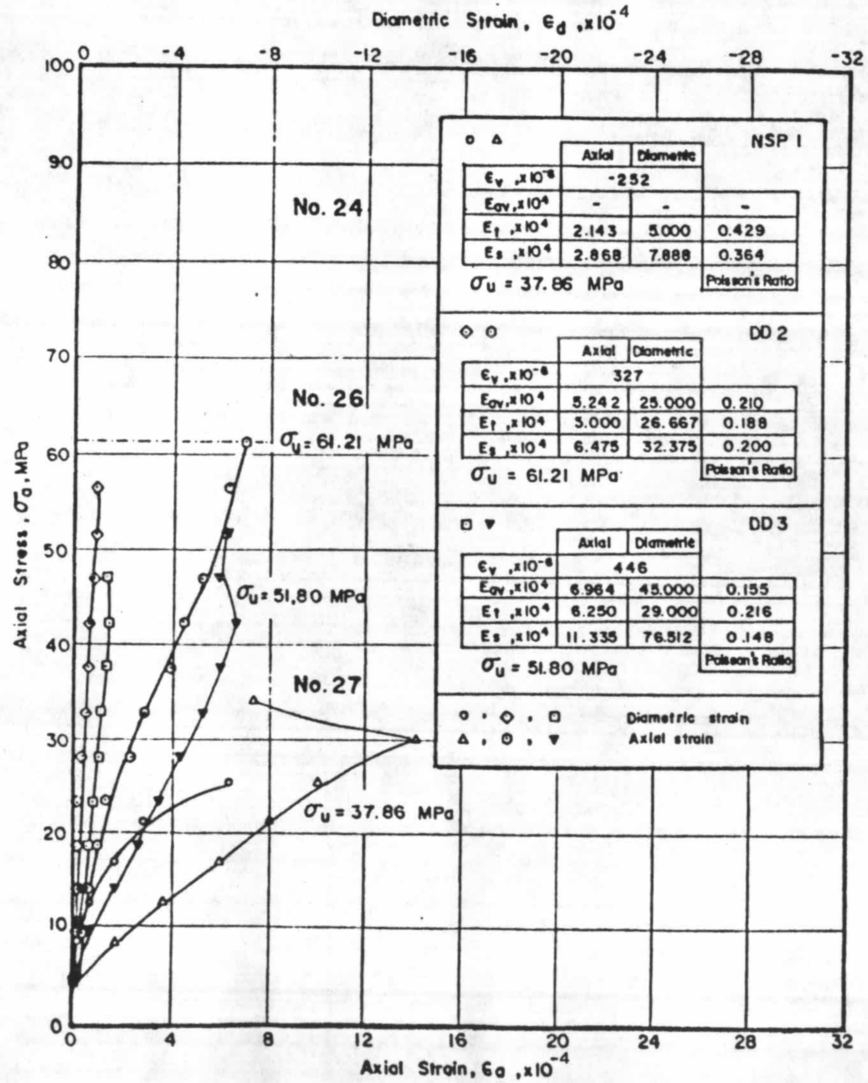
Diametric Strain, ϵ_d, x10^{-4}
Axial Stress, σ_a, MPa
Axial Strain, ϵ_a, x10^{-4}
No. 24
No. 26
No. 27
σ_u = 61.21 MPa
σ_u = 51.80 MPa
σ_u = 37.86 MPa
NSP 1
	Axial	Diametric	
ϵ_v, x10^{-6}	-252		
ϵ_{av}, x10^4	-	-	-
E_t, x10^4	2.143	5.000	0.429
E_s, x10^4	2.868	7.888	0.364
σ_u = 37.86 MPa
Poisson's Ratio
DD 2
	Axial	Diametric	
ϵ_v, x10^{-6}	327		
E_{av}, x10^4	5.242	25.000	0.210
E_t, x10^4	3.000	26.667	0.188
E_s, x10^4	6.475	32.375	0.200
σ_u = 61.21 MPa
Poisson's Ratio
DD 3
	Axial	Diametric	
ϵ_v, x10^{-6}	446		
E_{av}, x10^4	6.964	45.000	0.155
E_t, x10^4	6.250	29.000	0.216
E_s, x10^4	11.335	76.512	0.148
σ_u = 51.80 MPa
Poisson's Ratio
Diametric strain
Axial strain

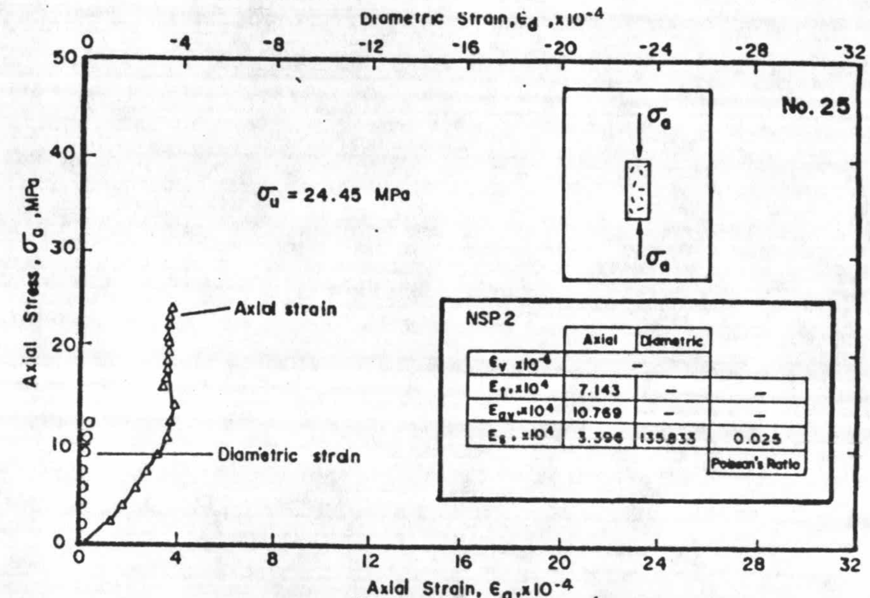
Diametric Strain, ϵ_d, x10^{-4}
No. 25
σ_a
σ_u = 24.45 MPa
Axial Stress, σ_a, MPa
Axial strain
Diametric strain
NSP 2
	Axial	Diametric	
ϵ_v x10^{-6}	–		
E_t, x10^4	7.143	–	–
E_{av}, x10^4	10.769	–	–
E_s, x10^4	3.396	135.833	0.025
Poisson's Ratio
Axial Strain, ϵ_a, x10^{-4}

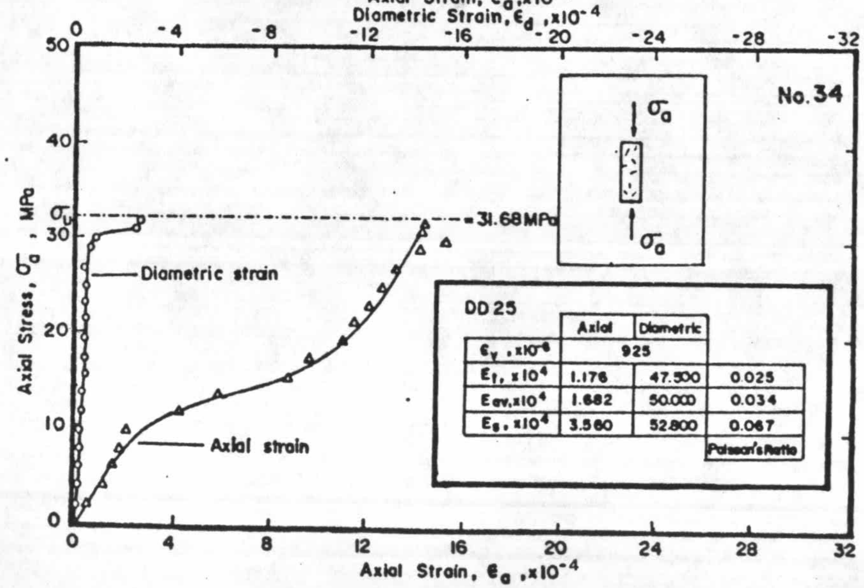
Diametric Strain, ϵ_d, x10^{-4}
No. 34
σ_a
σ_u
= 31.68 MPa
Axial Stress, σ_a, MPa
Diametric strain
Axial strain
DD 25
	Axial	Diametric	
ϵ_v, x10^{-6}	925		
E_t, x10^4	1.176	47.500	0.025
E_{av}, x10^4	1.682	50.000	0.034
E_s, x10^4	3.560	52.800	0.067
Poisson's Ratio
Axial Strain, ϵ_a, x10^{-4}

Figure 4.5 cont.

Rock sample no. 28, borehole DD 4 with depth 51.00 - 51.15 m.

Rock sample no. 29, borehole DD 20 with depth 9.00 - 9.34 m.

Rock sample no. 37, borehole DD 25 with depth 61.80 - 62.00 m.

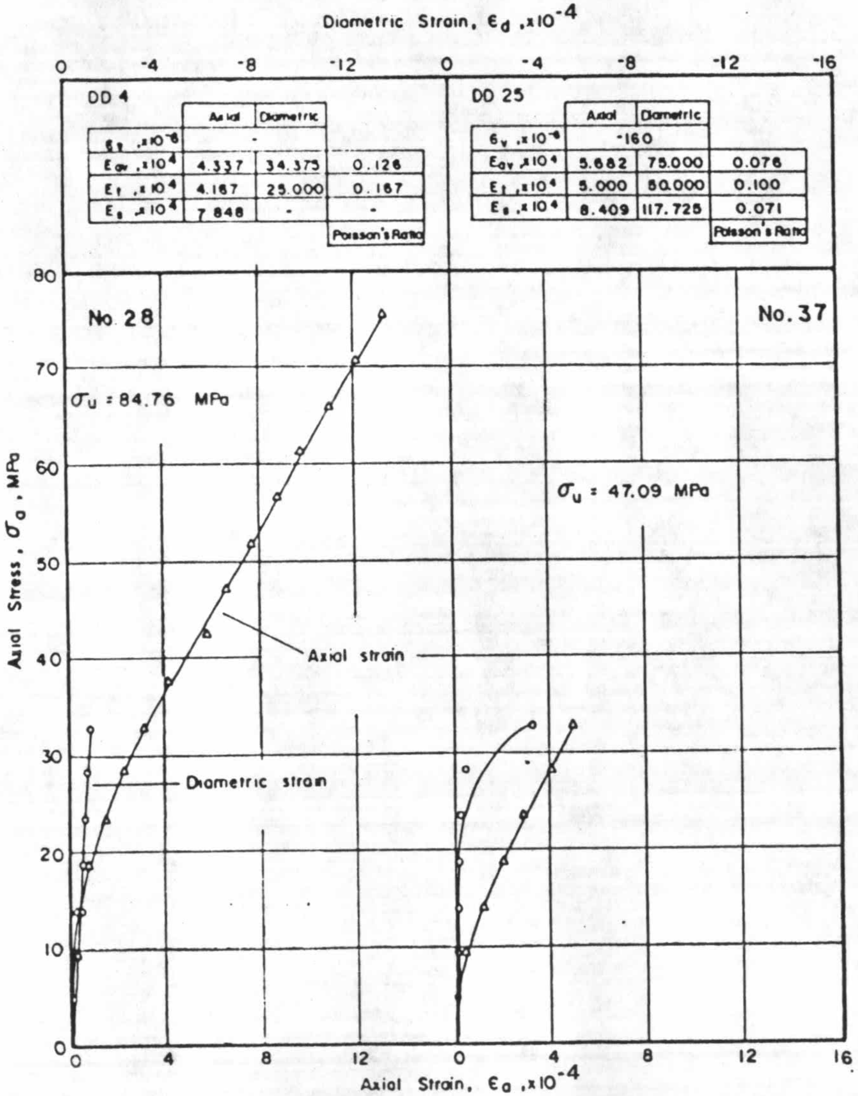

Diametric Strain, ϵ_d, x10^{-4}
DD 4
	Axial	Diametric	
ϵ_v, x10^{-6}	-		
E_{av}, x10^4	4.337	34.375	0.126
E_t, x10^4	4.167	25.000	0.167
E_s, x10^4	7.848	-	-
			Poisson's Ratio
DD 25
	Axial	Diametric	
ϵ_v, x10^{-6}	-160		
E_{av}, x10^4	5.682	75.000	0.076
E_t, x10^4	5.000	50.000	0.100
E_s, x10^4	8.409	117.725	0.071
			Poisson's Ratio
No. 28
σ_u = 84.76 MPa
No. 37
σ_u = 47.09 MPa
Axial strain
Diametric strain
Axial Stress, σ_a, MPa
Axial Strain, ϵ_a, x10^{-4}

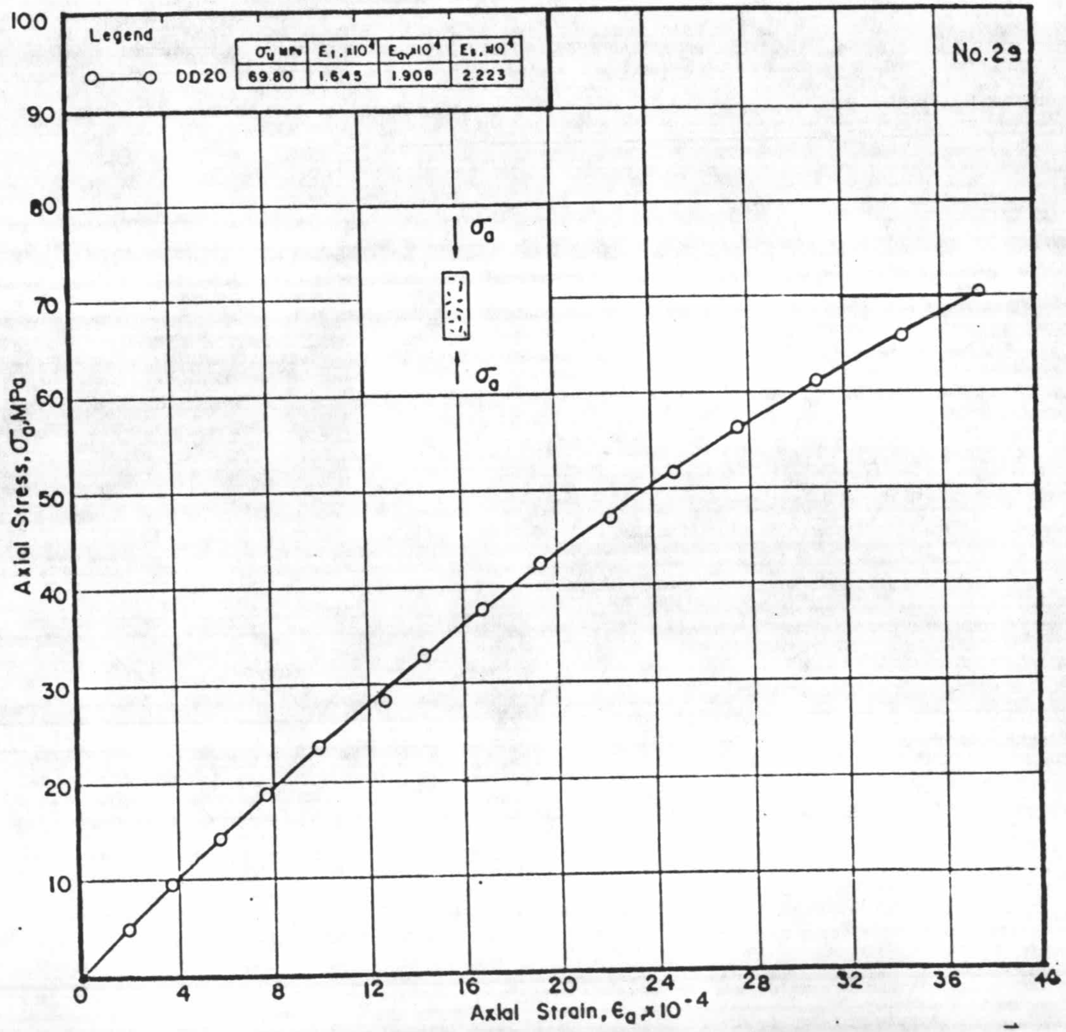

Legend
	σ_u MPa	E_t, x10^4	E_{av} x10^4	E_s, x10^4
DD20	69.80	1.645	1.908	2.223
No. 29
σ_a
σ_a
Axial Stress, σ_a, MPa
Axial Strain, ϵ_a x10^{-4}

Figure 4.5 cont.

Rock sample no. 30, borehole DD 22 with depth 30.25 - 30.53 m.

Rock sample no. 31, borehole DD 23 with depth 41.28 - 41.48 m.

Rock sample no. 32, borehole DD 24 with depth 43.00 - 43.34 m.

Rock sample no. 33, borehole DD 25 with depth 7.00 - 7.21 m.

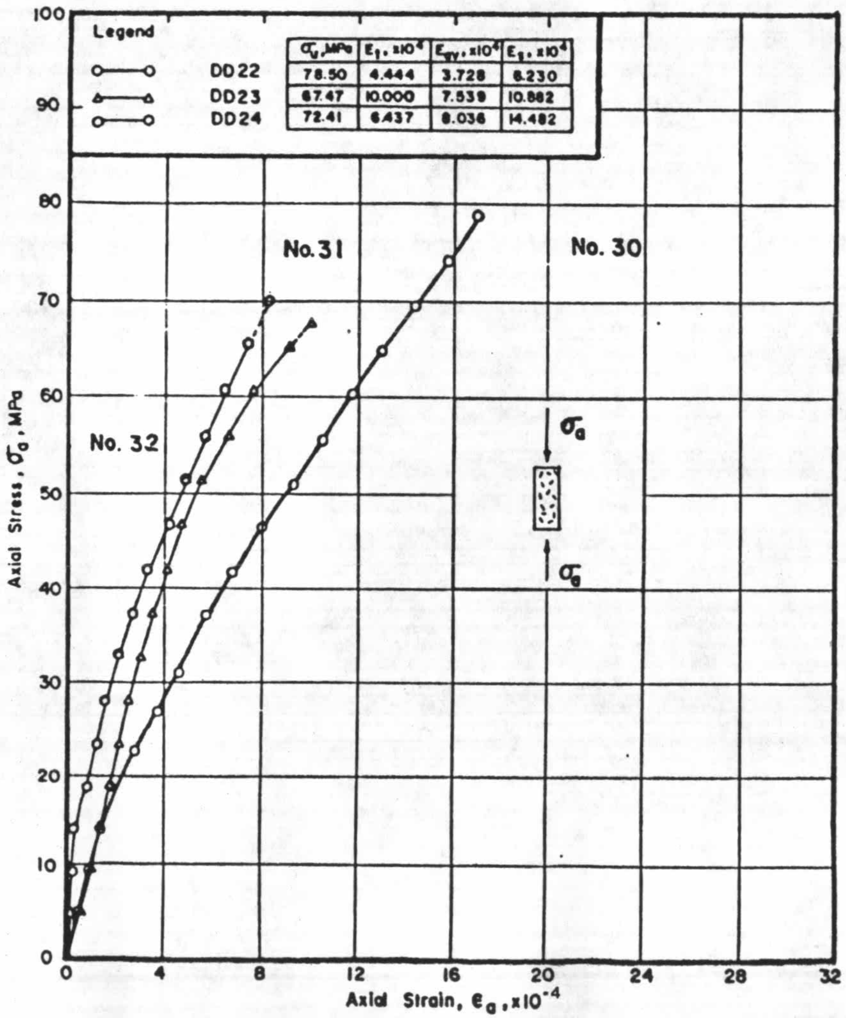

Legend
DD22
DD23
DD24
σu, MPa | E1, x10^4 | Eqy, x10^4 | Es, x10^4
78.50 | 4.444 | 3.728 | 6.230
67.47 | 10.000 | 7.539 | 10.882
72.41 | 6.437 | 8.036 | 14.482
No. 31
No. 30
No. 32
σa
σa
Axial Stress, σa, MPa
Axial Strain, εa, x10^-4
0
4
8
12
16
20
24
28
32
10
20
30
40
50
60
70
80
90
100

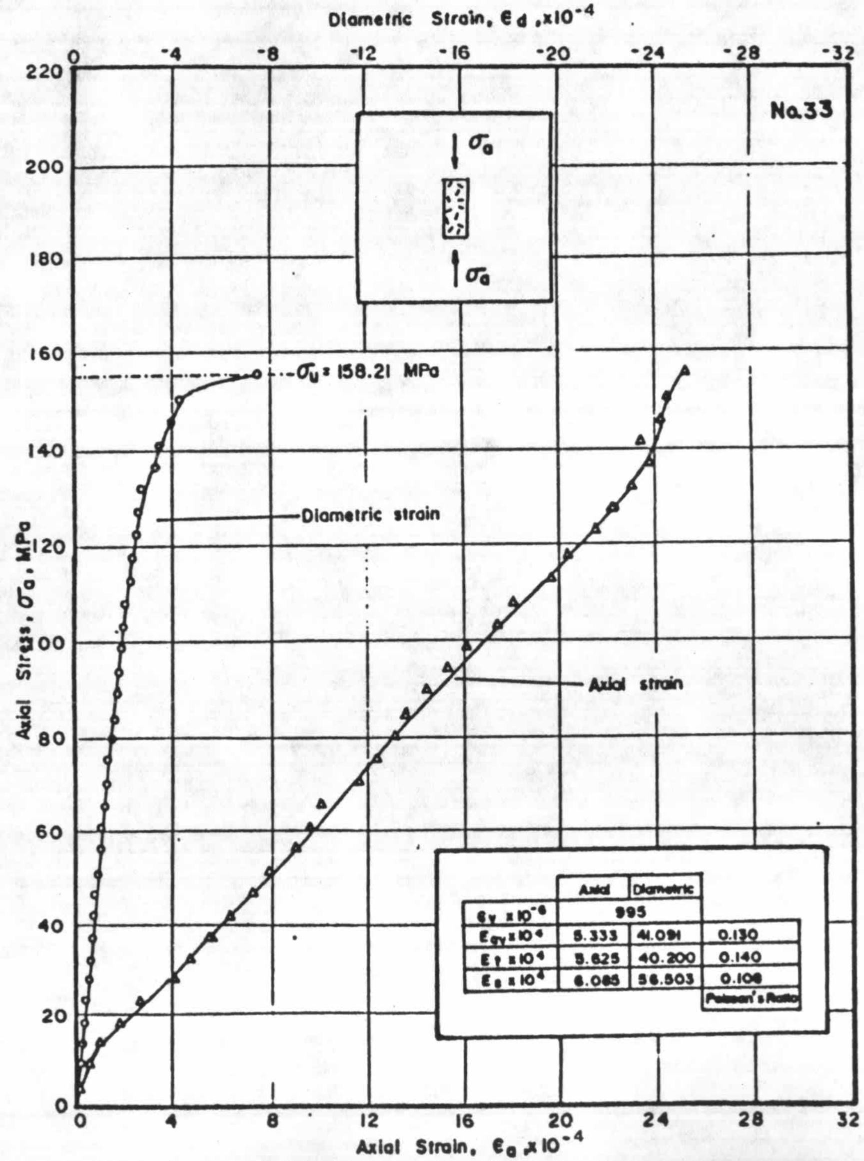

Diametric Strain, εd, x10^-4
0
-4
-8
-12
-16
-20
-24
-28
-32
No.33
σa
σa
σu = 158.21 MPa
Diametric strain
Axial strain
Axial Stress, σa, MPa
Axial Strain, εa, x10^-4
220
200
180
160
140
120
100
80
60
40
20
0
4
8
12
16
20
24
28
32
Axial | Diametric
εy x10^-6 | 995
Eqy x10^4 | 5.333 | 41.091 | 0.130
Et x10^4 | 5.625 | 40.200 | 0.140
Es x10^4 | 6.085 | 56.503 | 0.108
Poisson's Ratio

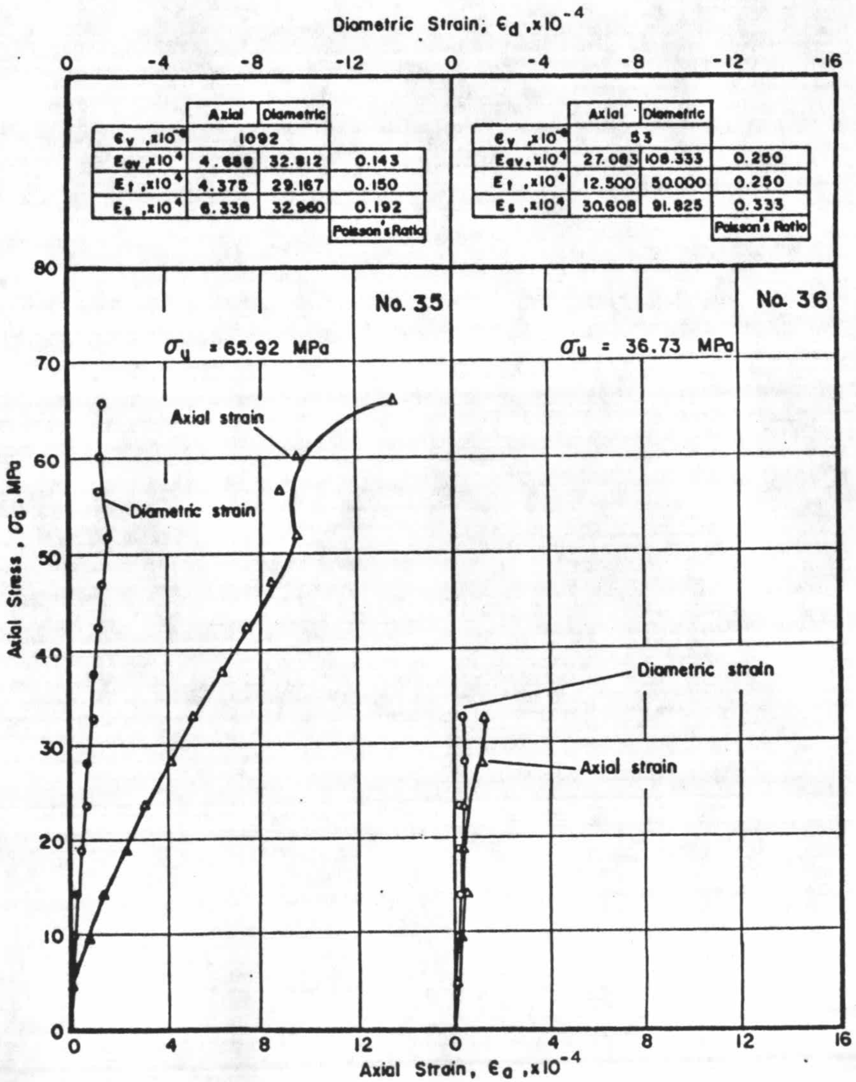

Figure 4.5 cont.
Rock sample no. 35, borehole DD 25, with depth 61.12 - 61.30 m.
Rock sample no. 36, borehole DD 25, with depth 64.06 - 64.26 m.

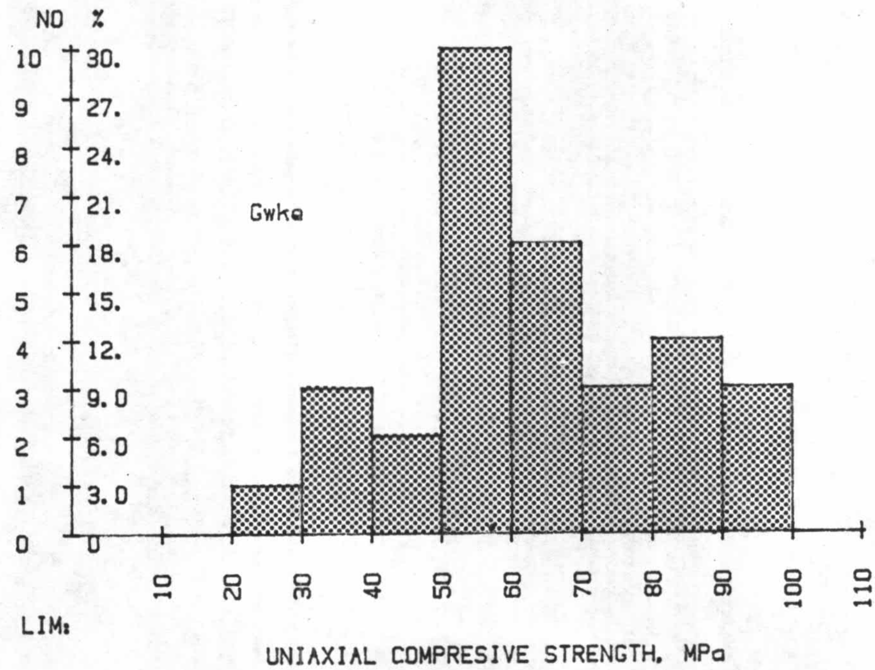

Figure 4.6 Histogram showing distribution of the uniaxial compressive strength values for pebbly graywacke specimens tested.

stress-strain curves behavior is seen in the test of specimens no. 3, 5, 6, 11, 16, 17, 18, 19, 20, 21, 27, 33 and 36.

(b) Type B (convex toward the stress axis)

This type of relationship is seen where there is pronounced strain with every increment in load. The value of the elasticity modulus is of the highest at the stages of the loading, but gradually decreases. Such a type a behavior is called as strain-softening behavior. These types of stress-strain curves are presented in specimen no. of 4, 13, 22, 24, 28, 29, 30, 31, 32, 35, and 37.

(c) Type C (convex towards the strain axis)

This type of stress-strain ecurves is occured where there is a decreasing strain with every increment in load. The value of the elasticity modulus is the lowest at the start of loading but continuosly increases. Such a behavior, termed as strain-hardening behavior, is illustrated in specimen no. 2, 7, and 10.

(d) Type D (convex variably towards the stress and strain axis)

This type of relationship depicts a variable stress strain curve for nonelastic material, as shown in specimen no. 1 8, 9, 12, 14, 15, 23, 25, 26 and 34.

The failure under this test along the discontinuities in the pebby graywacke core specimens was detected as illustrated in Figure 4.7. The results indicate that the different orientation of the discontinuities to the applied axial stress gives rise to variation in uniaxial compressive strength (Figure 4.8). Because only a few specimens failed by the effect of discontinuities and with a limitation of variation in the inclination, a conclusion can insufficient be made. However, it was observed that the uiti-mate compressive strength is at the minimum when the angle between the discontinuity and applied stress is in range of 0° - 20° and the strength becomes higher when the angle increases. The results incate a wide range of the strength values. This may be because of the effect of discontinuity condition such as separation, infilled material, etc. It should be noted that only one discontinuity is considered.

The discussions of these results can be more explained that the different orientation of the cleavage in the intact rocks to the direction of applied axial stress gives rise to variation in uniaxial compressive strength as illustrated in Figure 4.9. Depending on a small number of specimens tested and a limited variation of the cleavage orientation, an exact conclusion can not be made. However, it was always noticed that whenever the cleavage is making an angle of 20° - 30° to the direction of axial stress, the minimum value of the ultimate compressive strength resulted while a higher value is recieved when it makes an angle smaller than 20°. When the angle is greater than 30°, it is noted that the highest strength can be as much as three times its lowest strength, depending on the orientation of the cleavage to the direction of the applied load. The results presented in Figure 4.9 is a crude estimation from the scatter diagram. This dispersion may be because of the variation of the mineral compositions, micro-fabrics, micro-cracks, etc., in the different specimens of the same rock type.

There are three broad modes of failure observed in the compression test. The first, the catcclasis, consists of a general internal crumbling by formation of multiple cracks in the direction of the applied load. When the specimen collapses, conical end fragments are left, together with the long slivers of rock from around the periphery. The third is the shearing displacement in the test specimen along a single oblique plane.

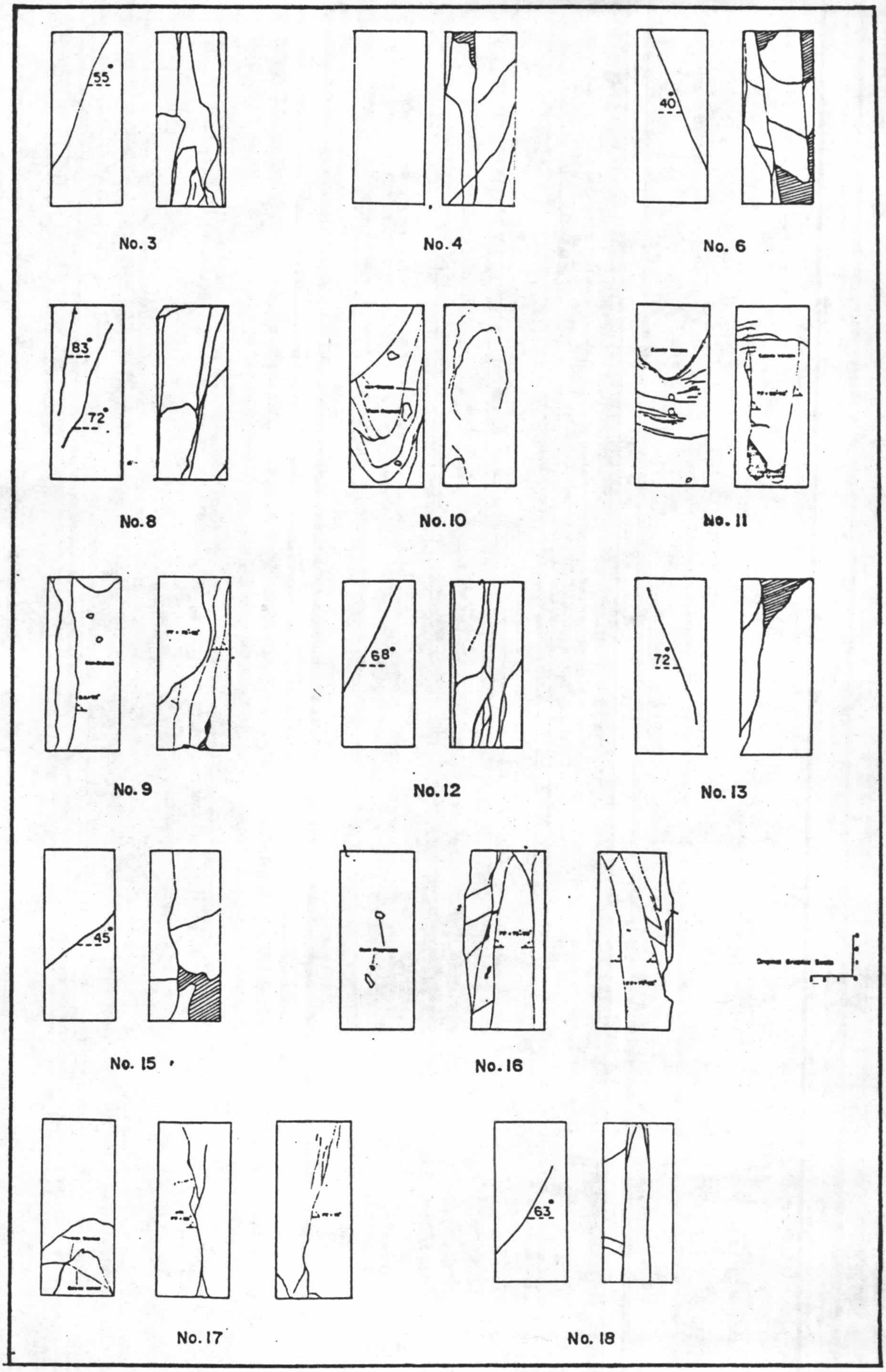

Figure 4.7 Sketch of typical main phase of failure of Chiew Larn pebbly graywackes core specimens under the uniaxial compression tests. Sample numbers are accnding to those in Fignre 4.5.

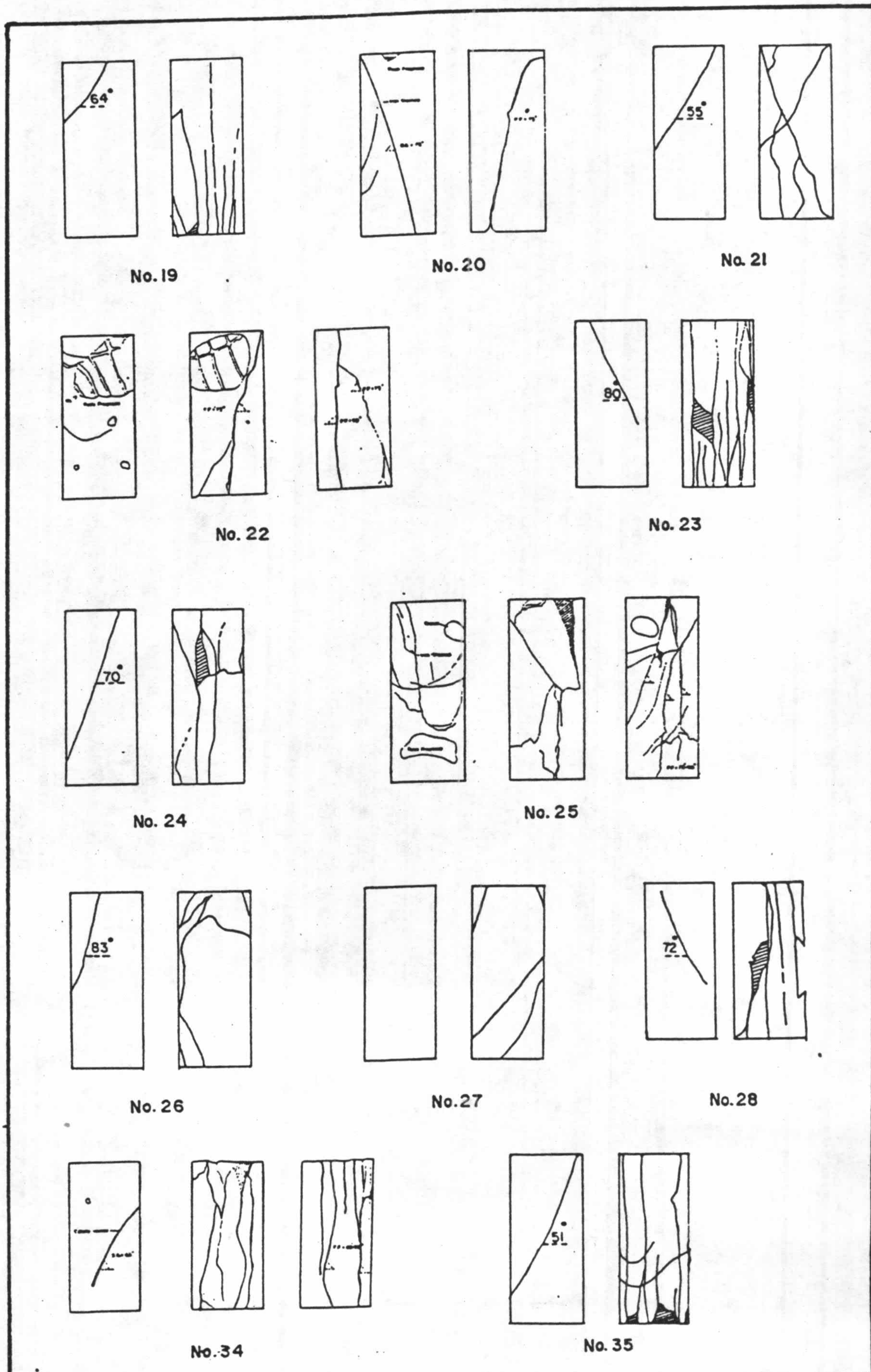

Figure 4.7 cont.

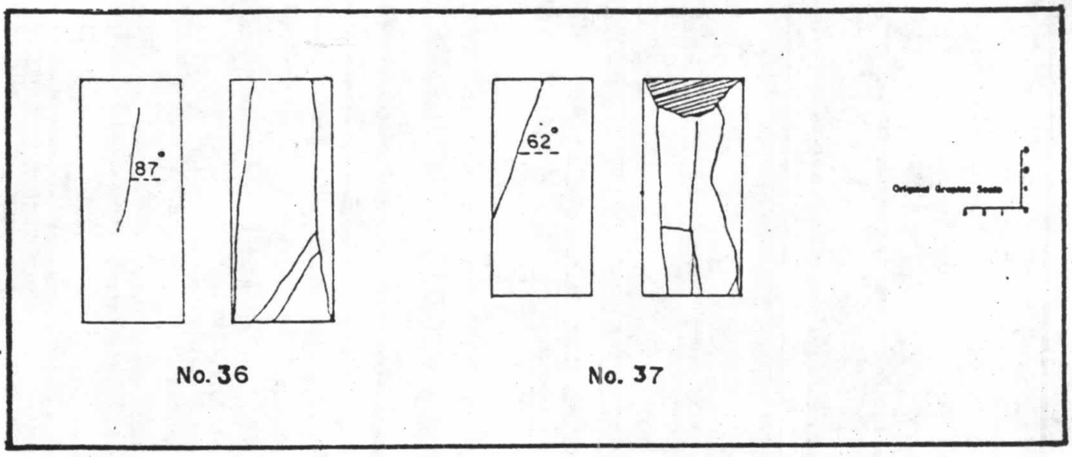

Figure 4.7 cont.

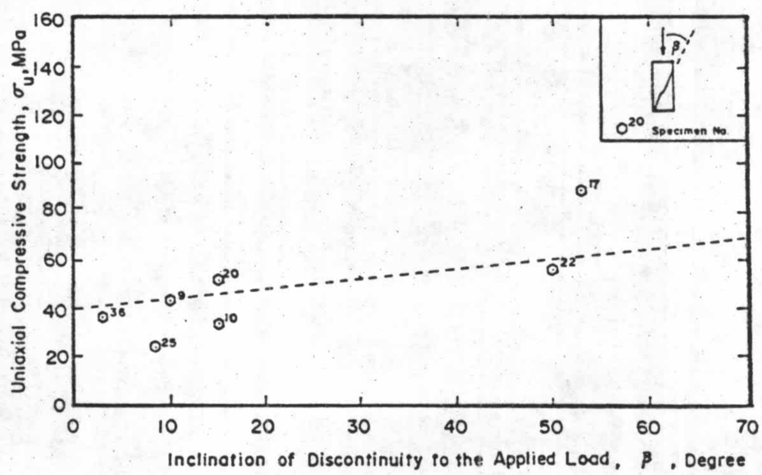

Figure 4.8 Uniaxial compressive strength versus inclination of discontinuity.

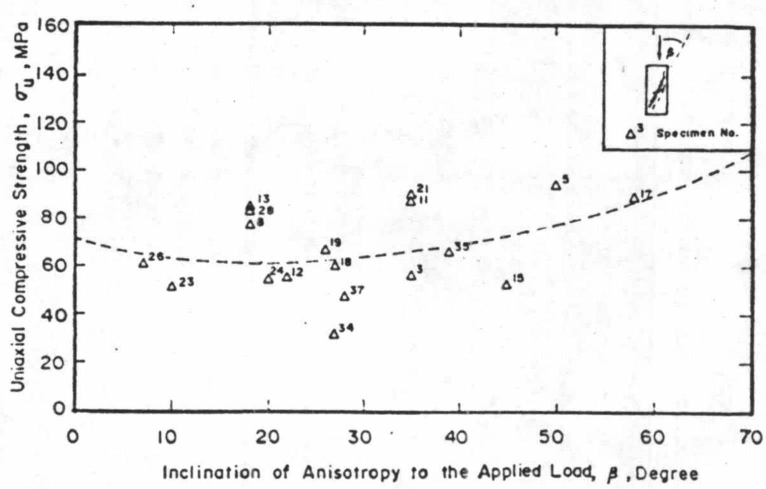

Figure 4.9 Uniaxial compressive strength versus inclination of anisotropy.

In some cases it is difficult to distinguish these different modes in a failed specimen, and occasionally all three appear together. The modes of failure of the Chiew Larn pebbly graywackes under the uniaxial compression test are illustrated in Figure 4.7.

4.4.2.2 Tensile Strength

The tensile strength of a material is defined as "the maximum tensile stress which a material is capable of developing"
(ASTM D 653-67, 1977). In Rock Mechanics, the knowledge about tensile strength of rocks is important for an analysis of the rock mass strength and stability of roofs and domes of underground opening in the tensile zone, for a design of the rock drilling and blasting programs, and possible for other endeavors in the rock engineering.

Rzhevoky and Novik (1971) and Jumikis (1979) stated that the tensile strength of a rock is much less than perhaps only about 10 percent. That is its compressive strength $\sigma_t = (0.10) . \sigma_c$

Roberts (1977) stated that the brittle failure theory predicted a ratio of compressive strength to tensile strength to be about 8 to 1. The critical evaluation of the test for the tensile strength can be noted in the works of Obert et al. (1946), Fairhhurst (1961), Grosvenor (1961), Brace (1963), Belikov et al. (1964), Hawkes and Mellor (1970), Barla and Goffi (1974).

The test performed in the pressent study provides a simple mean of estimating the uniaxial tensile strength and is of great interest in connection with the failure of rock under the quitecomplicated stresses. In the Brazilian test, a cylindrical testspecimen is placed on its side between the bearing plates of a testing machine and loaded to failure by a compression. In such configuration, the horizontal stresses perpendicular to the loaded diameter are uniform and the tensile stress is with a magnitude

$$\sigma_t = 2P/\pi Dt = 0.636\ P/Dt \qquad \ldots\ldots\ldots (4.27)$$

where P = compression load at failure, in Newton

D = cylinder specimen diameter, in mm

t = thickness of the test specimen, in mm

The method given by ISRM (1981) was used for this study. The load-plates touch the side of a disc-shaped rock specimen at the opposite ends of a diametric line. The diameter of the specimen was measured in the loading direction at the mid-length and at both ends of the specimen, then a the average value was taken from these measurements. The thickness (axial length) of the specimen was obtained by averaging the measurements taken along the lines of contact with the two plates of the loading machine. These measurements were done using a vernier caliper to the nearest 0.1 mm. After placing the specimen in between the plates, the specimen was centered and the spherical seat formed by a half-ball bearing at the center of the top surface of the upper plate was aligned with the half-ball bearing fixed to the botton of the proving ring attached to the Leonard Farnell (England) Compression Machine. The load was then applied through the spherical seat by controlling the loading rate as 0.5 $kg/cm^2/sec$. The bearing load at failures was record and the time duration of the test measured by a stop watch.

This procedure was adopted for all the test specimens. The tensile strength of the rock was calculated according to the equation 4.27 and was sunnarized in Table 4.16. Figure 4.10 show the histograms of a number of pebbly graywacke and subarkose specimens tested.

The tensile strength can also be obtained in a pointload test. Its originator, Reichmuth (1963), described that the point - load test is a measure of tensile strength of rock obtained by an indirect method. The point-load tensile strength test, so widely used as a laboratory and field tool that been developed by Professor John Franklin, gives a rapid and accurate strength index in the harder rocks The conducted experimental studies in detail were done by McWilliams (1966), Hiromatsu and Oka (1966), Reichmuth (1968), Franklin (1970), Franklin et al. (1971), Broch and Franklin (1972), Guidicini et al. (1973), Beiniawski (1974, 1975), Brook (1977, 1980), Peng (1980), and Greminger (1982). These investigators had pointed out that the following factors mainly affected the point-load strength of rocks. They are the size of the test specimen, shape of specimens, ratio of length-to-diameter (L/D ratio), water content, etc.

A further study of the scale effect in a point-load testing had been conducted by Greminger (1982), who proposed the correction

Table 4.16 Summary of Brazilian tests results

Core Specimen		Ranging Value	W %	Sr %	D/t	Ultimate Load $\times 10^3$ N.	Apparent Tensile Strength Mpa
Rock Type	No. of Tests						
Sark	12	Minimum	0.09	-	1.94	20.97	10.28
		average	0.39 $\pm$ 0.11	-	2.03 $\pm$ 0.08	28.32 $\pm$ 7.26	17.48 $\pm$ 7.52
		maximum	0.60	-	2.25	66.95	29.65
Gwke	96	minimum	0.04	0.24	1.76	6.49	2.79
		average	0.41 $\pm$ 0.28	0.83 $\pm$ 0.52	2.03 $\pm$ 0.14	23.65 $\pm$ 7.27	10.46 $\pm$ 2.95
		maximum	1.73	2,27	2.63	39.68	17.34

Note : Gwke = pebbly graywackes to pebbly mudstones

Sark = subarkosic sandstones

a)

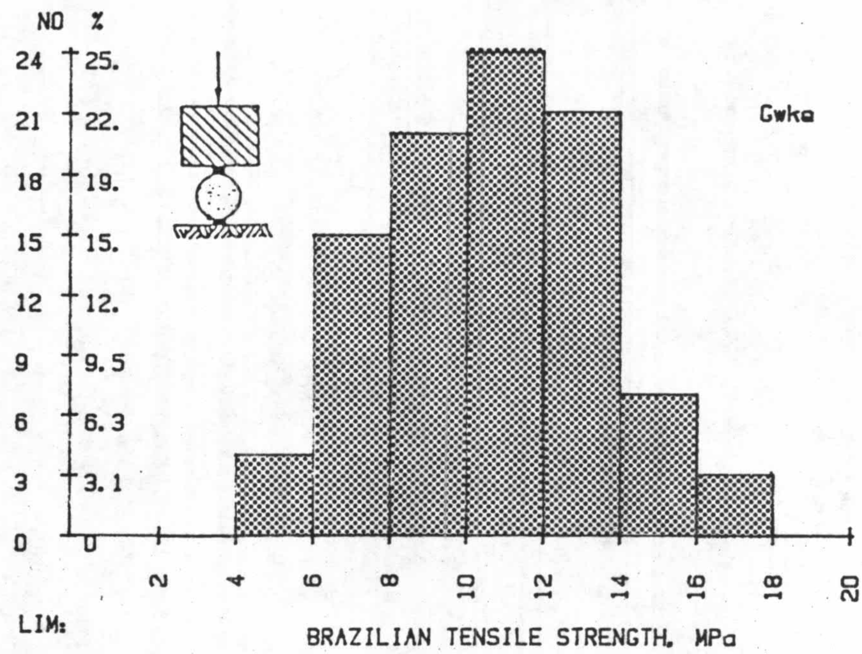

b)

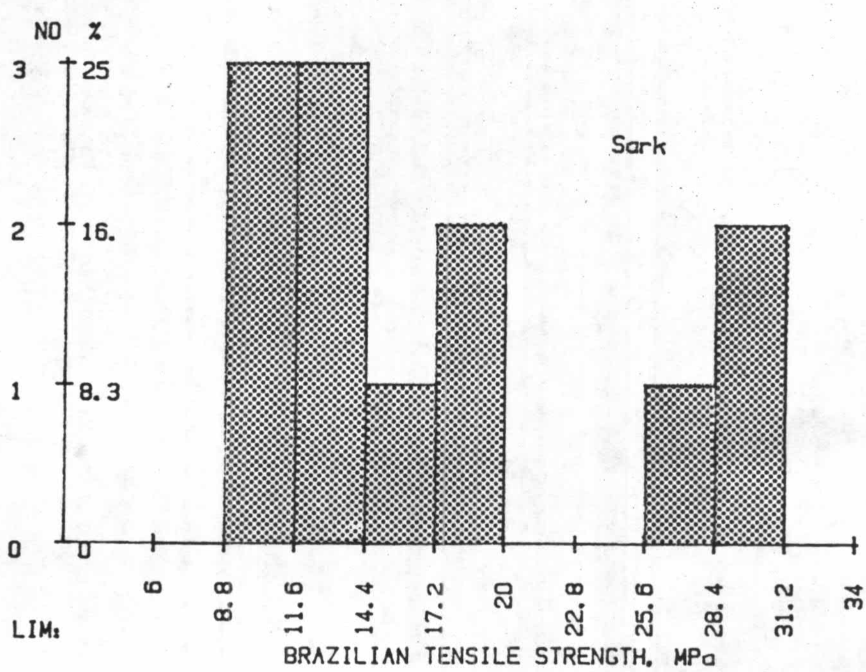

Figure 4.10 Histogram of a) pebbly graywackes and b) subarkosic sandstones specimens tested for the Brazilian tensile tests.

formulae for the different sample size and shape. His correction formulae are for three simple cases of the test specimens with a circular, elliptical and rectangular cross-section while the mormalizing diameter used is always 50 mm.

(a) for circular section specimen

$$Is\ (50) = P/\ (D^{1.5}.D^{*0.5}) \qquad \text{..........(4.28)}$$

(b) for elliptical section specimen

$$Is\ (50) = P/\ (D.L)^{0.75}.D^{*0.5} \qquad \text{.........(4.29)}$$

(c) for rectangular section specimen

$$Is\ (50) = 0.834\ P/\ (D.L)^{0.75}.D^{*0.5} \text{ .....(4.30)}$$

where Is (50) = point-load strength reference-index

D* = core of 50 mm diameter

D = diameter of width of specimen

L = length of specimen

ISRM (1973) and Greminger (1982) defined the strength anisotropy index (Ia) as the ratio of point-load strength in the strongest and weakest direction. The index works as a quantitative measure for the anisotropy of point-load strength.

$$Ia\ (50) = \frac{Is\ (50)\ \text{perpendicular to plane of weakness}}{Is\ (50)\ \text{parallel to plane weakness}} \qquad \text{.... (4.31)}$$

D'Andrea et al. (1965), Franklin et al. (1971), and Broch and Franklin (1972) had shown that the empirical relation between the uniaxial compressive strength and the point-load strength reference-index examined for the anisotropic rocks, is

$$\sigma_c = 24.Is\ (50) \qquad \text{.............. (4.32)}$$

Their result had been confirmed later by ISRM (1973), Bieniawski (1975), and Brook (1977, 1980) but none of these investigators took the strength anisotropy into a consideration. Pells (1975) and Greminger (1982) compared the measured values of the compressive strength of respectively twelve and four rock types, concurrently with those predicted by Equation 4.32 that the relationship between the uniaxial compressive strength and point-load strength is the most significant.

The method used for the point-load strength index determination in the present study follows ISRM's (1972) method. The specimens in the form of Nx cores with a height-to-diameter ratio of 1.5 and 1.1 were used for the diametrical point-load test and axial point-load test respectively, while the square shape specimens were used for the irregular lump lest.

The specimens were compressed by the point-load wedge (Figure 4.11) and cone until fail. The point-load strength index was then obtained from the formulae 4.28, 4.29 and 4.30. The value Is(50) was then used to obtain the compressive strength using the relationship give in Equation 4.32.

The point-load strength index was defined in a field test by the axial, diametrical, and lump methods. Two hundred and thirty-nine specimens were used for the diametrical point-load test and ninty-six specimens for the axial point-load test. One thousand and eigty-nine graywacke specimens and sixty-seven subarkosic sandstones were used for the lump test. The median value is found from the test results by systematically deleting the highest and lowest values until only two remain. The required median valur is the average of these two remain values. The results of point-load strength index are summarized in Table 4.17 and Figure 4.12.

4.4.2.3 Direct Shear Strength

The shear strength is another important strength characteristic of the rock mass where it is needed in the analysis of the stabillity problem of the underground openings, the limiting equilibrium analysis of the degree of slope stability, and the analysis of the suitability of foundation and abutments.

Protodyakonov (1969) defined the ultimate shearing strength of a rock to be the ratio of the maximum resistance-overcoming shearing area of the specimen. The definition is expressed as the following equation.

$$\tau = Ps/A \qquad \text{...............} \qquad (4.33)$$

where τ = shear strength

Ps = shearing force necessary to cause failure along a plane and

A = cross-sectional area along with failure occurs

The mechanical effect on the rock shear strength depends on a number of factors, e.g. the size and shape of test specimen, tolerences of demensions, loading rate, number of tested specimens, etc.

The method used for the shear strength determination followed that of Kenty's (9170). The principle of rock core direct shear is illustrated schematically in Figure 4.13.

Table 4.17 Summary of point-load tests results

Rock Type	No. of Tests	Test Type	W	Sr	I_{max}	I_{min}	I_{med}	c_{med}	$I_{s_{50}}$	σ_c	I_{a_D}
			%		MPa						
Gwke	241	Diametrical	0.41 ± 0.19	0.85 ± 0.33	8.30	0.38	3.64	87	3.71 ± 1.26	89 ± 30	0.94 ± 0.32
	96	Axial	0.42 ± 0.20	0.91 ± 0.39	9.91	1.23	4.36	104	4.26 ± 1.50	102 ± 36	
	998	Lump	0.61 ± 0.34	0.59 ± 0.36	8.95	0.14	3.69	88	3.39* ± 0.65	81* ± 15	–
									3.76 ± 0.67	90 ± 16	
Sark	67		0.14 ± 0.05	0.67 ± 0.37	12.04	1.39	6.43	154	4.61* ± 0.52	110* ± 12	
									5.37** ± 1.00	129** ± 24	

Table 4.17 (cont.)

Rock Type	No. of Tests	Test Type	W	Sr	I_{max}	I_{min}	I_{med}	c_{med}	$I_{s_{50}}$	σ_c	I_{a_D}
			%		MPa						
Gwke W IV-V	88	Lump	0.96 $\pm$ 0.40	1.05 $\pm$ 0.40	1.52	0.68	0.08	19	1.14* $\pm$ 0.74	27 $\pm$ 18*	—
									1.33** $\pm$ 0.91	32 $\pm$ 22**	
Msh	8		0.76	2.69	2.14	0.65	0.39	33	1.26* 1.35**	30	

Note : * = All Values Tests

** = Excluding Extreme Low's Values Tests

Gwke = Pebbly greywacke to pebbly mudstones

Sark = Subarkosic to arkosic sandstones

Msh = Mudshales

$I_{s_{50}}$ = Point-Load Strength Index, MPa

$_c$ = Approximate Uniaxial Compressive Strength, MPa

I_{a_D} = Strength Anisotropy Index

Figure 4.11 The point-load test machine being worked on the pebbly graywacke core specimens.

a)

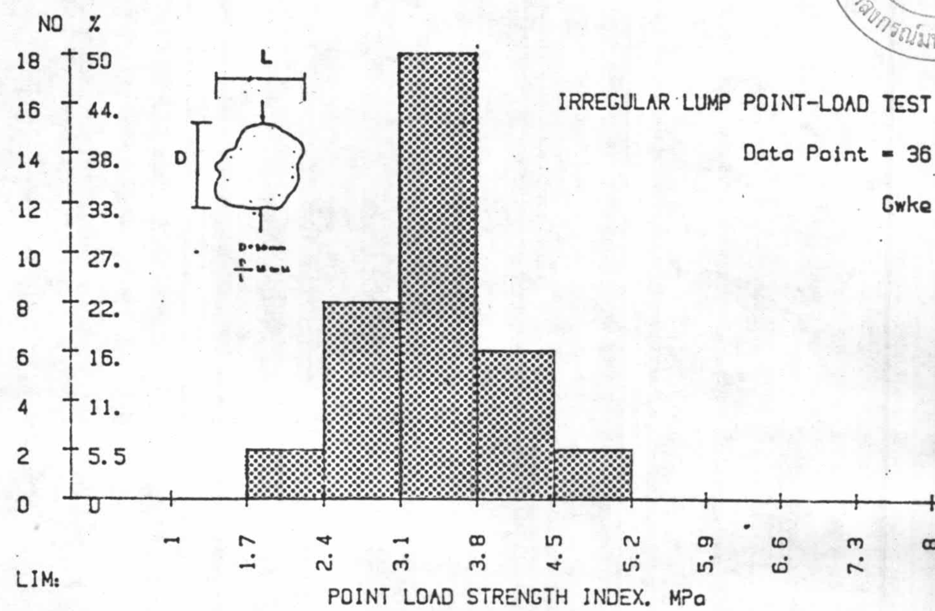

Figure 4.12 Histogram of pebbly graywacke specimens tested for the tensile strength. The point-load tests are a) irregular lump, b) diametrical, and c) axial.

b)

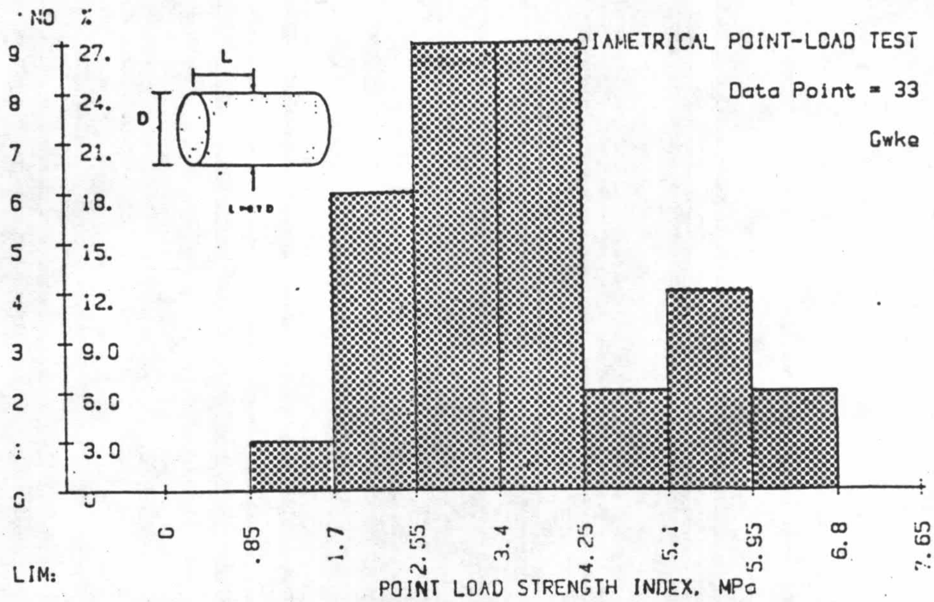

c)

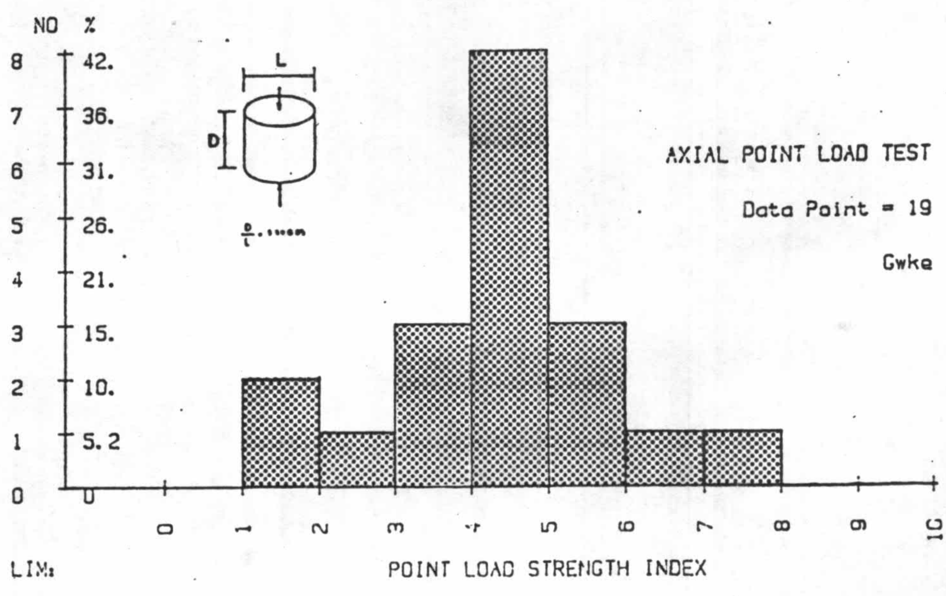

Figure 4.12 (cont.)

The core specimen was placed in an iron box made up with two separate parts (blocks), each part having a recess of 5.40 cm in diameter and 2 cm-deep to receive NX core size test specimens. The two blocks assembled with the specimen are placed within a framework consisting of two plates connected by four tie rods each with a nut on each end. One block is fitted with a pair of ball bearing races in the baseplate for minimizing friction of the moving block. A hydraulic jack is inserted between the other block and its companion cover plate to hold the normal load on the specimen (Figure 4.14).

A hydraulic jack was turned over 90 degrees so that the flange of the block B was resting on the table and the shear plate was centered under the loading head. The shear load was then applied onto the flange of block A at a rate between 0.0343 MPa (0.35 kg/cm^2) for the soft rocks to 0.69 MPa (7.03 kg/cm^2) for the very hard rocks. The shear deformation was measured from the dial gage to an accuracy of 0.01 mm. The concurrent time, shear load, and deformation (i.e. displacement) were also recorded. In the test, the normal stresses between 1.42 MPa (14.49 kg/cm^2) to 9.83 MPa (100 kg/cm^2) were used.

The shear stress was computed by dividing the shear load by the cross-sectional area of the specimen. The generally linear failure envelopes for the samples indicated by the relationship between the applied normal stress (abscissa) and the shear stress at failure (ordinate) are illustrated in Figure 4.15a, where the plots for the pebbly graywackes and subarkosic sandstones are

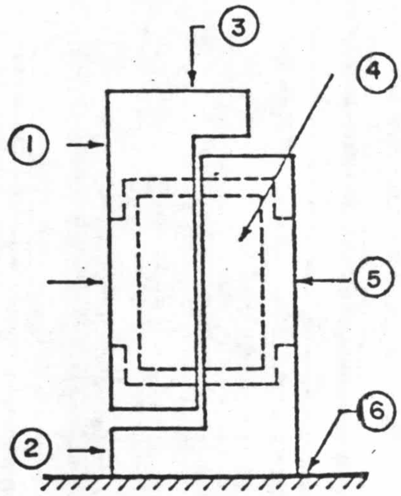

1 Block A
2 Block B
3 Shearing (testing machine) load
4 Rock core specimen cast in gypsum cement within cylindrical opening
5 Normal load applied by hydraulic jack
6 Testing machine table

Figure 4.13 Direct shear of rock core-shematic (after Kenty, 1970)

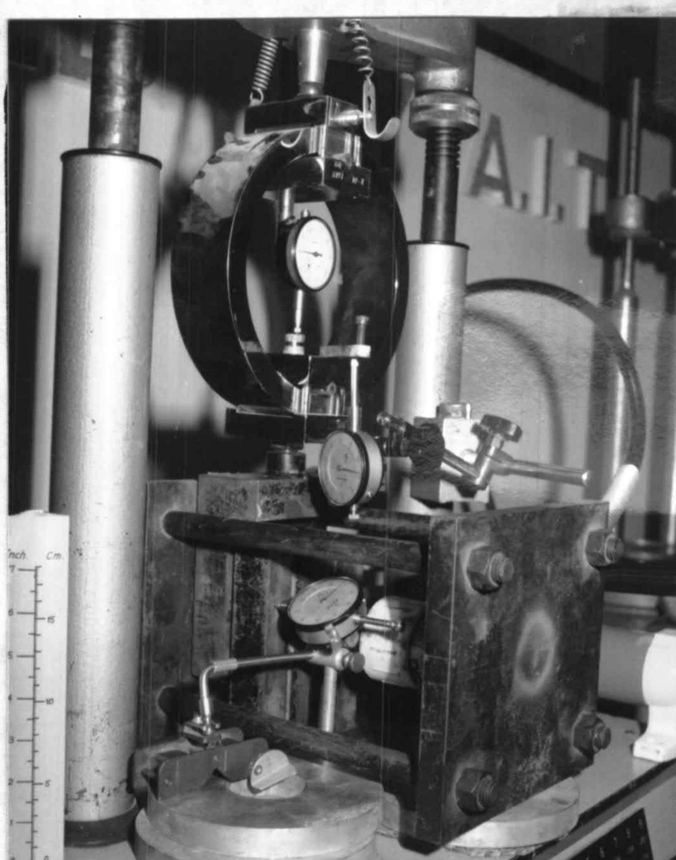

Figure 4.14 Dial gages and prooving ring of direct shear test

given. The failure envelopes may be extrapolated in a parabolic curve to the origin on the assumption that under the very small normal stresses the cohesion may be considered as zero (Patton, 1966). A tangent constructed to this curve over the stress range applicable to the Chiew Larn portal slopes indicated the values of the effective cohesion (c) and effective angle of friction (ϕ), the values are summarized in Table 4.18 and Figure 4.16. In order to account for the roughness of the rock discontinuities and for any slight tilt of the plane when assembled in the shear box, the angle of the plane of movement of the upper block relative to the lower was measured, and a correction is then applied to the measured value ϕ to give a basic friction angle (Figure 4.15c).

The specimens were divided into two groups. The first group was tested initially in an air-died condition and the others were saturated to determine the strength mobilised along a wet surface. In several instances, a large strain was applied to the samples such that most of the asperities were sheared, and a residual strength of the discontinuity thereby determined.

4.4.3 Determination of Hardness

The rock hardness is considered to be a complement of the resistance of rock to the displacement of surface materials by a tangential abrasive force, as well as its resistance to a normal, penetrating force, whether static or dynamic (Deere and Miller, 1966). The hardness measurment usually falls into three main categories, i.e., an abrasion or scratch hardness, indentation hardness, and rebound or dynamic hardness. For the laboratory study

Table 4.18 Summary of direct shear tests results

Core Specimen		Ranging Value	Condition	W %	Peak		Residual	
Rock Type	No. of Tests				ϕ_p (°)	c, MPa	ϕ_r (°)	c, MPa
Sark	12	minimum	air-dry	0.31	-	-	-	-
		average		0.36 ± 0.05	64	7	32	0
		maximum		0.18	-	-	52	5
Gwke	23	minimum	air-dry	0.18	42	7	22	1
		average		0.53 ± 0.07	55.67 ± 9.07	15.33 ± 1.03	34 ± 12.17	3.33 ± 2.16
		maximum		0.85	67	17	55	6
	18	minimum	Saturated	0.25	42	7	24	1
		average		0.54 ± 0.27	52.17 ± 6.59	14.00 ± 3.88	40.83 ± 13.63	3 ± 1.41
		maximum		1.04	60	17	59	5

Note : Sark = subarkosic sandstones; Gwke = pebbly graywackes to pebbly mudstones

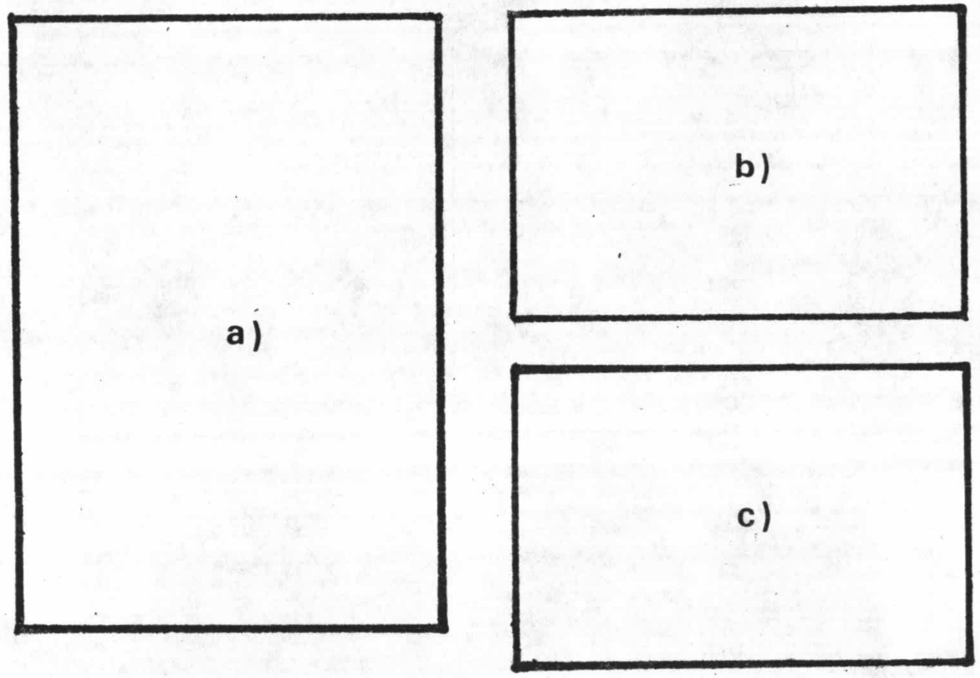

(Sample number, with depth
if mentioned)

Figure 4.15 Correlations of the results of direct shear strength tests on Chiew Larn rock samples.

a) Normal displacement versus shear displacement.

b) Shear strength versts normal stress.

c) Shear stress versus shear displacement.

Note : The correlation diagrams are arranged as shown above.

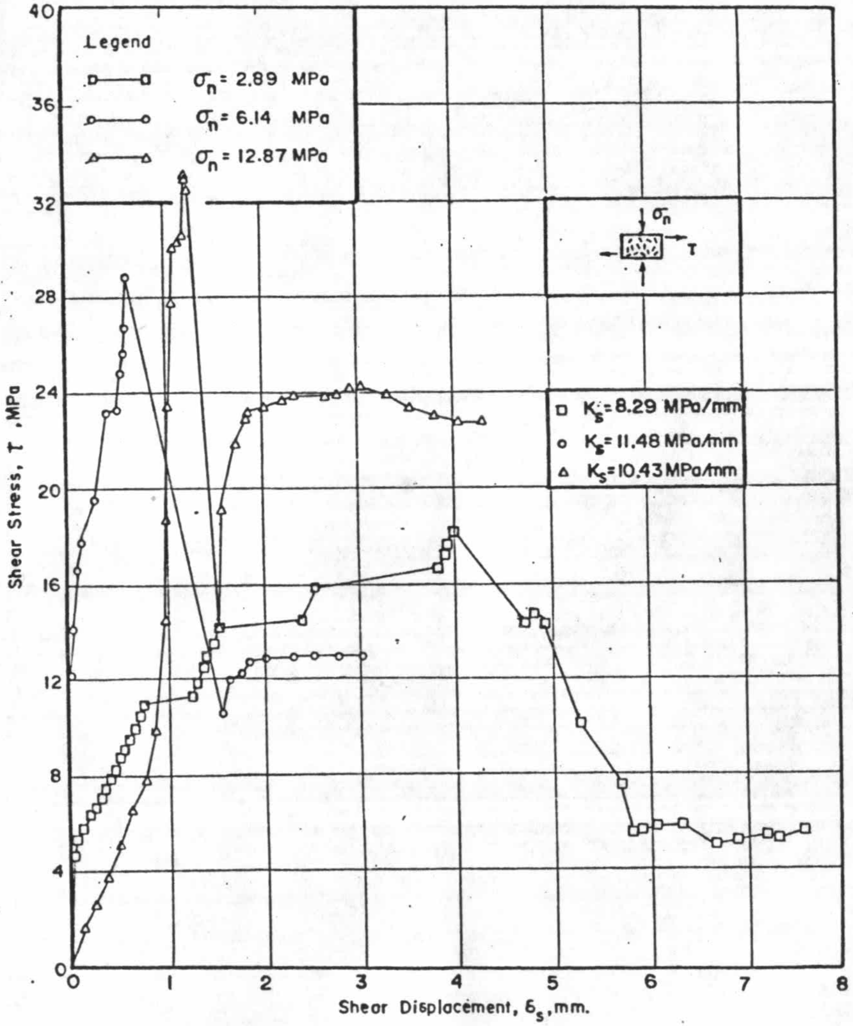

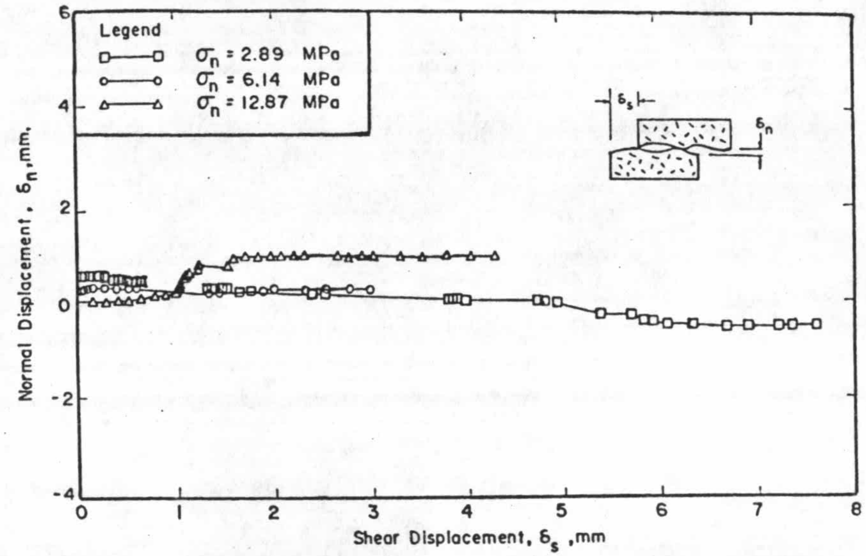

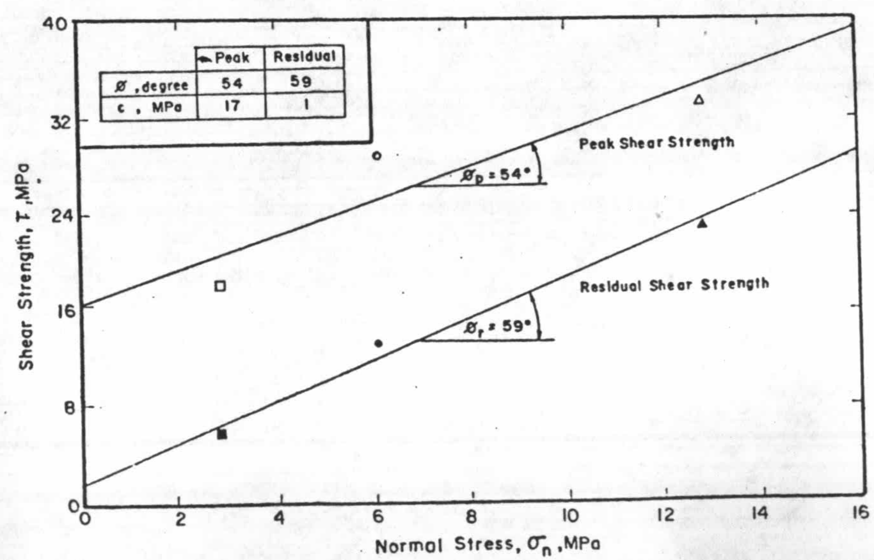

(Rock sample CHR-1)

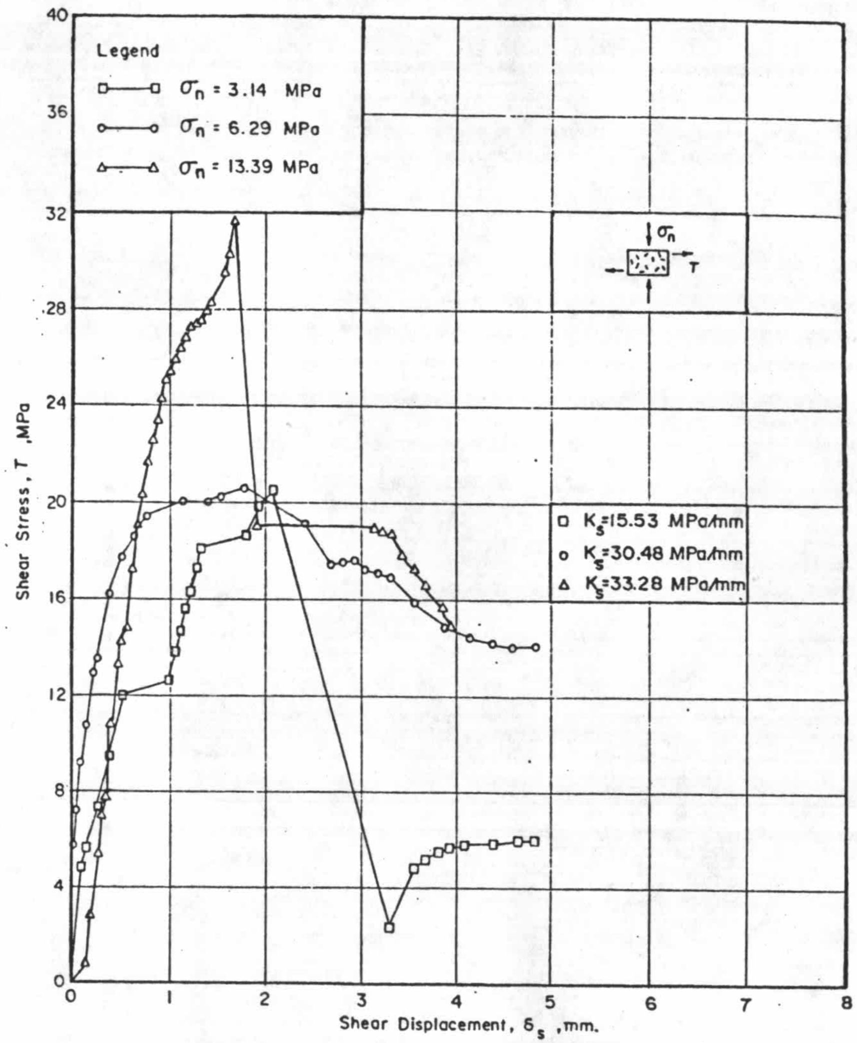

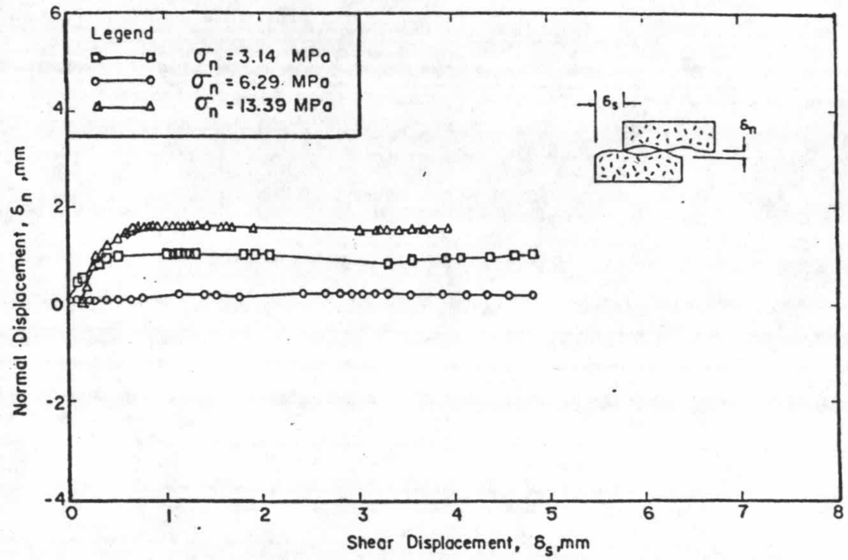

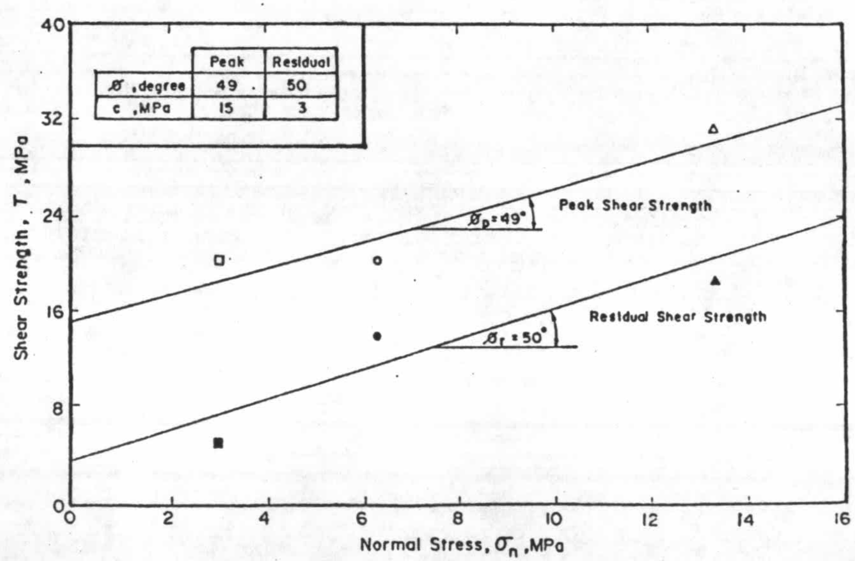

Figure 4.15 cont. (Rock sample CHR-2)

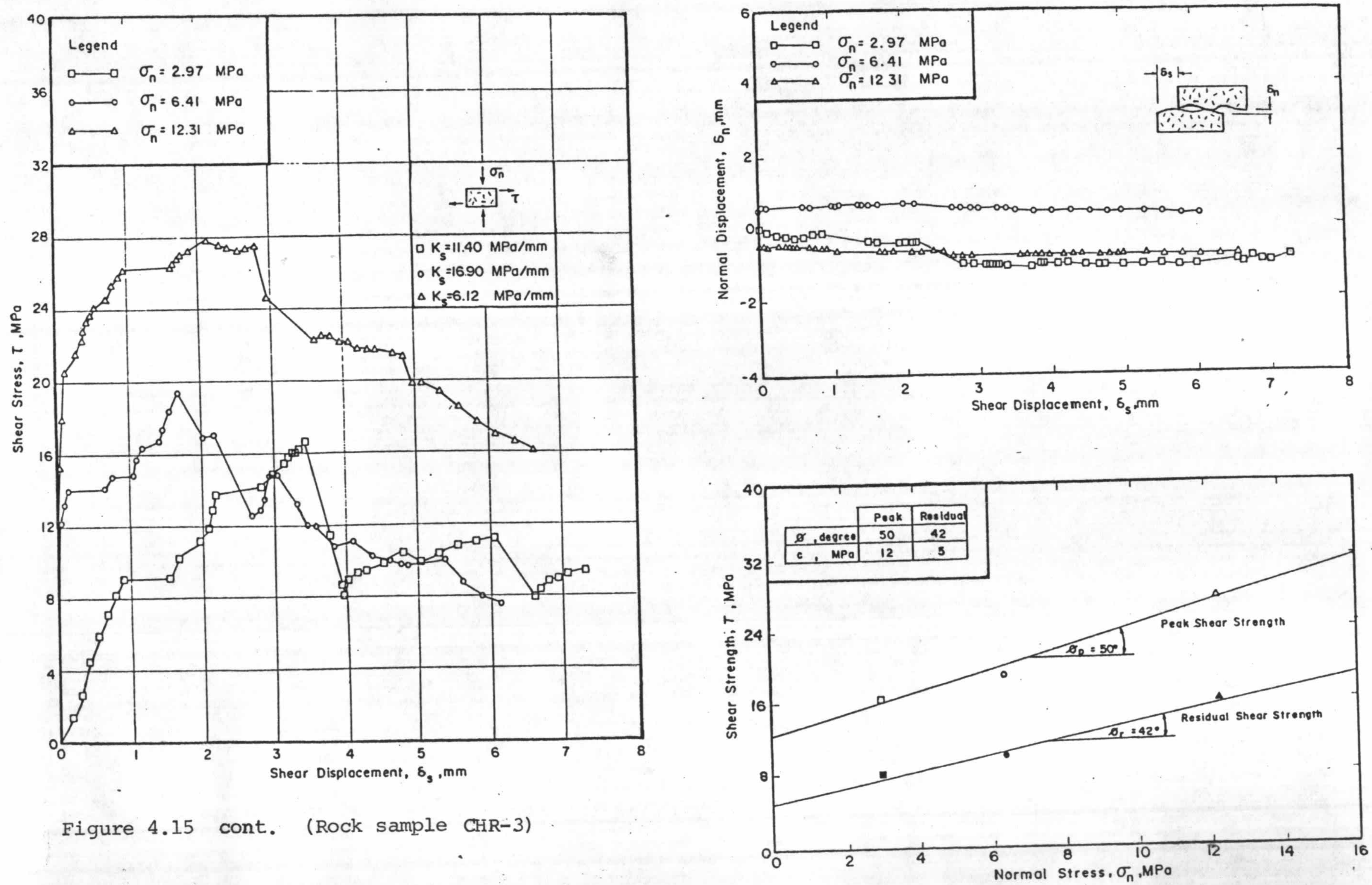

Figure 4.15 cont. (Rock sample CHR-3)

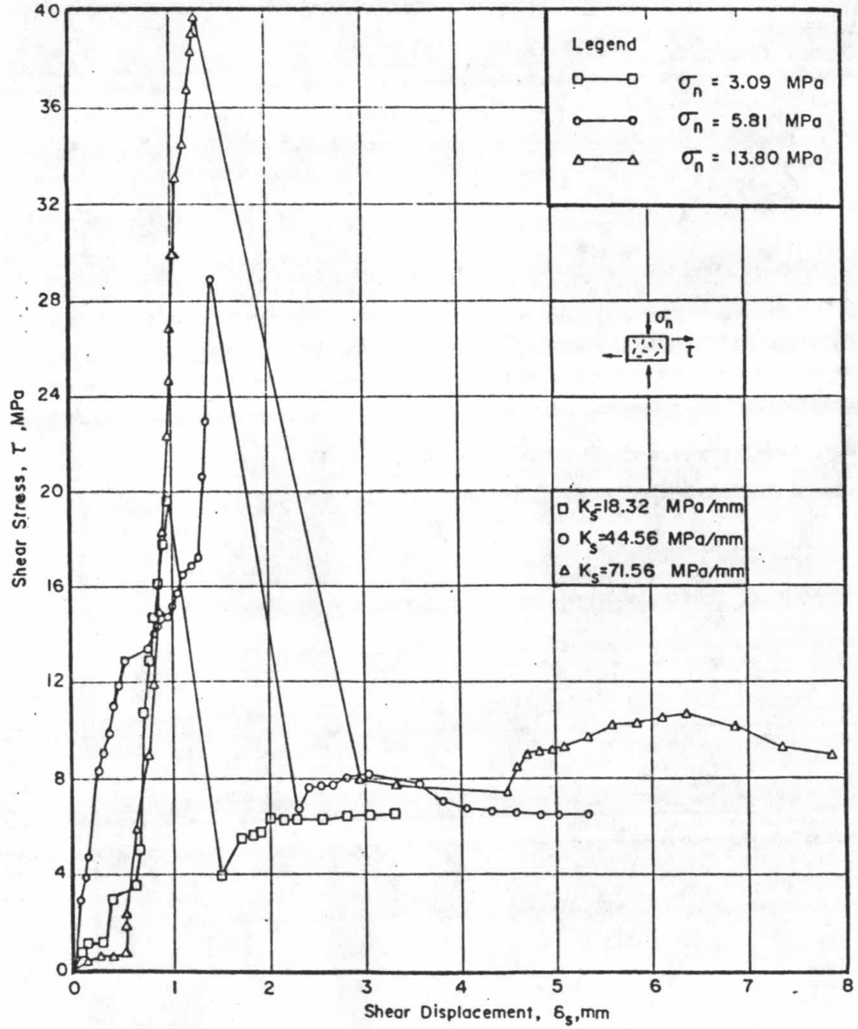

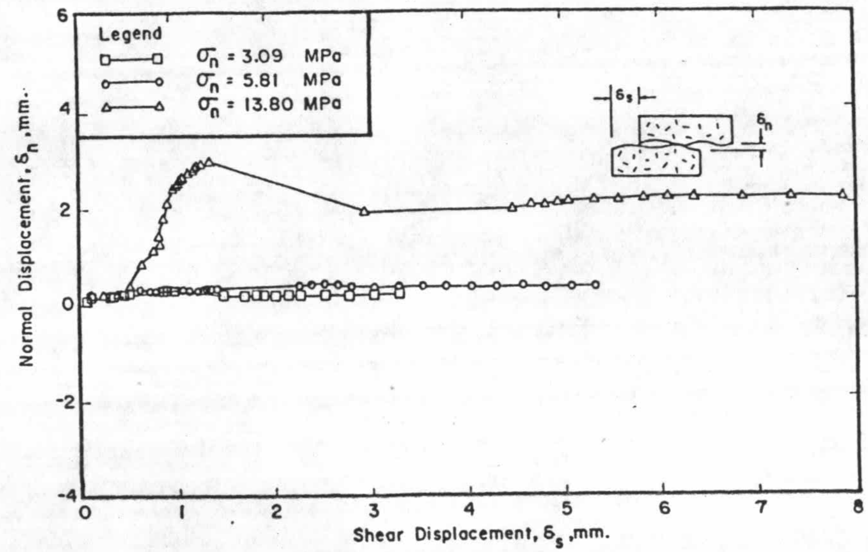

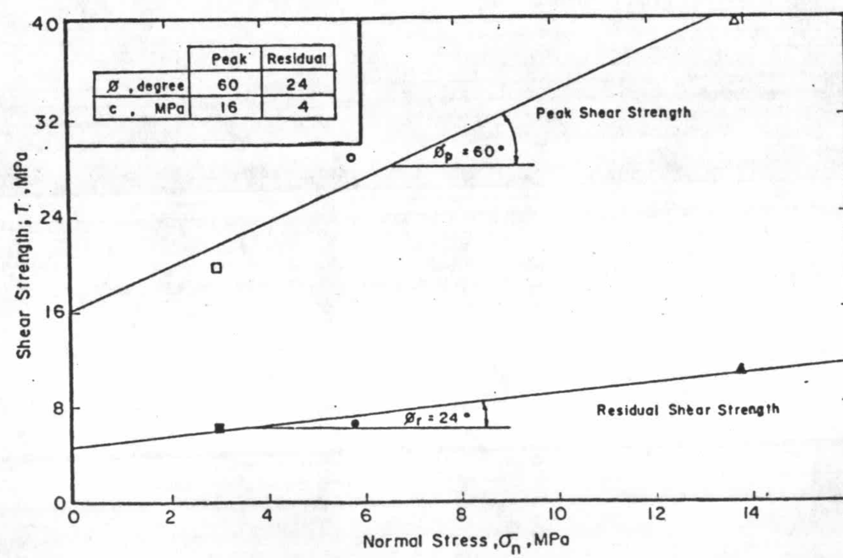

	Peak	Residual
Ø , degree	60	24
c , MPa	16	4

Figure 4.15 cont. (Rock sample CHR-4)

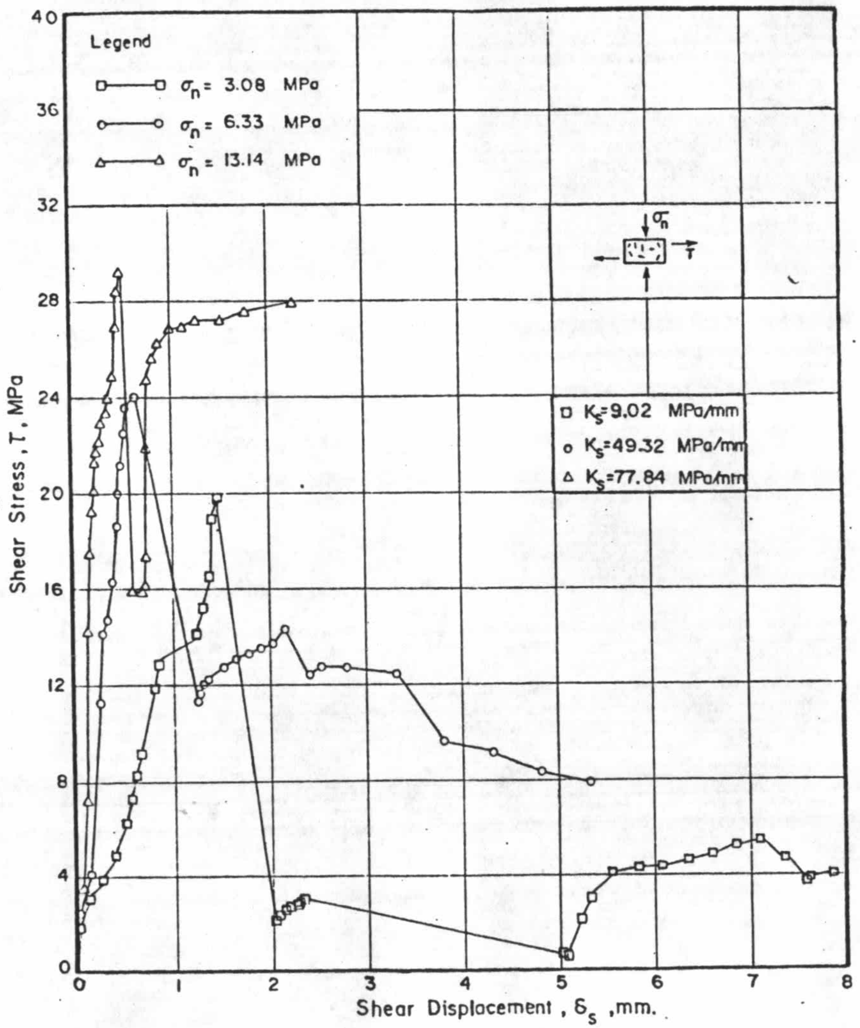

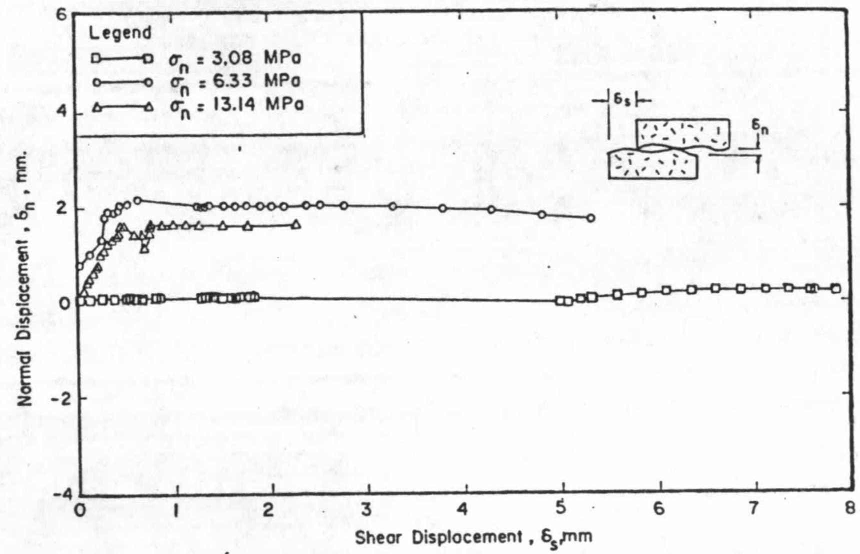

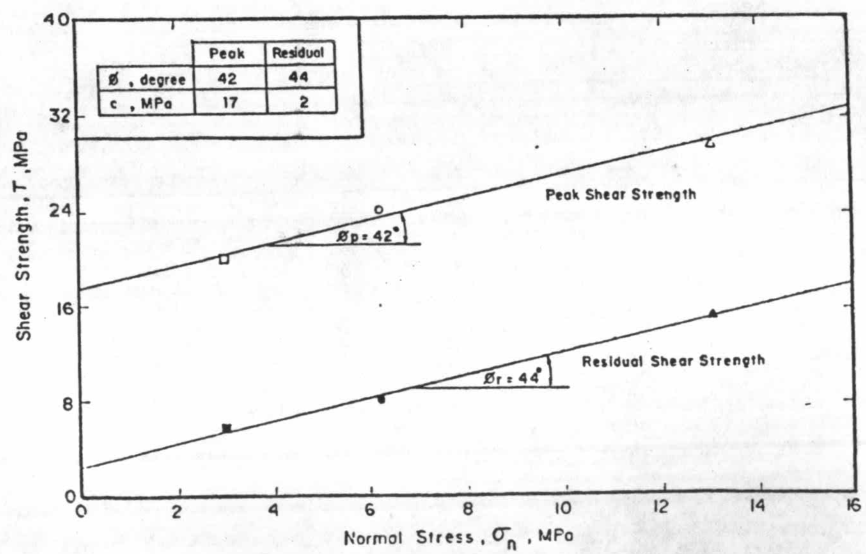

Figure 4.15 cont. (Rock sample CHR-5)

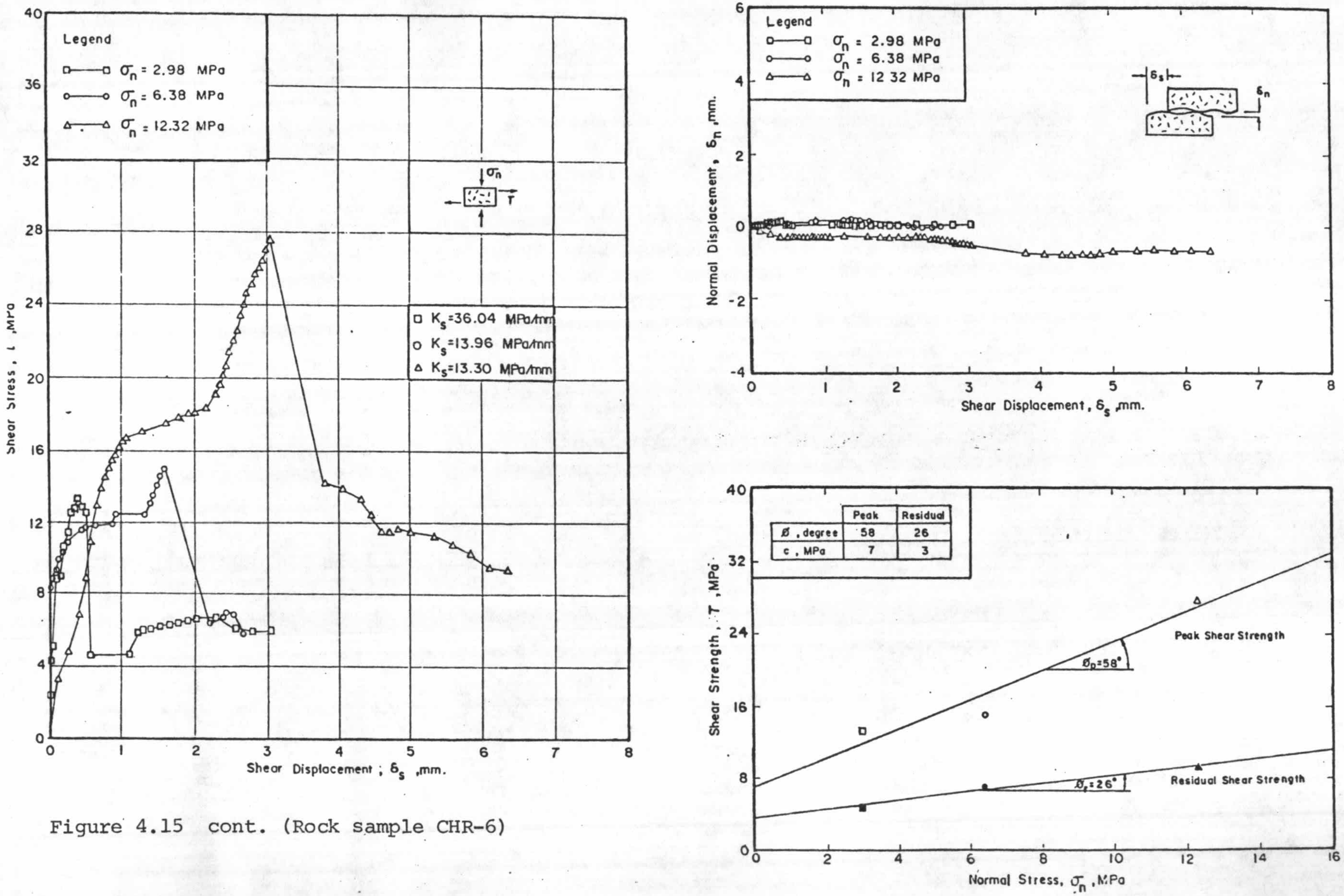

Figure 4.15 cont. (Rock sample CHR-6)

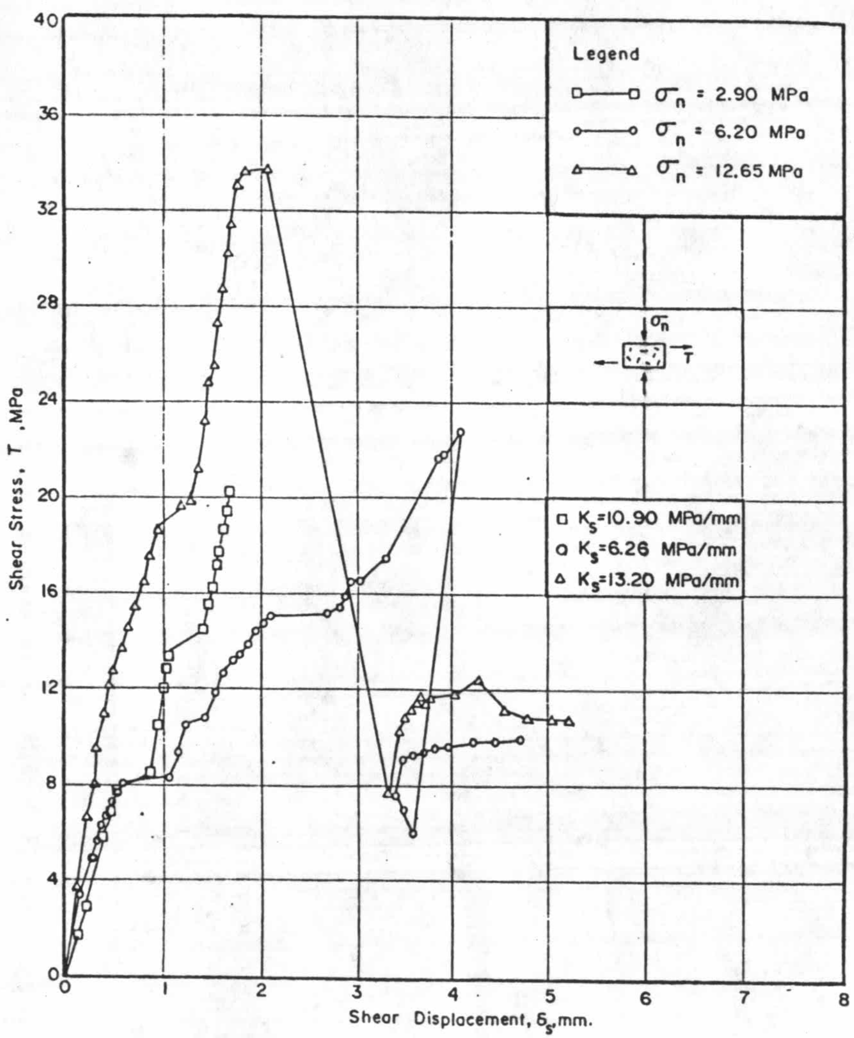

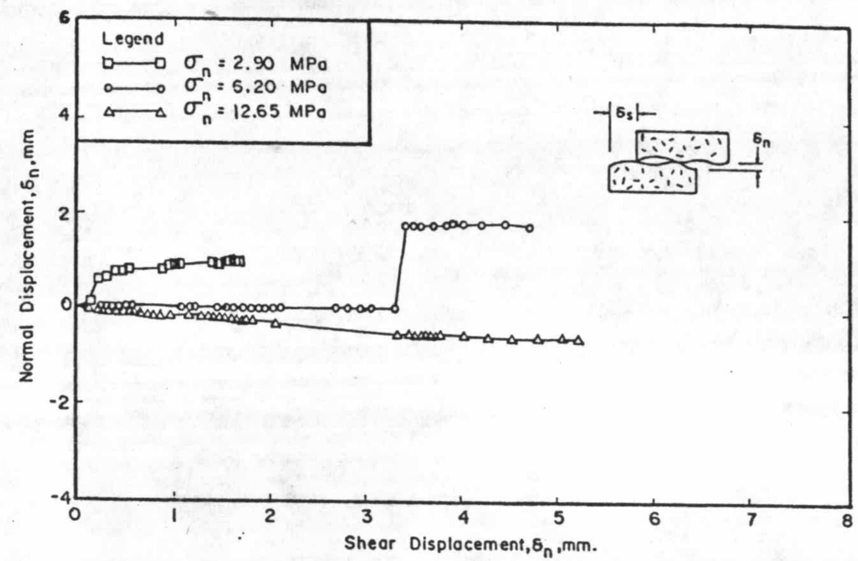

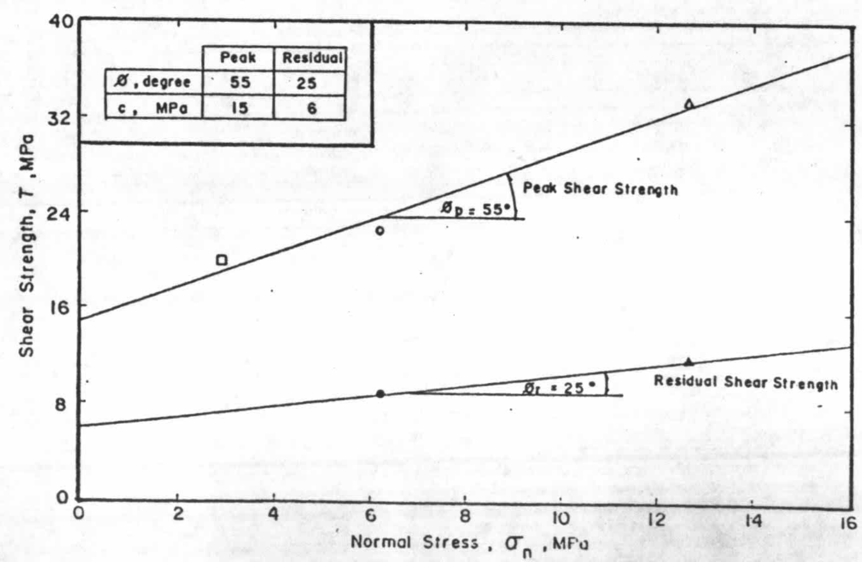

Figure 4.15 cont. (Rock sample DH-3, with depth 15.05 - 15.33 m)

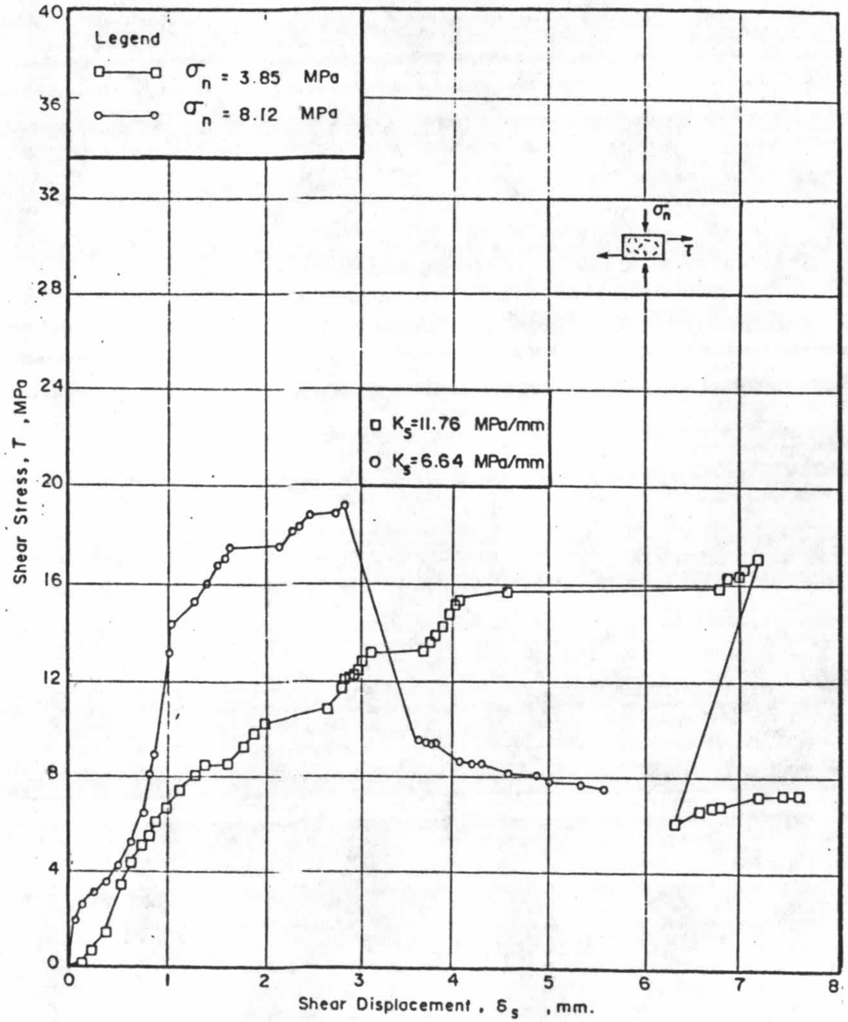

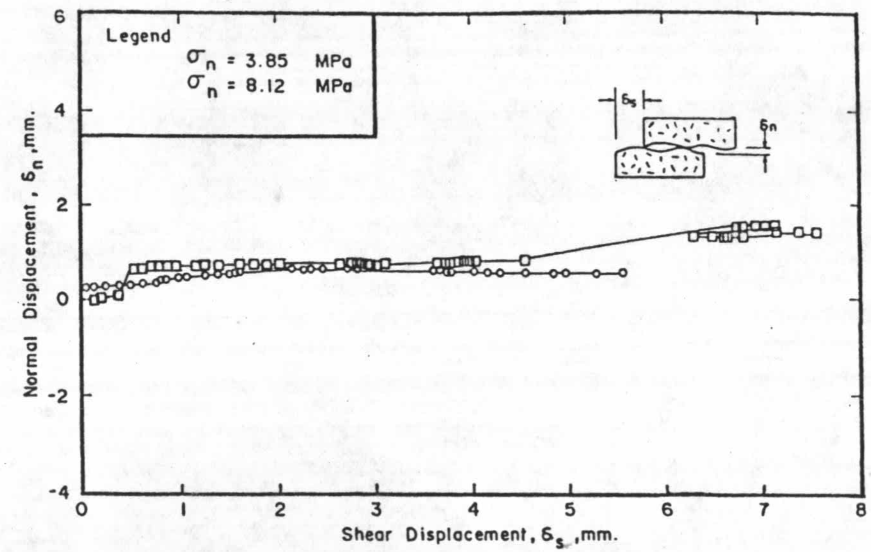

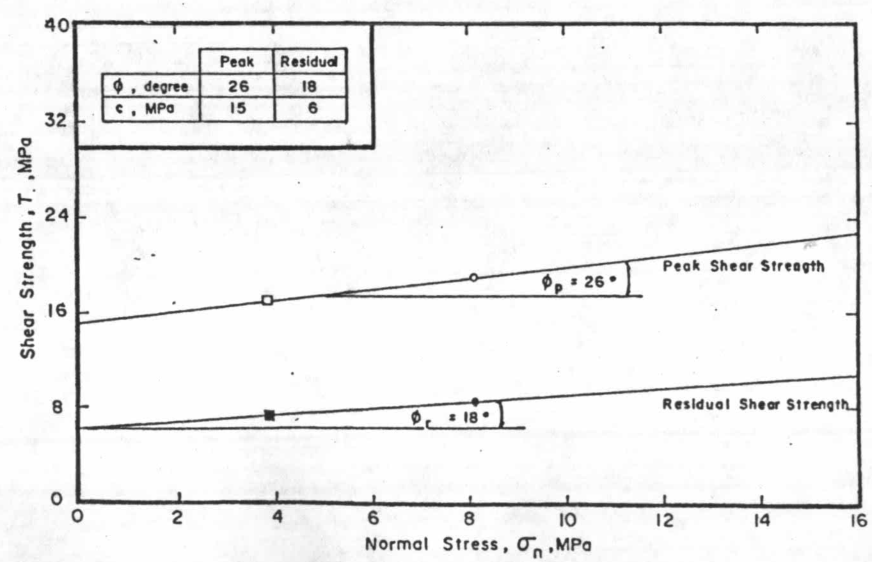

Figure 4.15 cont. (Rock sample DH-4, with depth

21.71 - 22.13 m)

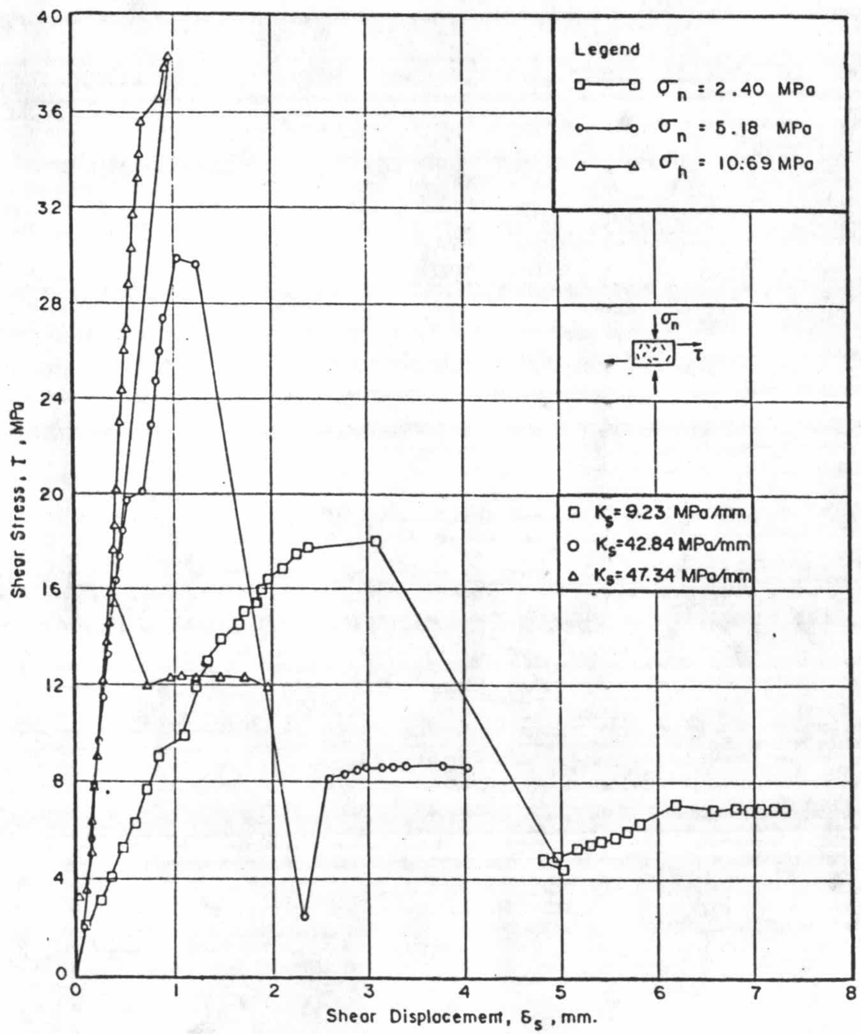

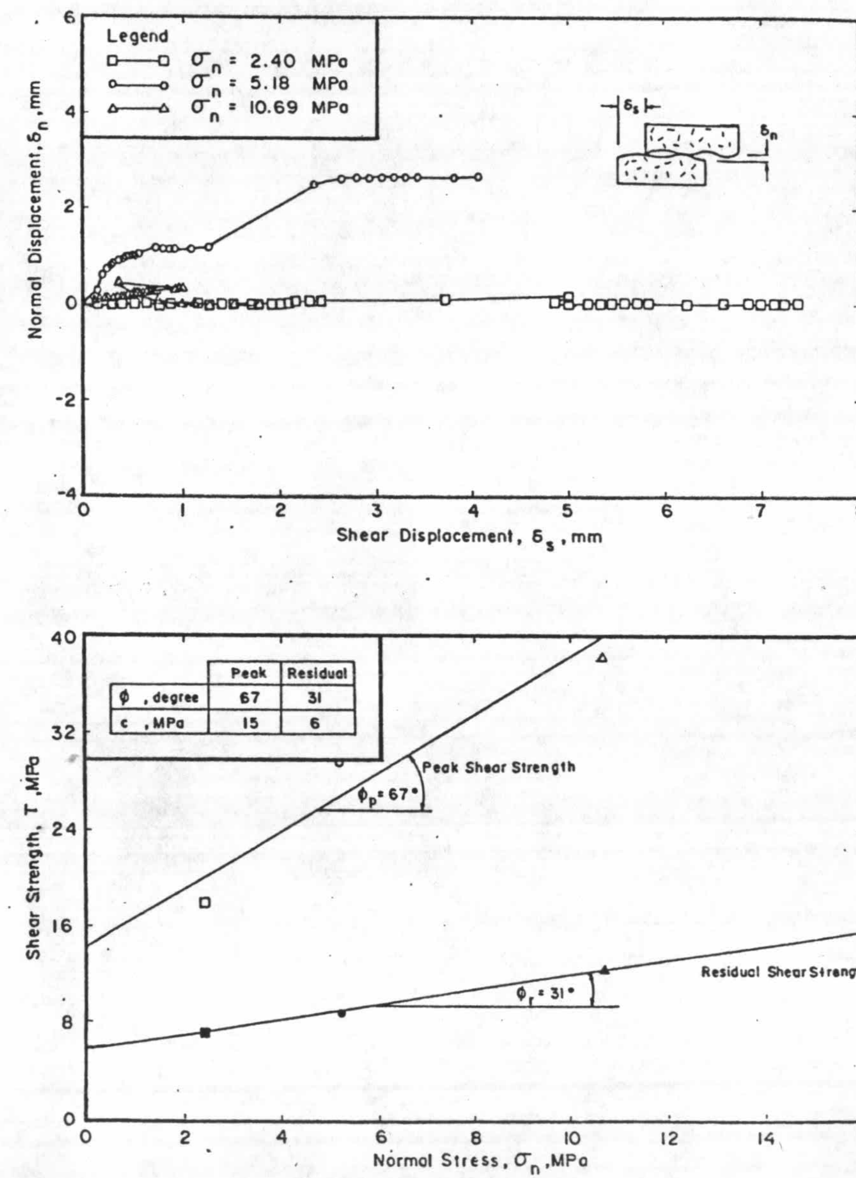

Figure 4.15 cont. (Rock sample DH-5, with depth

14.90 - 15.40 m)

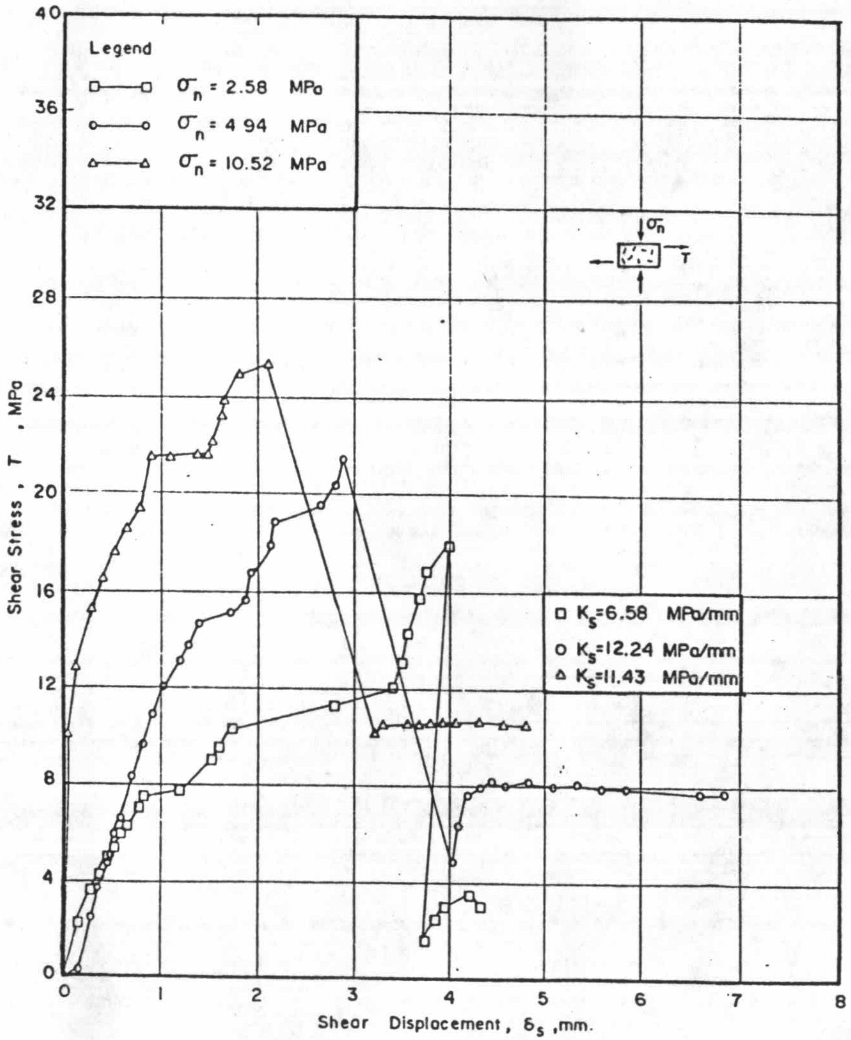

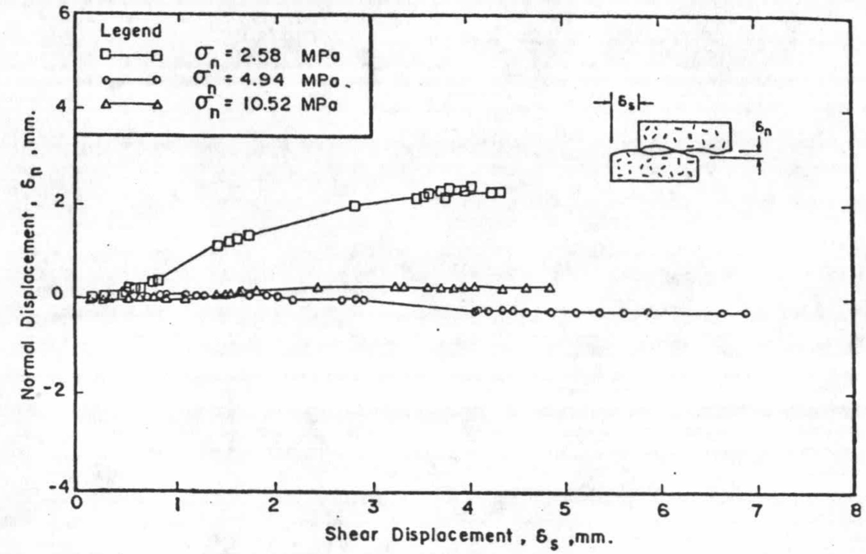

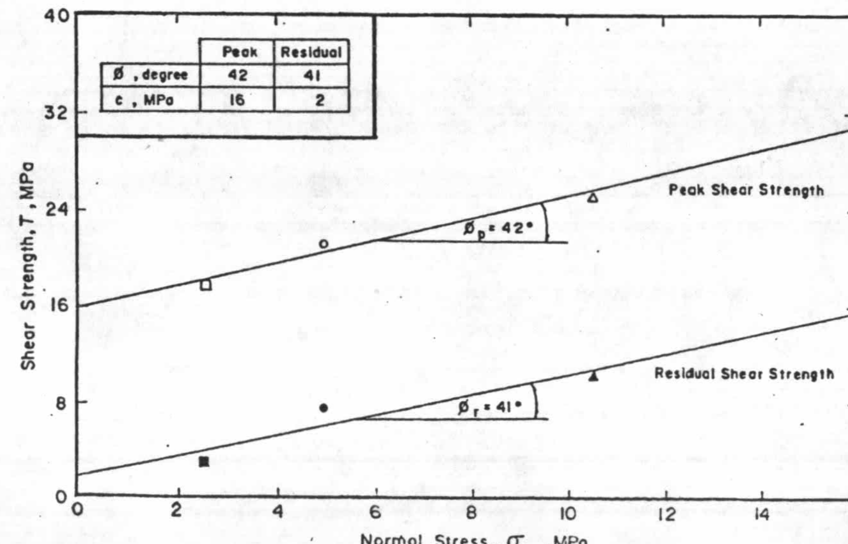

Figure 4.15 cont. (Rock sample DH-6, with depth 35.40 - 35.80 m)

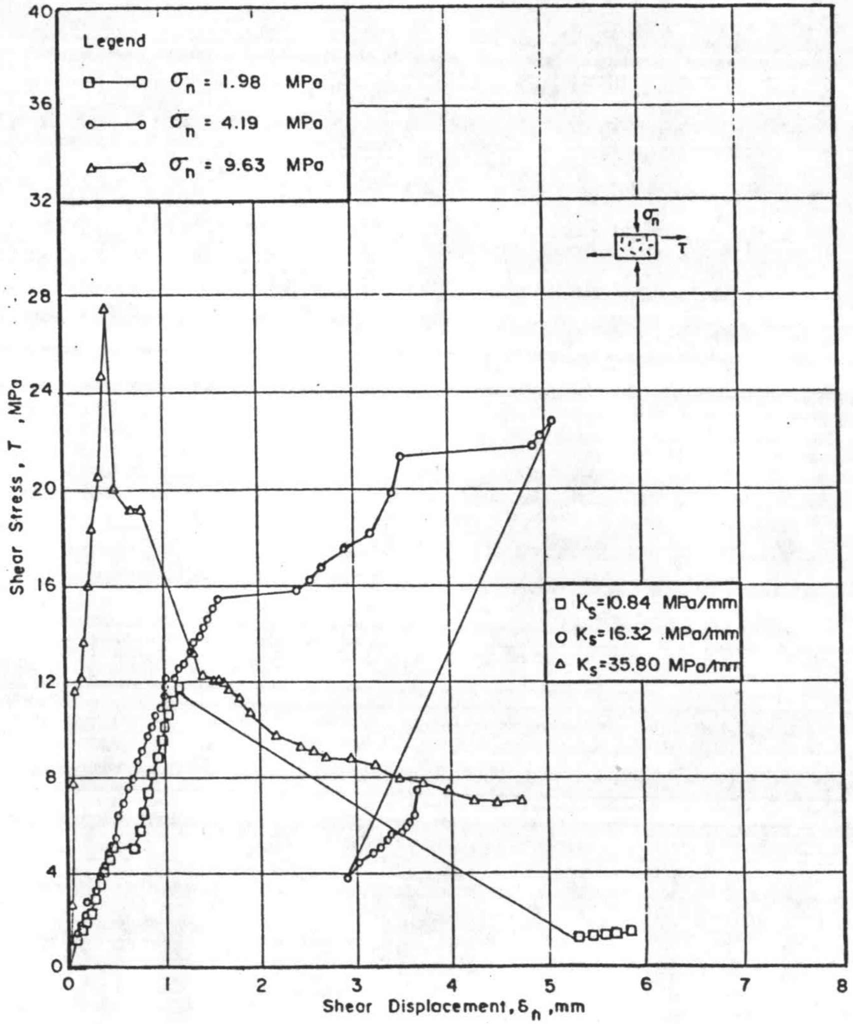

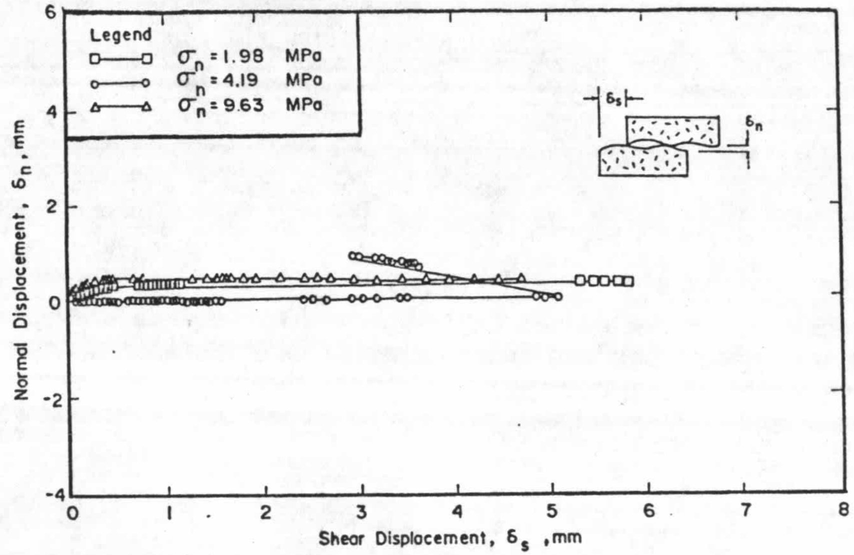

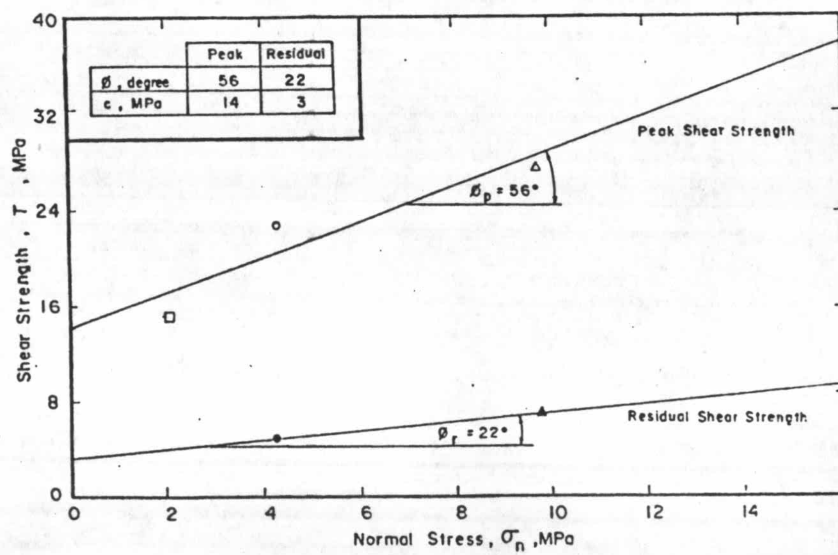

Figure 4.15 cont. (Rock sample DH-7, with depth 42.00 - 42.34 m)

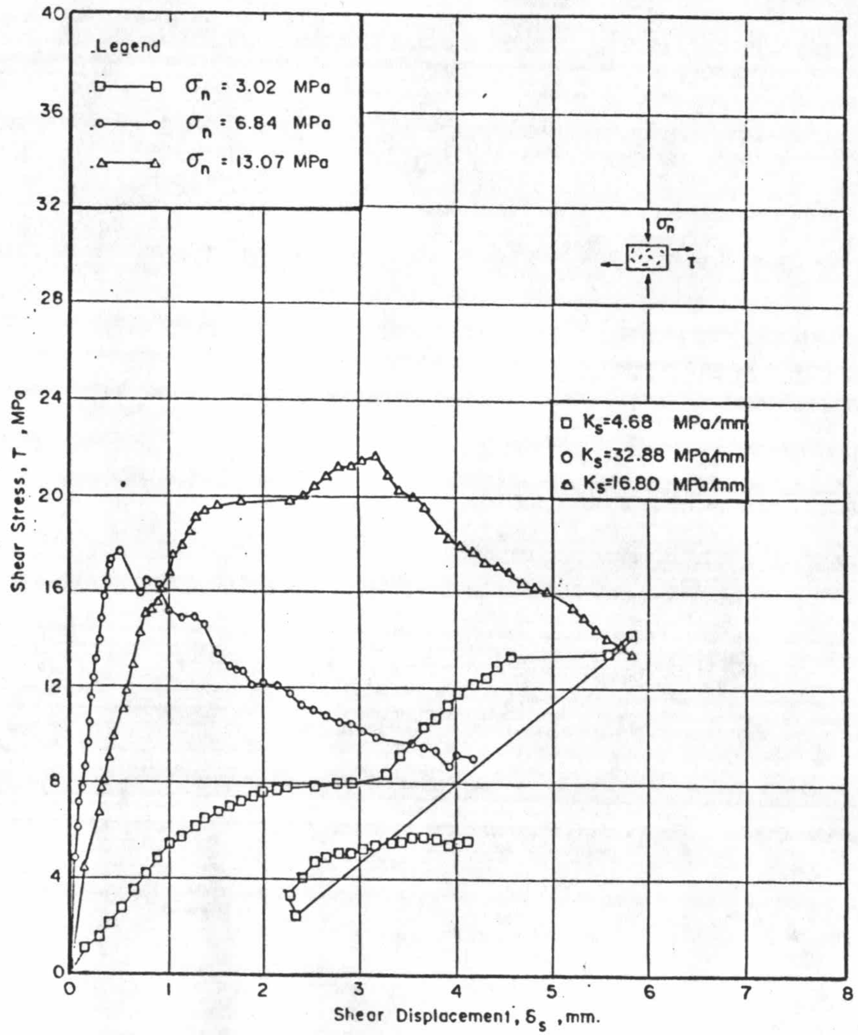

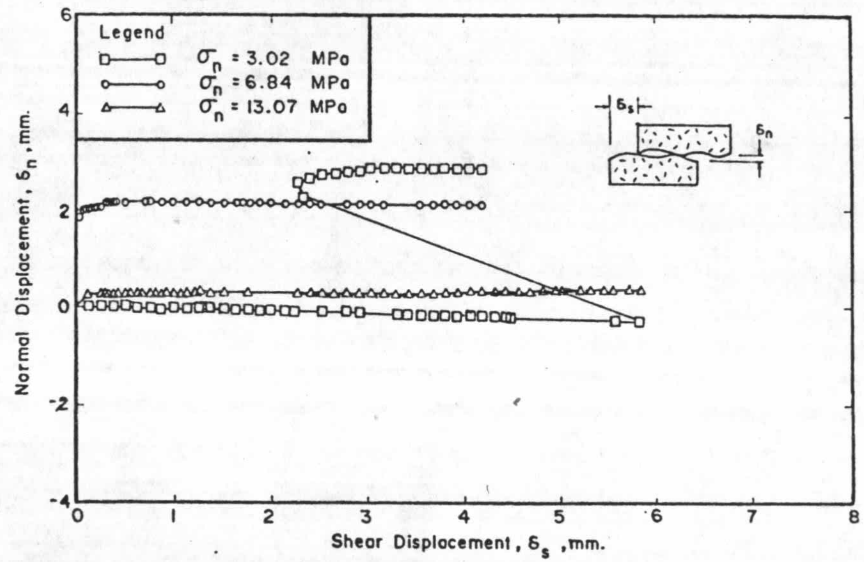

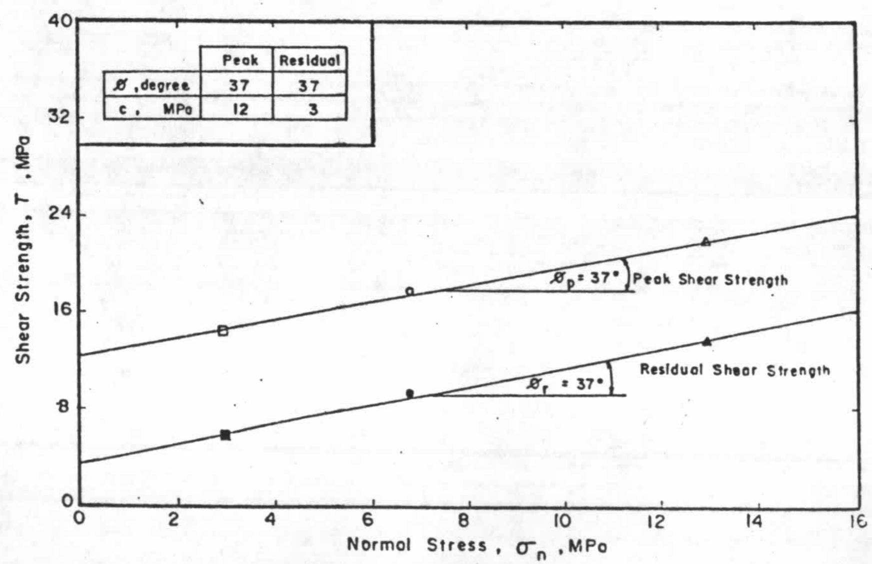

Figure 4.15 cont. (Rock sample DH-8, with depth 43.00 - 43.35 m)

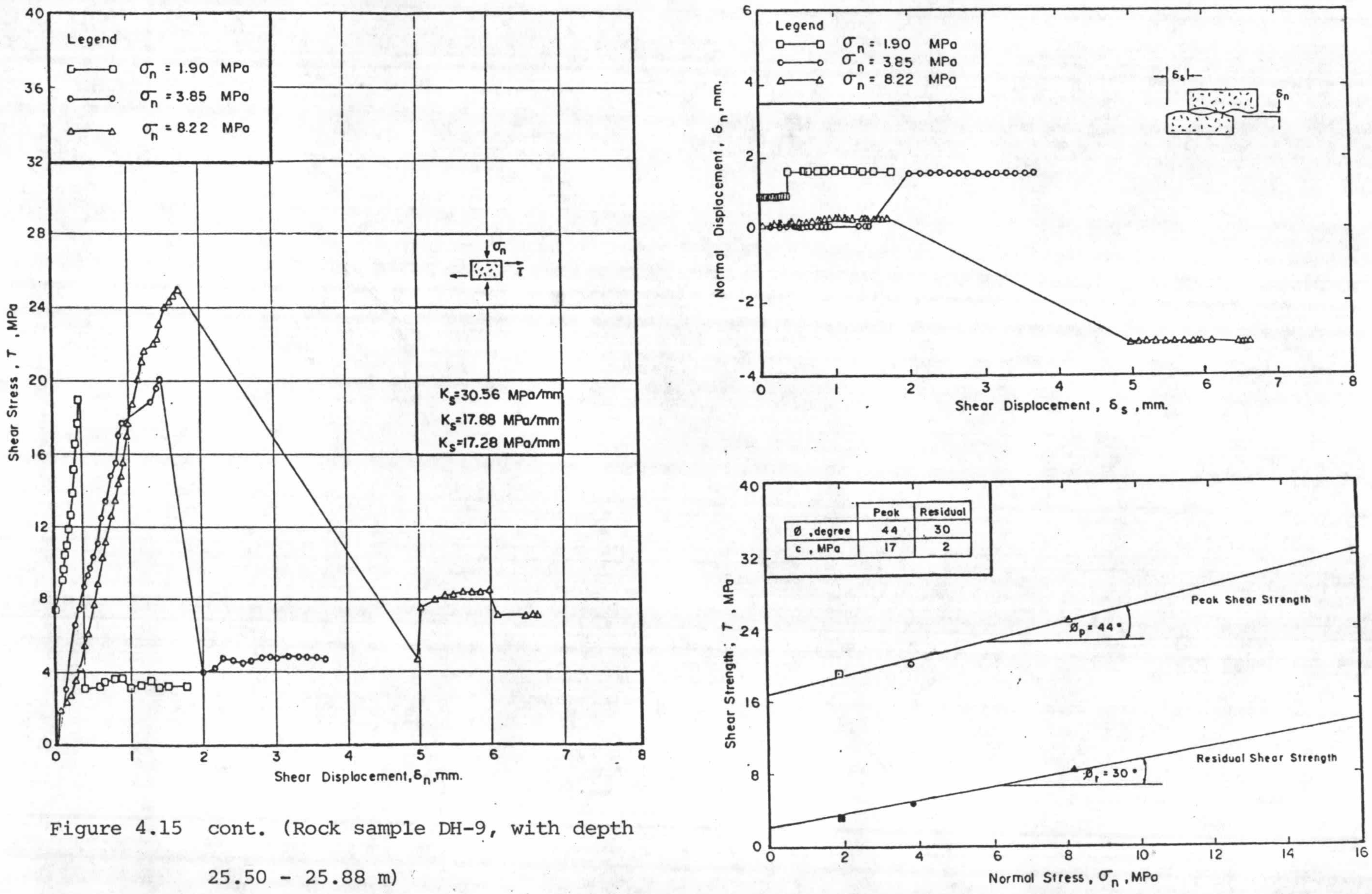

Figure 4.15 cont. (Rock sample DH-9, with depth 25.50 - 25.88 m)

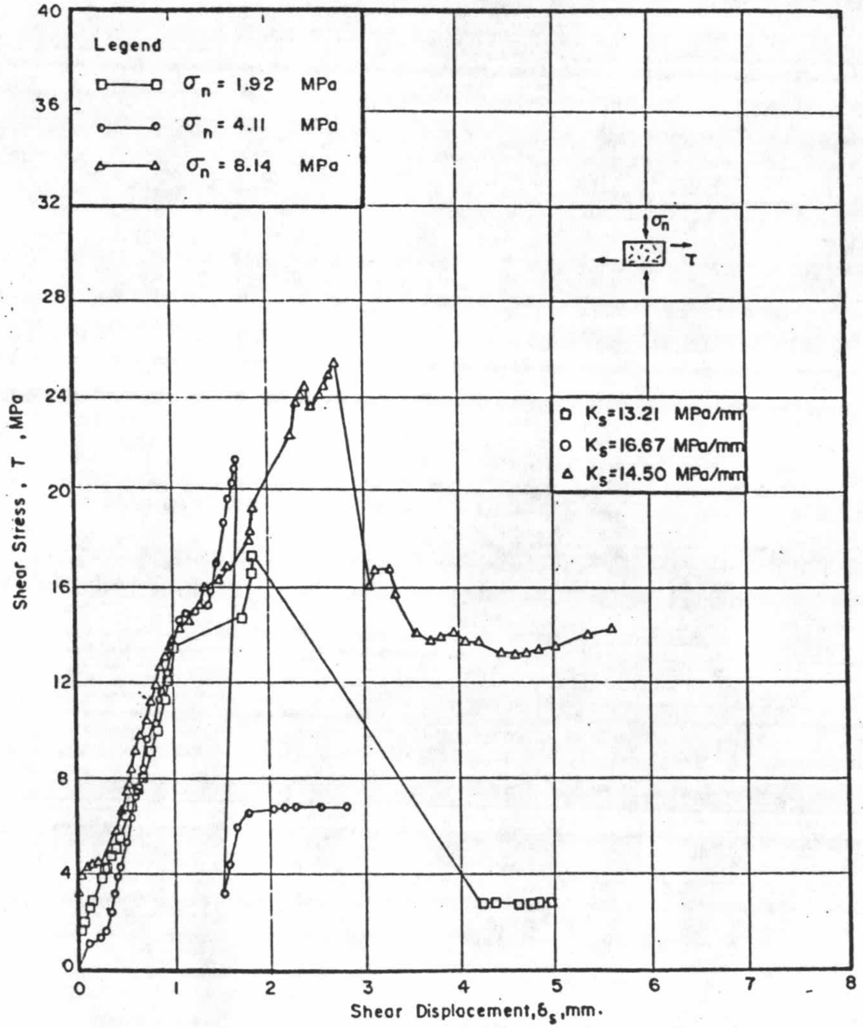

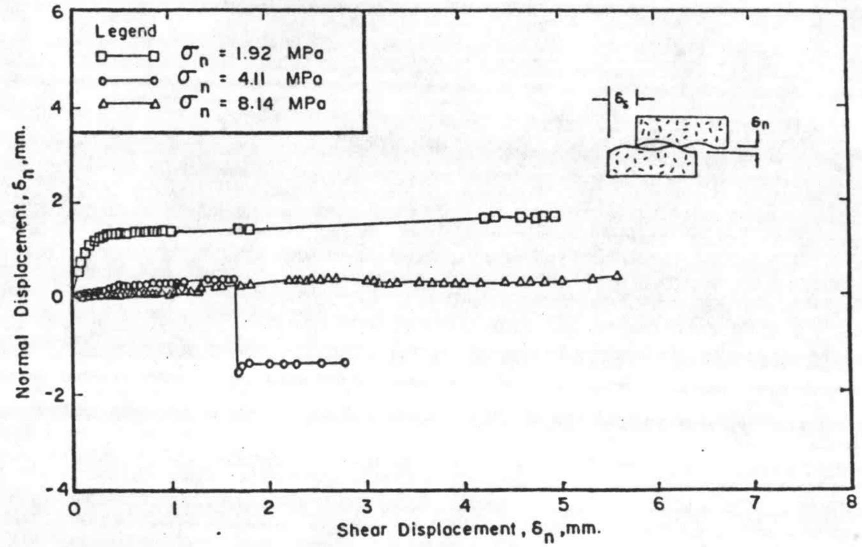

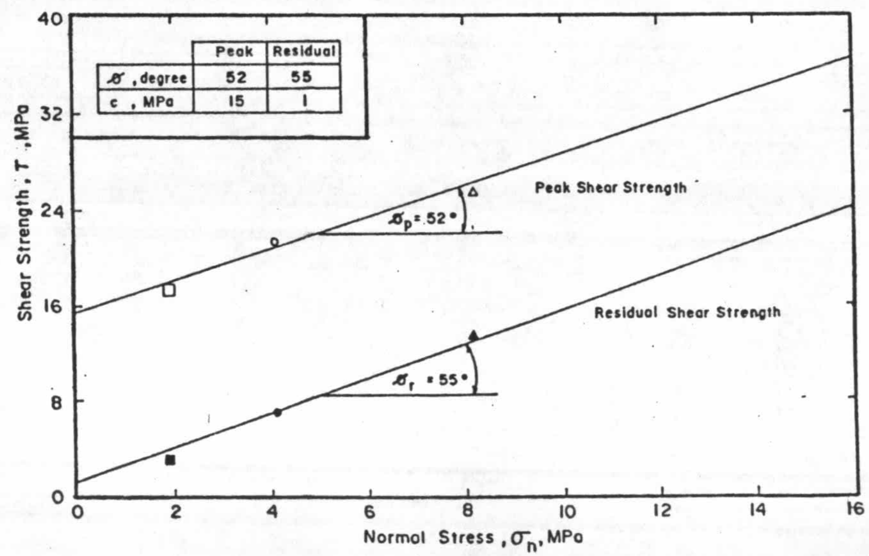

Figure 4.15 cont. (Rock sample DH-11, with depth 60.65 - 61.05 m)

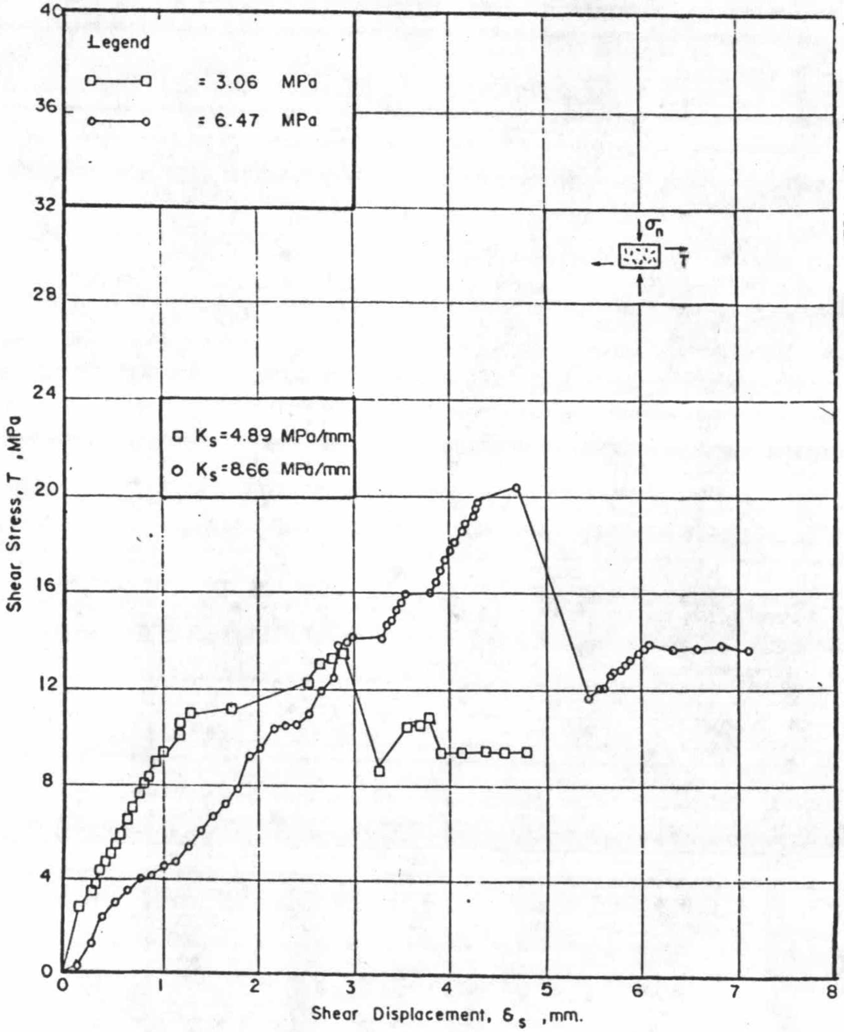

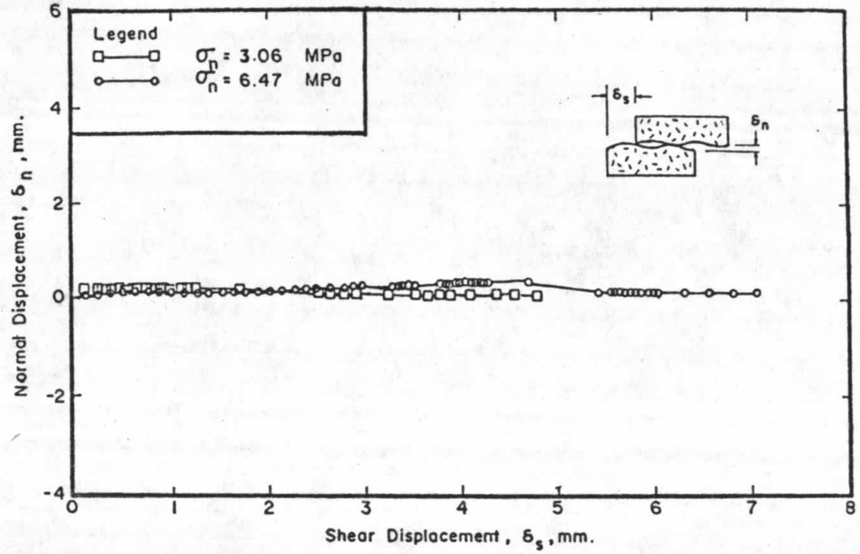

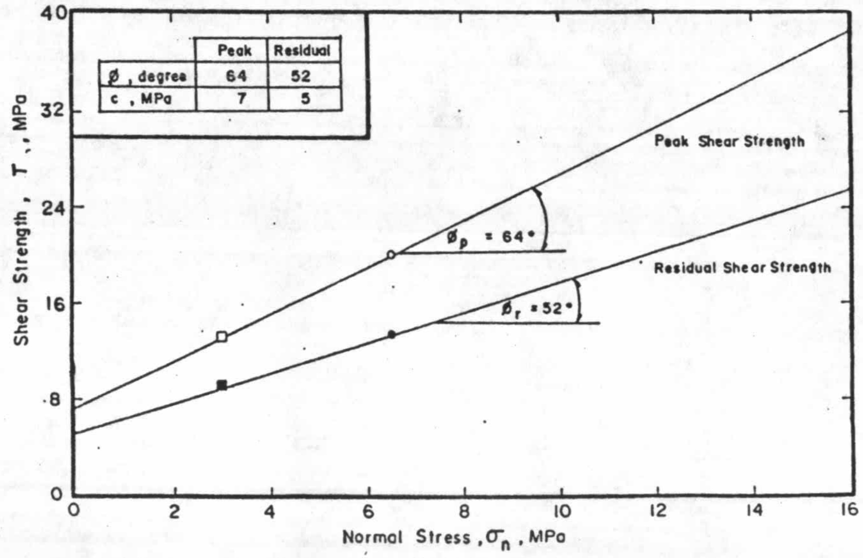

Figure 4.15 cont. (Rock sample DD 25, with depth 15.43 - 15.73 m)

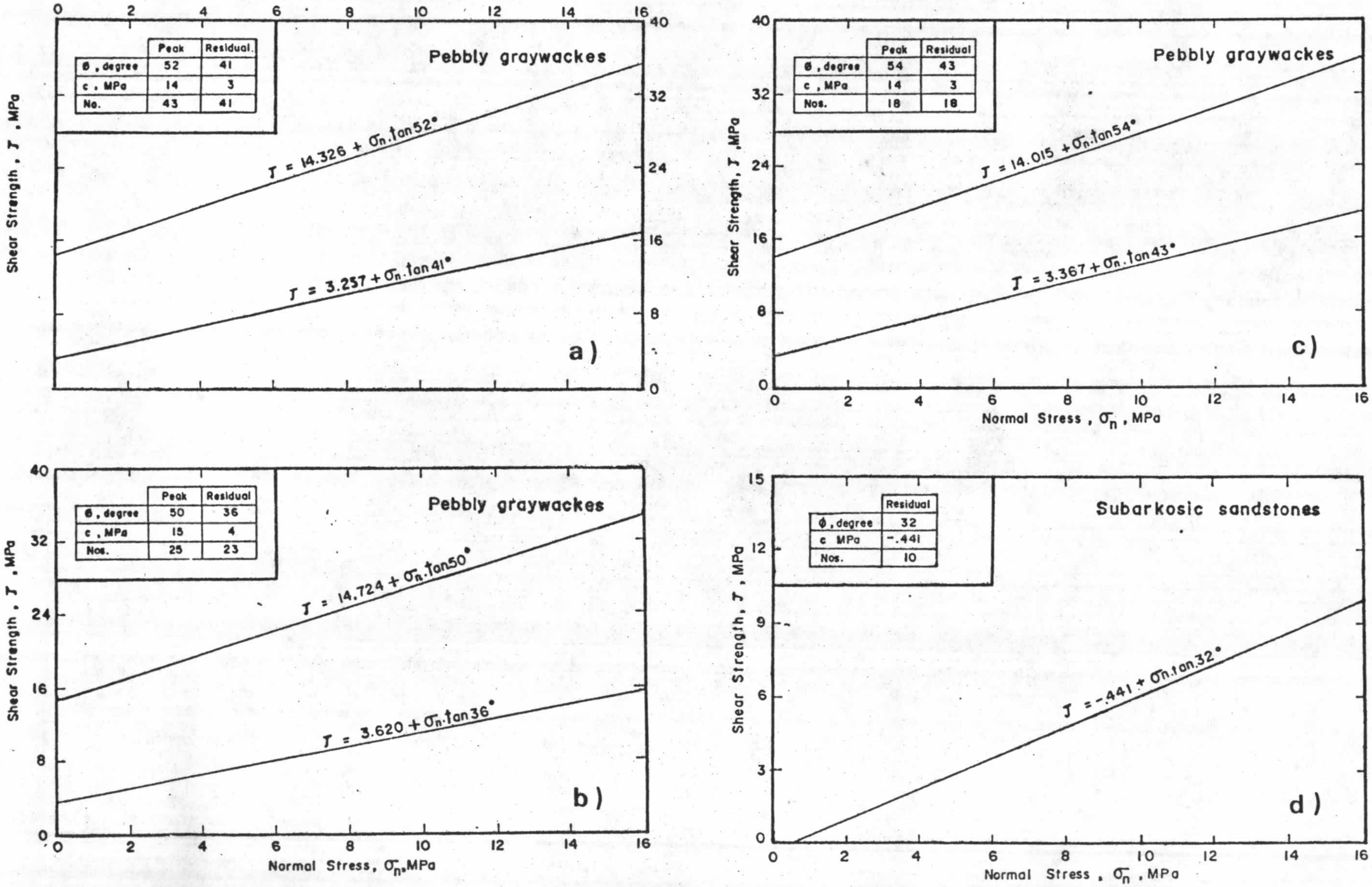

Figure 4.16 Shear strength vs. normal stress, for direct shear tests, a) total rock samples (CHR and DH), b) air-dry samples (DH), c) saturated samples (CHR), d) subarkosic sandstone samples.

of rocks, some form of abrasion hardness and the Scleroscope rebound hardness and Schmidt hardness have been investigated by many workers to a great extent.

4.4.3.1 Schmidt Rebound Hardness

The amount of rebound of an object, consisting of a sefinite amount of stored energy, after impacting on surfaces of various materials was found to indicate the strength of those materials.

The rebound hammer, to be used for this purpose, release the plunger from the locked position by pressing it gently against a hard surface where the harness was required to be measured. The spring-loaded weight is released from its locked position, thus causing an impact. With the rebound of the hammer the indicator was locked by pressing the push-botton at its side and the rebound number was read to the nearest whole number.

Proceq Sa Co. (9177) proposed that a surface area of about 4 by 4 in^2 is required to permit 5 to 10 test hammer impacts. ISRM (1981) proposed that at least 20 individual tests should be conducted on one rock sample and the test locations should be separated by at least the diameter distance of the plunger.

This test can be conducted horizontally, vertically upward or downward, or at any intermediate angle (Malhotra, 1976; ISRM, 1981). At any position, the rebound number may be different in the same material therefore the separate calibration or correction charts (Figure 4.17) were required. Zoldners (1957) showed that five numver values are needed to be added to the readings in the downward manner in order to translate these readings into the values for horizontal testing.

According to Maholtra (1976), the results of this test were affected by the smoothness of the surface unrface under test, size, shape and rigidity of the specimen, age of the rock sample tested, surface and internal moisture condition of the specimen, and the type material under test.

The graph of rebound number versus the compressive strength of the cubic and cylindrical test specimen is shown in Figure 4.18.

A caution must be excercised in implying the Schmidt rebound hammer to the soft, loosely cemented, or partially fractured rocks because of the tendency of these materials to fail under impact (Aufmuth, 1974).

The Schmidt hammer used for the present test was the L-type rebound hammer. The piston was held perpendicularly in contact with the surface of the rock. The bottom and the piston were pressed against the anvil simultaneously. The piston rebound after striking the anvil, and the hight of rebound indicated on an arbitrary scale of 0 to 100 was recorded. The indicator was locked by pressing the push bottom and the reading was recorede. The number of readings were taken by following this procedure for the in-situ tests, both in the diversion tunnel and on its portals.

a)

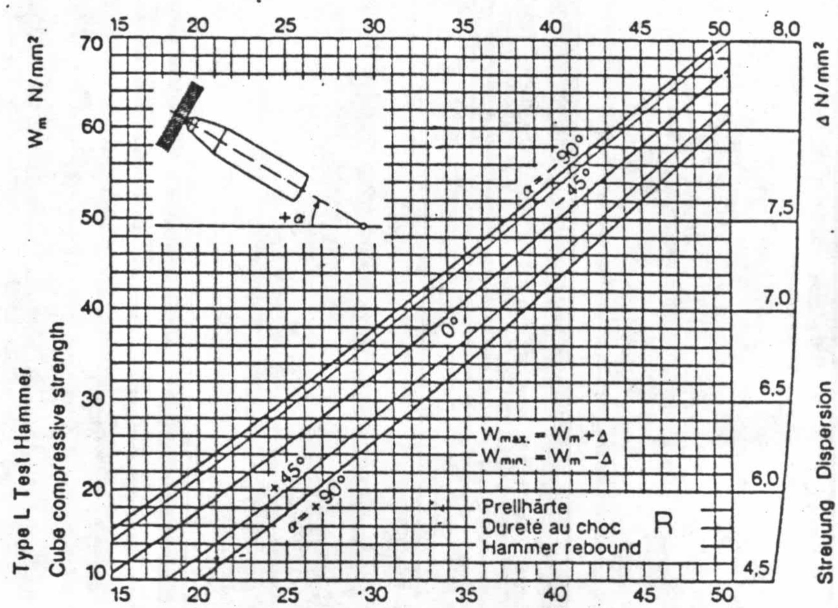

b)

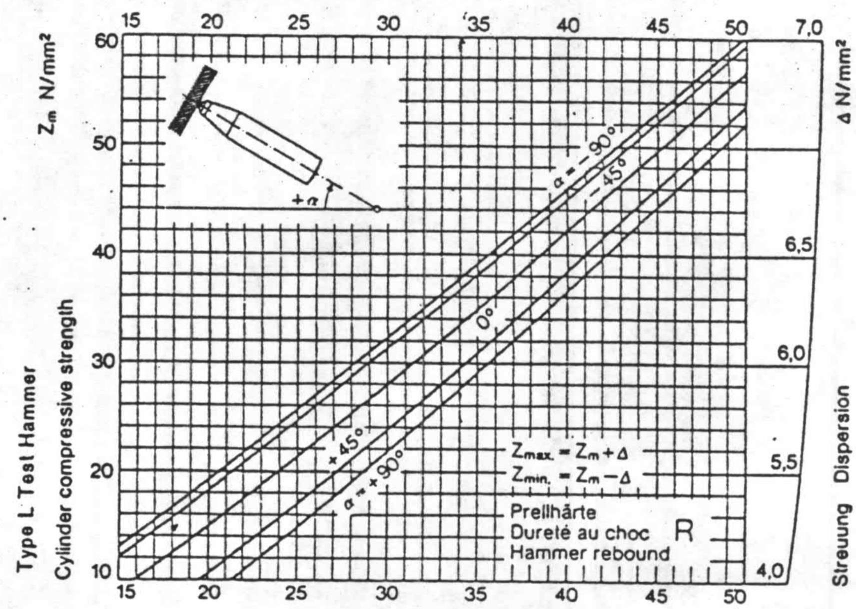

Figure 4.17 Graph of the rebound number plotted against a) cubic compressive strength and b) cylindrical compressive strength (after Proceq Sa, 1977).

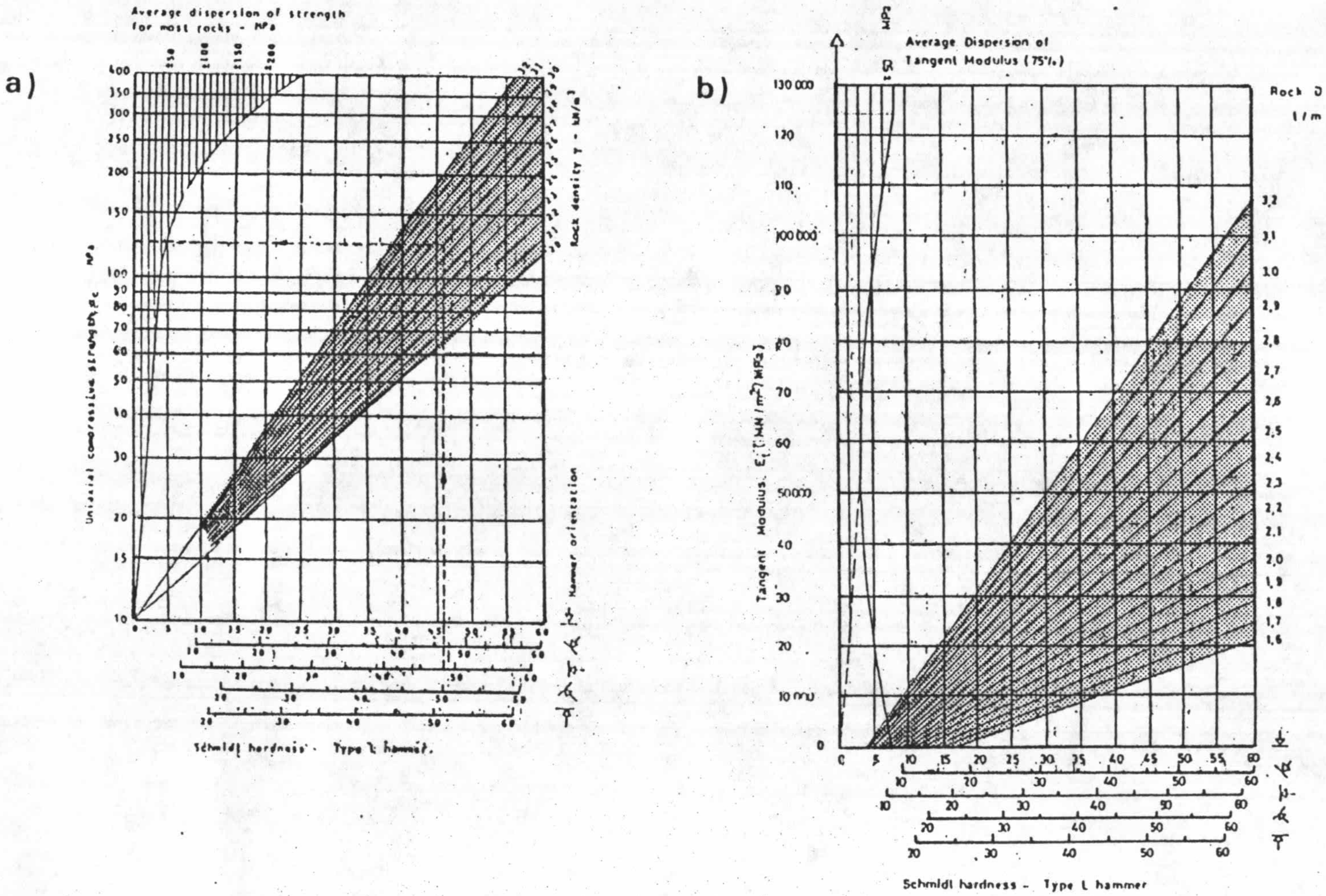

Figure 4.18 Relationship between Schmidt hardness versus the uniaxial compressive strength and tangent modulus of rock (after Deere and Miller, 1966).

The Schmidt rebound hardness results for the pebbly graywackes to pebbly mudstones, subarkosic sandstones, weathered pebbly graywackes to pebbly mudstones, and mudshales are summarized in Tables 4.19 and 4.20.

4.4.3.2 Los Angeles Abrasion Hardness

The Los Angeles abrasion hardness is expressed as the percentage of wear due to the relative rubbing action between the aggregates and steel balls used as the abrasive chsrge. The pounding action of these steel balls also exists during the Los Angeles abrasion test. ASTM (C131-69, 1975) and ISRM (1981) proposed the standard method of test for the resistance to abrasion of the smallsize coarse aggregates using a Los Angeles testing machine and suggested a procedure for testing sizes of coarse-aggregates smaller than 38 mm by placing the test sample of a known weight and the abrasive charge in the Los Angeles abrasion testing machine and rotate the cylinder at a speed of 30-33 rpm. for 500 revolutions. The materials are then discharged from the machine, separate the aggregates that do not pass the sieve no.12 US (1.70 mm), ovendried at 105°- 110°C to a substantially constant weight, then weight to the nearest 1 gm. The value of wear is expressed as the percentage of the difference between the original weight and the final weight of the test sample to the original weight of the sample.

ISRM (1981), ASTM (C131-69, 1975) suggested that the ratio of the loss after 100 revolutions to the loss after 500 revolutions should not exceed 0.02 for the material of uniform hardness.

Table 4.19 Summary of Schmidt rebound hammer tests results in tunnel

Rock Type	NO. of Tests	Ranging Value	R	R_c	σ_c (MPa)	E_t^{lin} (MPa)	E_t^{sq} (MPa)
Gwke*	1041	minimum	21.00	25.73	40.27	21228.22	26956.57
		average	43.20 $\pm$ 5.40	43.18 $\pm$ 5.39	107.84 $\pm$ 29.48	49095.58 $\pm$ 9490.95	50328.72 $\pm$ 8318.70
		maximum	58.00	54.29	206.23	64273.60	63045.10
Gwke**	846	minimum	18.00	25.25	29.93	12383.50	19541.30
		average	35.99 $\pm$ 5.22	34.60 $\pm$ 5.74	65.08 $\pm$ 13.64	35544.40 $\pm$ 6871.29	38959.01 $\pm$ 6439.43
		maximum	56.00	53.65	182.51	66287.87	64733.83

Notes : * = fresh wall strength

** = joint wall strength

Gwke = pebbly grayeackes to pebbly mudstones

$_c$ = uniaxial compressive strength

E_t^{lin} = linear tangent modulus of elasticity

E_t^{sq} = square tangent modulus of elasticity

Table 4.20 Summary of Schmidt rebound hammer tests reslts

Rock Type	No. of Tests	Ranging Value	R	R_c	σ_c	E_t^{lin}	E_t^{sq}
					MPa		
Gwke*	578	minimum	31.80	31.10	53.85	29895.40	34222.99
		average	42.67 ± 5.52	43.20 ± 5.66	109.56 ± 33.27	49876.76 ± 9071.39	50939.05 ± 7672.11
		maximum	54.60	55.16	198.08	68728.24	66779.79
Gwke W III -IV	49	minimum	20.40	20.40	29.20	11646.40	18126.80
		average	27.40 ± 3.96	27.52 ± 3.38	43.02 ± 7.15	22803.28 ± 5302.44	27202.36 ± 4313.27
		maximum	33.67	31.80	53.14	29498.80	32648.83

Note : * = fresh wall strength at portal slopes

Gwke = pebbly graywackes to pebbly mudstones

Gwke W III-IV = weathered (grade III-IV) pebbly graywackes to pebbly mudstones

R_c = Schmidt hammer number reading correct

Table 4.20 (cont.)

Rock Type	No. of Tests	Ranging Value	R	R_c	σ_c	E_t^{lin}	E_t^{sq}
					MPa		
Sark	103	minimum	36.14	36.14	66.26	36078.40	37825.30
		average	44.88 ± 4.55	45.90 ± 4.44	112.65 ± 24.48	51184.14 ± 6897.14	49965.03 ± 5565.60
		maximum	52.00	53.54	164.68	63222.40	59820.98
Msh	66	minimum	21.14	21.14	31.14	13566.28	20321.82
		average	27.34 ± 4.74	29.14 ± 4.33	49.05 ± 11.30	26385.19 ± 6932.22	30989.08 ± 5768.65
		maximum	35.60	35.60	67.73	36731.20	39598.51

Note : Sark = subarkosic sandstones

Msh = mudshales

R_c = Schmidt hammer number reasing correct

In the present test, the aggregates were washed and dried in the oven at 105° C to a substantially constant weight then separated into individual size fractions, weighted (Wi) and re-combined to the grading. The A grade and E grade of ASTM designation C131-69 was used. The sample and the abrasive charge were placed in the Los Angeles abrasion machine. The machine was rotated at 100 revolutions with uniform speed 30-33 rpm. the sample was sieve out suing sieve no. 12 and the coarser fraction weighted. The whole sample was combined back in the machine. A care must be taken that no part of sample was left out. The rotated machine was for 400 more revolutions at the same speed mentioned above. The aggregate was again removed and separated. The fraction with the size smaller than sieve no. 12 was completely removed. The remaining aggregate was washed, dried and weighted (W_{500}). The percentage of the difference between the original aggregate weight and the final weight to the original weight was reported as Los Angeles abrasion hardness. The uniformity of sample (U.F.) was calculated by

$$U.F. = \frac{W_i - W_{100}}{W_i - W_{500}} \qquad \text{............ (4.34)}$$

The Los Angeles abrasion hardness was performed on the aggregated which were crushed from the pebbly graywackes core specimens and the test results are summarized in Table 4.21.

Table 4.21 Summary of Los Angeles abrasion tests results

Rock Type	No. of Tests	Ranging Value	Grade	Percentage of Wear %	Uniformity Factor (U.F.)
Gwke	6	minimum	A	19.01	0.21
		average		28.04 ± 11.76	0.22 ± 0.12
		maximum		50.78	0.24
	2	minimum	E	28.26	
		average		44.30 ± 22.69	
		maximum		60.35	

Note : Gwke = pebbly graywackes to pebbly mudstones

4.4.4 Correlations of Various Mechanical Properties

The uniaxial compressive strength values and Yonge's modulus derived from the various types of tests are compared in Tables 4.22, 4.23 and 4.24. The correlation between the point-load strength and unconfined was significant, the coefficients being 0.59 and 0.62 (Figures 4.19a and 4.19b) whilst that between the Brazilian strength and unconfined compressive strength was 0.86, (Figure 4.19c) indicationg a highly significant relationship. There are also a highly significant relationship between the two strengths and pulse wave velocity. Their correlation coefficients are 0.77 and 0.87 (Figures 4.19d and 4.19e).

There is a highly significant correlation between the cohesion and ultimate compressive strength, their correlation coefficient being 0.96 (Figure 4.19f). This suggests that as the ultimate compressive strength increases, a higher cohesion. The correlation between cohesion and Brazilian tensile strength is 0.69 (Figure 4.19g). As far as the hardness is concerned, there was a significant correlation between the Schmidt hammer values and those of the point-load strength, in this instance the coefficient being 0.50 of the left wall and 0.68 of the right wall of the diversion tunnel (Figures 4.19h and 4.19i).

4.5 Relationship Between Index Properties

In order to see if any significant relationship exist between the composition of sandstones from Chiew Larn on the one hand and their various physical and mechanical properties on the other, a number of correlations were made (Table 4.25). It was

Table 4.22 Comparison of uniaxial compreeive strength values obtained from various tests types

<table>
<tr><th rowspan="2">Test Type / Rock Type</th><th colspan="2">Schmidt Rebound Hardness Tests</th><th colspan="3">Point Load Strength Index Tests</th><th colspan="2">Uniaxial Compression Tests</th></tr>
<tr><th>No. of Tests</th><th>Schmidt Hardness*</th><th>Point Load Test Type</th><th>No. of Tests</th><th>Uniaxial Compressive Strength*</th><th>No. of Tests</th><th>Uniaxial Compressive Strength*</th></tr>
<tr><td>Sark</td><td>103</td><td>112.65 ± 24.48</td><td>Lump</td><td>67</td><td>129 ± 24</td><td>4</td><td>144.32 ± 43</td></tr>
<tr><td rowspan="3">Gwke</td><td rowspan="2">1619**</td><td rowspan="2">108.70 ± 31.37</td><td>Axial</td><td>96</td><td>102 ± 36</td><td rowspan="3">33</td><td rowspan="3">64.51 ± 24</td></tr>
<tr><td>Diametrical</td><td>230</td><td>89 ± 30</td></tr>
<tr><td>846***</td><td>65.08 ± 13.64</td><td>Lump</td><td>998</td><td>90 ± 16</td></tr>
</table>

Note : Sark = Subarkosic sandstones

Gwke = Pebbly greywacke to pebbly mudstones

* = MPa

** = fresh wall strength

*** = joint wall strength

Table 4.23 Comparative Young's modulus velues obtained from various tests types

Test Type / Rock Type	Schmidt Reboumd Hardness Tests		Sonic Velocity Tests		Uniaxial Compression Tests	
	No. of Tests	Young's Modulus* $\times 10^4$ MPa	No. of Tests	Young's Modulus** $\times 10^4$ MPa	No. of Tests	Young's Modulus*** $\times 10^4$ MPa
Sark	103	5.12 ± 0.67	2	3.36 ± 0.41**1	4	5.78 ± 2.01
				3.75 ± 0.43**2		
Gwke	1041	4.91 ± 0.95*1	36	4.24 ± 0.60**1	33	5.43 ± 2.87
	846	3.50 ± 0.69*2		4.33 ± 0.70**2		

Note : * = E_t^{lin}

*1 = fresh wall strength

*2 = joint wall strength

** = air-dry condition

**1 = ρ_b determined by gemetry

**2 = ρ_b determined by bmoyancy

*** = tangent Young's modulus

Table 4.24 Comparison between the static and dynamic elastic moduli.

Test Type / Core Specimen		Uniaxial Compression Test*					Sonic Velocity Test**				
		E_{sta}	G_{sta}	K_{sta}	λ_{sta}	ν_{sta}	E_{dyn}	G_{dyn}	K_{dyn}	λ_{dyn}	ν_{dyn}
Rock Type	No. of Tests	$\times 10^4$ MPa				—	$\times 10^4$ MPa				—
Sark	4	4.25 ± 1.51	2.48 ± 0.85	2.81 ± 1.11	1.23 ± 0.54	0.16 ± 0.02	3.75 ± 0.43	1.72 ± 0.19	3.22 ± 0.55	2.07 ± 0.08	0.27 ± 0.01
Gwke	37	5.48 ± 2.86	2.28 ± 1.21	2.88 ± 1.74	1.39 ± 1.20	0.16 ± 0.08	4.33 ± 0.58	1.71 ± 0.21	3.29 ± 0.68	2.11 ± 0.62	0.27 ± 0.03

Note : * = at 50 % Ultimate Strength

** = air-dry condition

Sark = subarkosic sandstones

Gwke = pebbly graywackes to pebbly mudstones

Figure 4.19 Correlations of various mechanical properties.

a) relationship between the point-load strength index (diametrical method) and the uniaxial compressive strength.

b) relationship between the point-load strength index (axial method) and the uniaxial compressive strength.

c) relationship between the Brazilizn tensile strength and the uniaxial compressive strength.

d) relationship between sonic velocity and the Brazilian tensile strength.

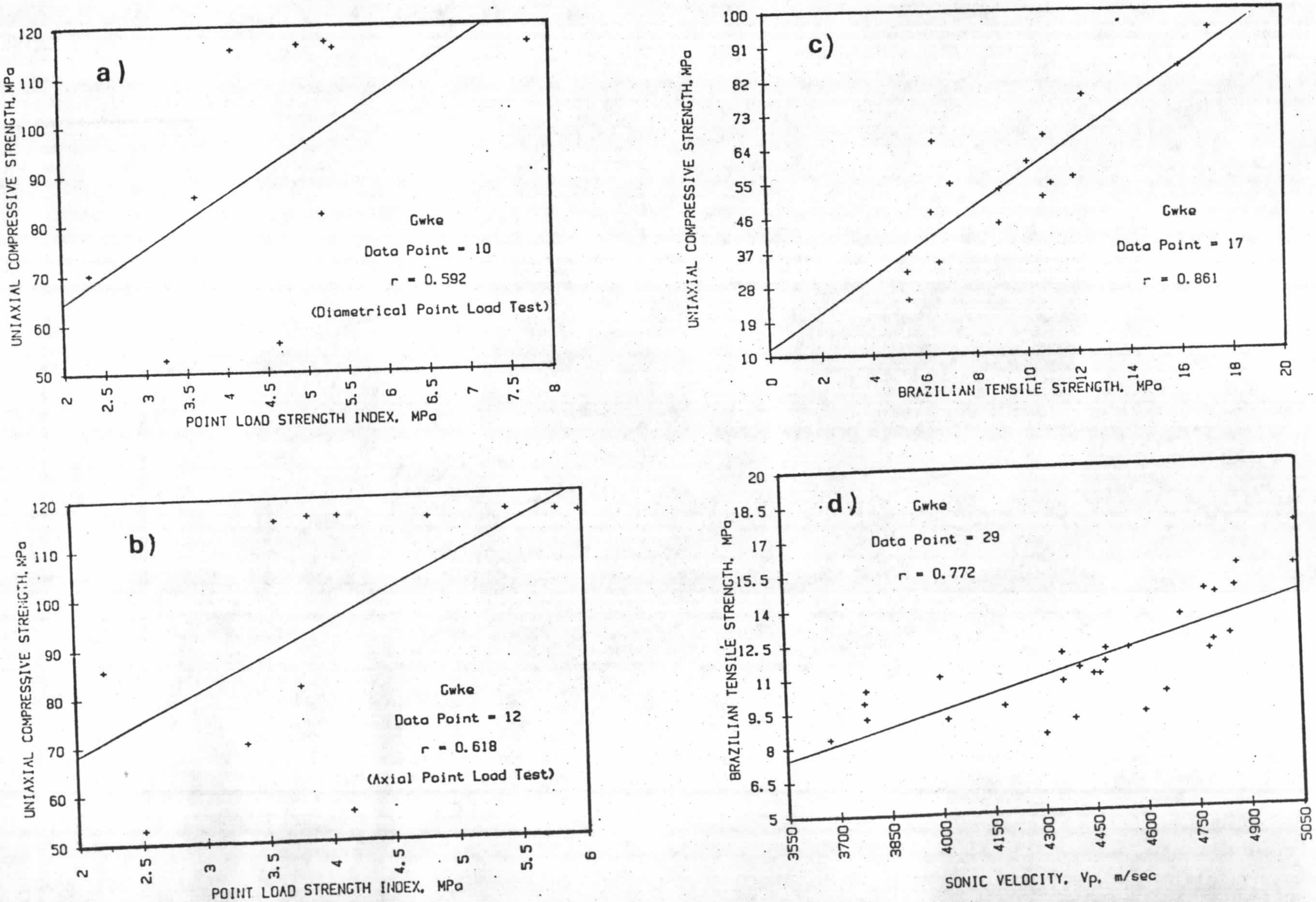
a)
UNIAXIAL COMPRESSIVE STRENGTH, MPa
POINT LOAD STRENGTH INDEX, MPa
Gwke
Data Point = 10
r = 0.592
(Diametrical Point Load Test)
b)
UNIAXIAL COMPRESSIVE STRENGTH, MPa
POINT LOAD STRENGTH INDEX, MPa
Gwke
Data Point = 12
r = 0.618
(Axial Point Load Test)
c)
UNIAXIAL COMPRESSIVE STRENGTH, MPa
BRAZILIAN TENSILE STRENGTH, MPa
Gwke
Data Point = 17
r = 0.861
d)
BRAZILIAN TENSILE STRENGTH, MPa
SONIC VELOCITY, Vp, m/sec
Gwke
Data Point = 29
r = 0.772

Figure 4.19 cont.

e) relationship between sonic velocity and compressive strength.

f) relationship between the cohesion and the uniaxial compressive strength.

g) relationship between the peak cohesion and the peak cohesion and the Brazilian tensile strength.

h) relationship between the Schmidt rebound hardness (left wall) and the point-load strength index.

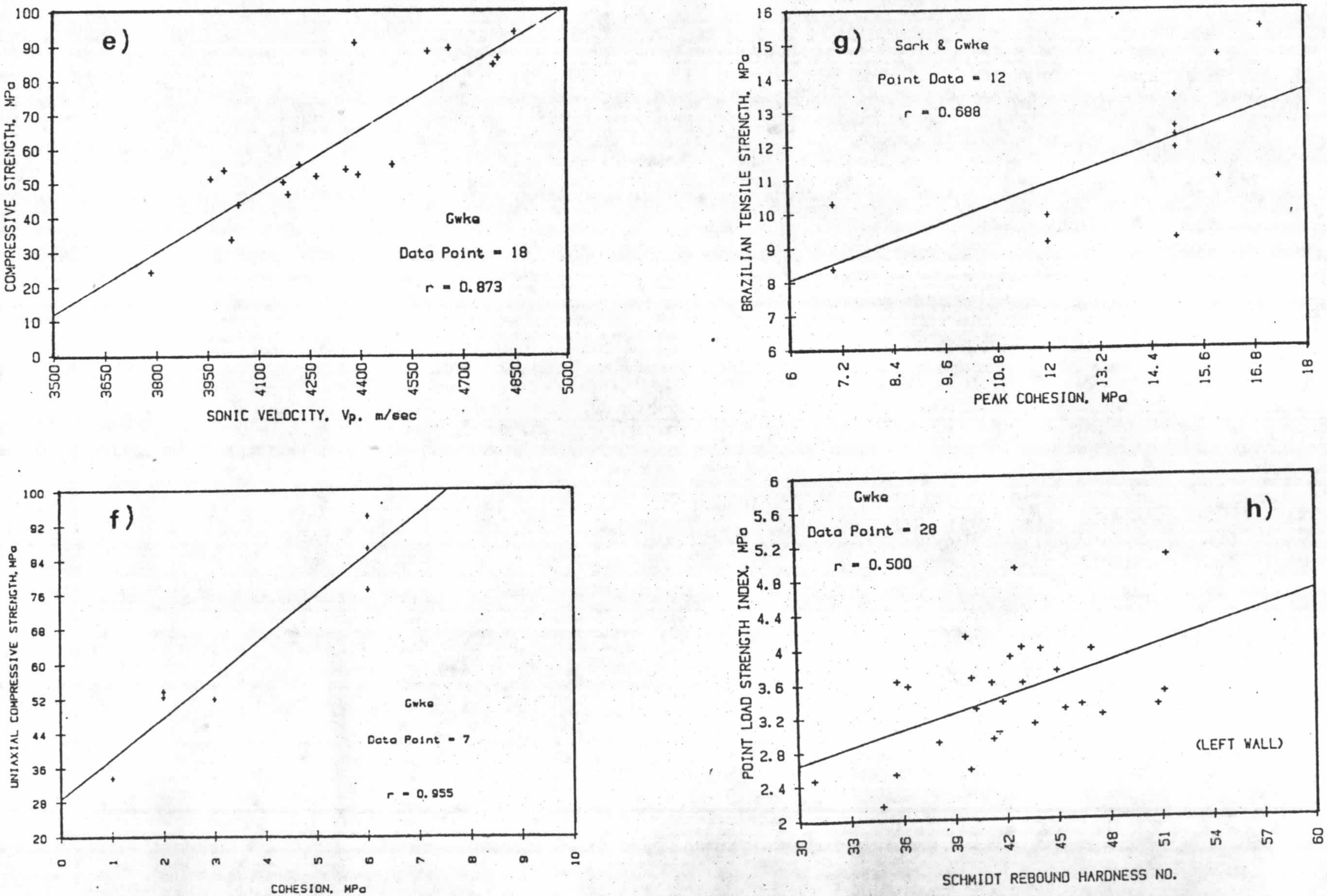
e)
COMPRESSIVE STRENGTH, MPa
SONIC VELOCITY, Vp, m/sec
Gwke
Data Point = 18
r = 0.873
g)
Sark & Gwke
Point Data = 12
r = 0.688
BRAZILIAN TENSILE STRENGTH, MPa
PEAK COHESION, MPa
f)
UNIAXIAL COMPRESSIVE STRENGTH, MPa
COHESION, MPa
Gwke
Data Point = 7
r = 0.955
h)
Gwke
Data Point = 28
r = 0.500
POINT LOAD STRENGTH INDEX, MPa
SCHMIDT REBOUND HARDNESS NO.
(LEFT WALL)

Table 4.25 Summary of relationship between various properties

Property Correlation	Dependent	Independent	Correlation Formula	Correlation Coefficient	Degree of Freedom and F Value	Confidence Level	Significant at the = 1%
Physical	Water Absorption	Bulk Density	$Sr = 23.39 - 8.48\ \rho_b$	0.77	1, 38, 53.8	99.99	Yes
	Void Index (Iv), %	Bulk Density	$Iv = 35.79 - 13.17\ \rho_b$	0.83	1, 41, 93.9	99.99	Yes
	Bulk Density	Porosity	$\rho_b = 2.73 - 0.05\ n$	0.65	1, 78, 57.0	99.99	Yes
	Bulk Density	Water Content	$\rho_b = 2.69 - 0.05\ W$	0.63	1, 56, 47.2	99.99	Yes
	Saturated Density	Dry-Density	$\rho_s = 0.22 + 0.93\ \rho_d$	0.95	1, 51,518.6	99.99	Yes
Mechanical	Compressive Strength	Brazilian Tensile Strength	$\sigma_c = 12.13 + 4.54\ \sigma_t$	0.86	1, 15, 43.2	99.99	Yes
		Point-Load Strength (axial)	$\sigma_c = 41.61 + 13.35\ \bar{I}_{s50}$	0.62	1, 10, 6.2	96.80	No
		Point-Load Strength (dia)	$\sigma_c = 43.02 + 10.70\ \bar{I}_{s50}$	0.59	1, 8, 4.3	92.82	NO
		Cohesion	$\sigma_c = 29.47 + 9.48\ c_r$	0.96	1, 5, 51.6	99.92	Yes
		P-wave Velocity	$\sigma_c = 196.17 + 0.06\ V_p$	0.87	1, 16, 51.4	99.99	Yes

Table 4.25 (cont.)

Property Correlation	Dependent	Independent	Correlation Formula	Correlation Coefficient	Degree of Freedom and F Value	Coefficient Level	Significant at the = 1%
Mineralogical, Physical and Mechanical	Point-Load Strength	Quartz Content	$\bar{I}_{s50} = 2.30 + 0.04\ Qz$	0.74	1, 10, 11.9	99.38	Yes
	Schmidt Rebound Number (left)	Bulk Density	$\bar{R}_c = -60.25 + 38.22\,\rho_b$	0.42	1, 21, 4.5	95.40	No
	Peak Internal Friction angle	Quartz Content	$\phi_p = 45.26 + 0.43\ Qz$	0.56	1, 7, 3.1	87.83	No
	Residual Internal Friction Angle	Quartz Content	$\phi_r = 19.02 + 0.66\ Qz$	0.56	1, 7, 3.2	88.32	NO
Others	Dynamic Young's Modulus	Static Young's Modulus	$E_{dyn} = 2.69 + 0.27E_{sta}$	0.65	1, 19, 13.9	99.86	Yes
	Rock Mass Rating	Rock Mass Quality	RMR =8.57inQ + 53.61	0.86	1, 38, 108.1	99.99	Yes

Table 4.25 (cont.)

Property Correlation	Dependent	Independent	Correlation Formula	Correlation Coefficient	Degree of Freedom and F Value	Coefficient Level	Significant at the = 1%
Mechanical	Brazilian Tensile Strength	Cohesion	$\sigma_t = 5.29 + 0.46\ c_p$	0.69	1, 21, 13	99.99	Yes
		P-wave Velocity	$\sigma_t = 8.83 + 0.01\ V_p$	0.77	1, 27, 39.9	99.99	Yes
	Point-Load Strength	Schmidt Rebound Number (left)	$\bar{I}_{s50} = 0.68 + 0.07\ \bar{R}_c$	0.50	1, 26, 8.7	99.34	Yes
		Schmidt Rebound Number (right)	$\bar{I}_{s50} = -1.05 + 0.13\ \bar{R}_c$	0.66	1, 12, 23	99.99	Yes
Mineralogical, Physical and Mechanical	Compressive Strength	Water Content	$\sigma_c = 96.27 - 47.00\ W$	0.41	1, 31, 6.3	98.22	No
		Quartz Content	$\sigma_c = 23.80 + 1.99\ Qz$	0.98	1, 4, 82.6	99.02	Yes
		Bulk Density	$\sigma_c = -2411.97 + 324.39\rho_b$	0.66	1, 13, 10	99.25	Yes
	Brazilian Tensile Strength	Bulk Density	$\sigma_t = -277.09 + 107\ 16\rho_b$	0.76	1, 26, 36.3	99.99	Yes
		Porosity	$\sigma_t = -13.42 - 4.18\ n$	0.75	1, 21, 26.7	99.96	Yes

found that the quartz content had a high influence on uniaxial compressive and point-load strengths (Figures 4.20a and 4.20b). Neither had it any influence on the internal faiction angles of pebbly graywackes (Figures 4.20c and 4.20d).

There is probably a highly significant relationship between the unconfined compressive and tensile strengths (Figures 4.19a, 4.19b and 4.19c).

The density is related to strength in those rocks which tend to show an increase in strenght with the increasing density. For example, the relationship between the Brazilian tenshile strength, uniaxial compressive strength and bulk density is highly significant (Figures 4.20e and 4.20f). There is a less tendency for hardness to increase with the increasing bulk density (Figure 4.20g).

As expected, there is an inverse relationship between the compressive strength and porosity, that is, as the porosity of the Chiew Larn sandstones increases, their strength decreases (Figure 4.20h).

The influence of water content on the strength reduction was surprisingly poor, the correlation coefficient between the two being -0.41 (Figure 4.20i), thus the relationship not being significant. This suggests that the amount of water contained is not the most important factor in this respect.

The index properties for the purpose of rock classification from the pebbly graywackes and subarksic sandstones have been summarized in Tables 4.26 and 4.27 respectively.

Figure 4.19 cont.

i) relationship between the Schmidt rebound hardness (right wall) and the point-load strength index.

Figure 4.20 Relationship between index properties.

a) relationship between the quartz content and the uniaxial compressive strength.

b) relationship between the quartz content and the point-load strength index.

c) relationship between the quartz content and internal friction angle (peak).

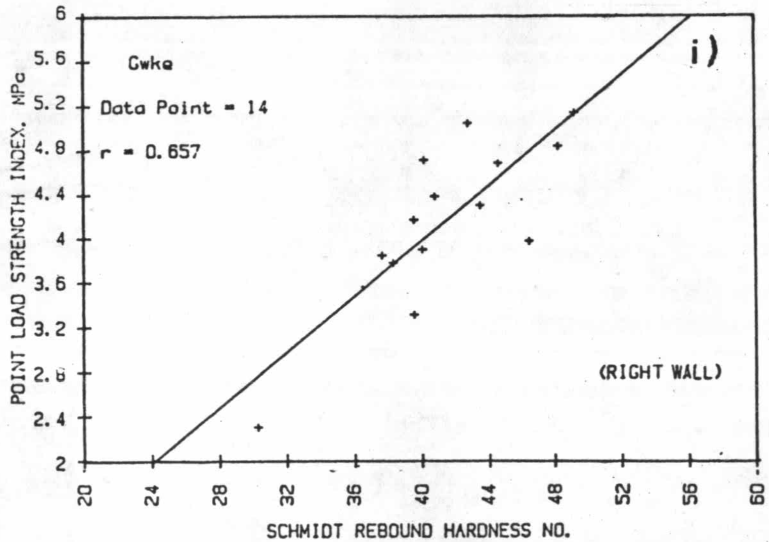
i)
Gwke
Data Point = 14
r = 0.657
(RIGHT WALL)
POINT LOAD STRENGTH INDEX, MPa
SCHMIDT REBOUND HARDNESS NO.

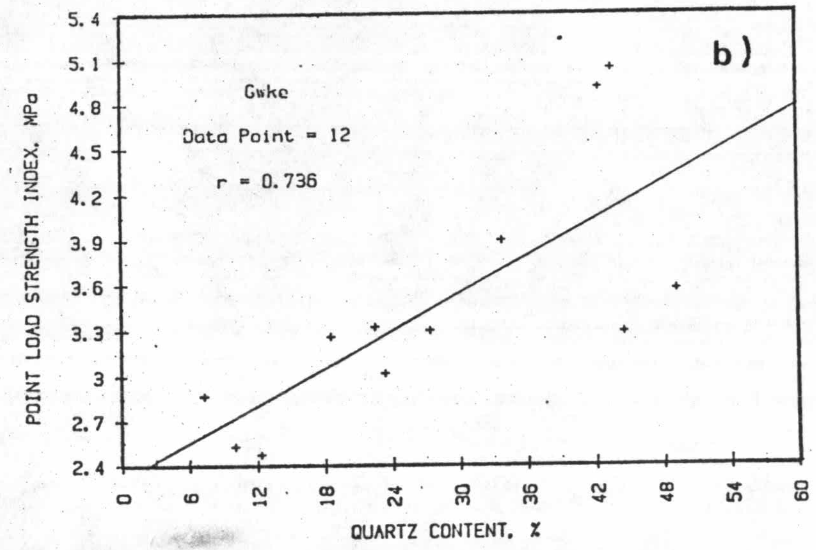
b)
Gwke
Data Point = 12
r = 0.736
POINT LOAD STRENGTH INDEX, MPa
QUARTZ CONTENT, %

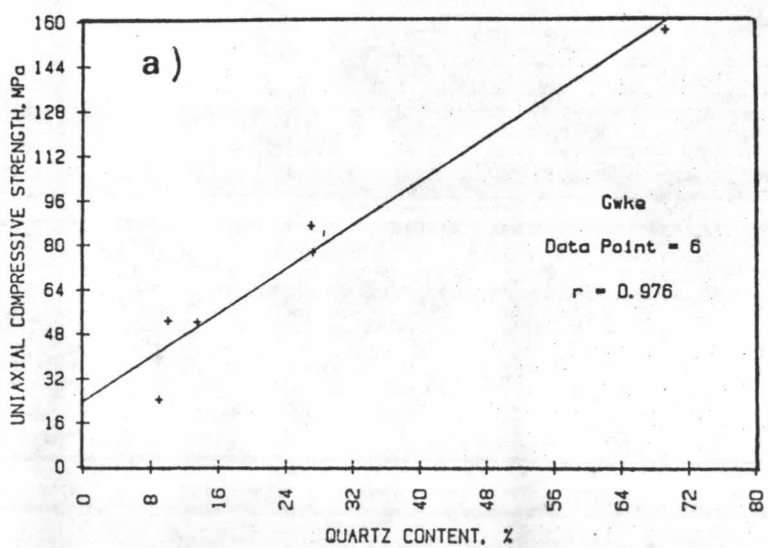
a)
Gwke
Data Point = 6
r = 0.976
UNIAXIAL COMPRESSIVE STRENGTH, MPa
QUARTZ CONTENT, %

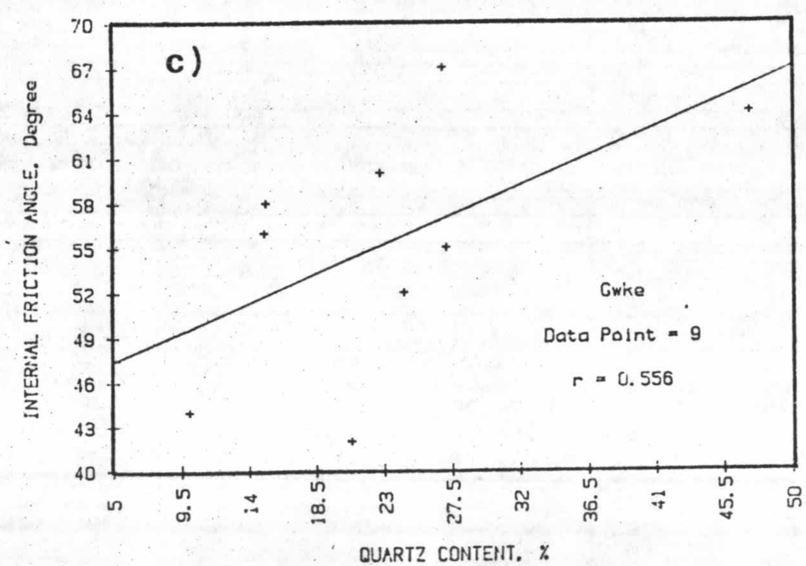
c)
Gwke
Data Point = 9
r = 0.556
INTERNAL FRICTION ANGLE, Degree
QUARTZ CONTENT, %

Figure 4.20 cont.

d) relationship between the quartz content and internal friction angle (residual).

e) relationship between the bulk density and the Brazilian tensile strength.

f) relationship between the bulk density and compressive strength.

g) relationship between the bulk density and the Schmidt rebound number.

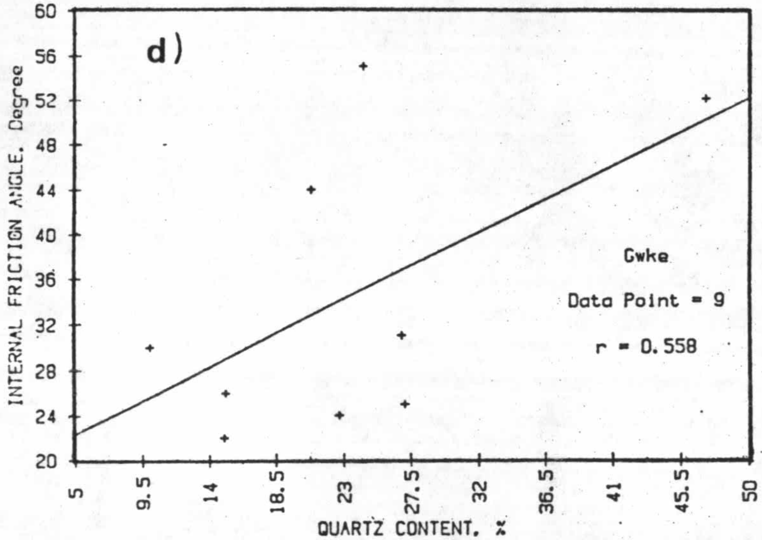
d)
INTERNAL FRICTION ANGLE, Degree
QUARTZ CONTENT, %
Gwke
Data Point = 9
r = 0.558
60
56
52
48
44
40
36
32
28
24
20
5
9.5
14
18.5
23
27.5
32
36.5
41
45.5
50

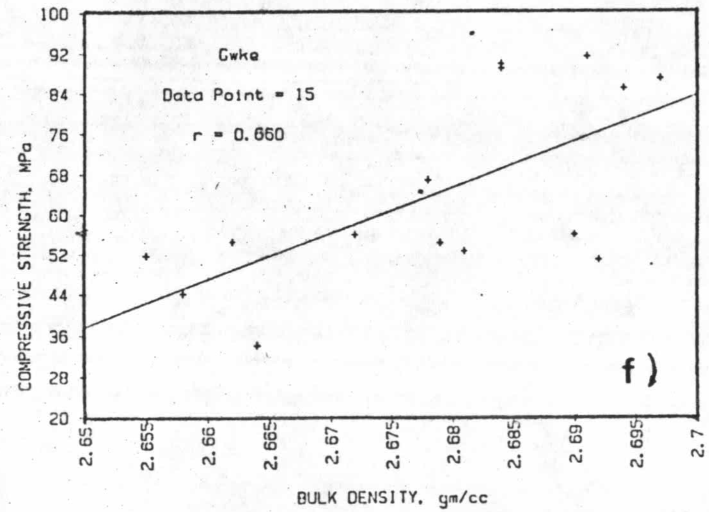
f)
COMPRESSIVE STRENGTH, MPa
BULK DENSITY, gm/cc
Gwke
Data Point = 15
r = 0.660
100
92
84
76
68
60
52
44
36
28
20
2.65
2.655
2.66
2.665
2.67
2.675
2.68
2.685
2.69
2.695
2.7

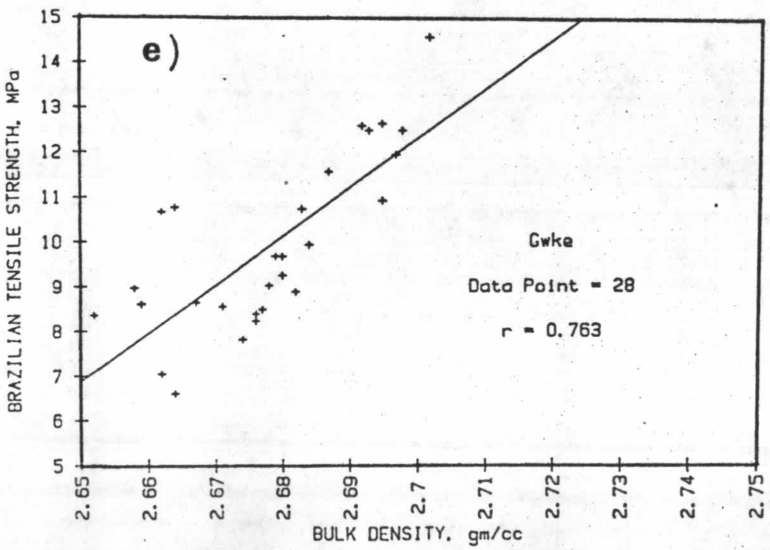
e)
BRAZILIAN TENSILE STRENGTH, MPa
BULK DENSITY, gm/cc
Gwke
Data Point = 28
r = 0.763
15
14
13
12
11
10
9
8
7
6
5
2.65
2.66
2.67
2.68
2.69
2.7
2.71
2.72
2.73
2.74
2.75

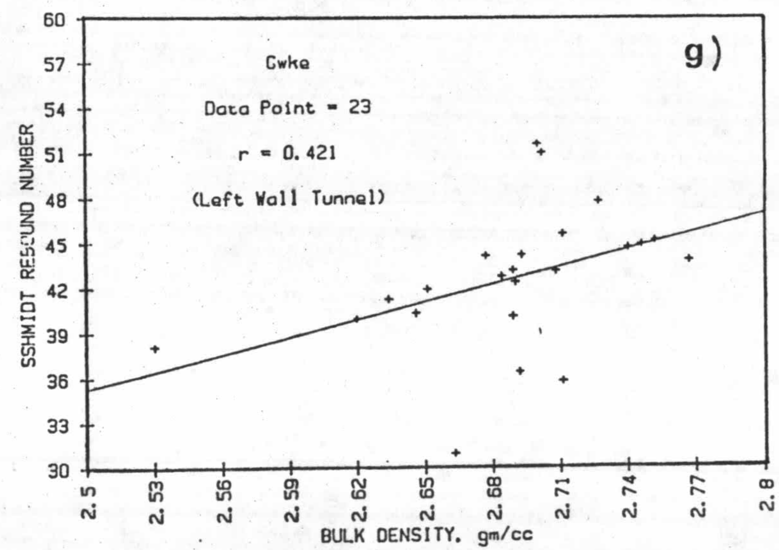
g)
SSHMIDT REBOUND NUMBER
BULK DENSITY, gm/cc
Gwke
Data Point = 23
r = 0.421
(Left Wall Tunnel)
60
57
54
51
48
45
42
39
36
33
30
2.5
2.53
2.56
2.59
2.62
2.65
2.68
2.71
2.74
2.77
2.8

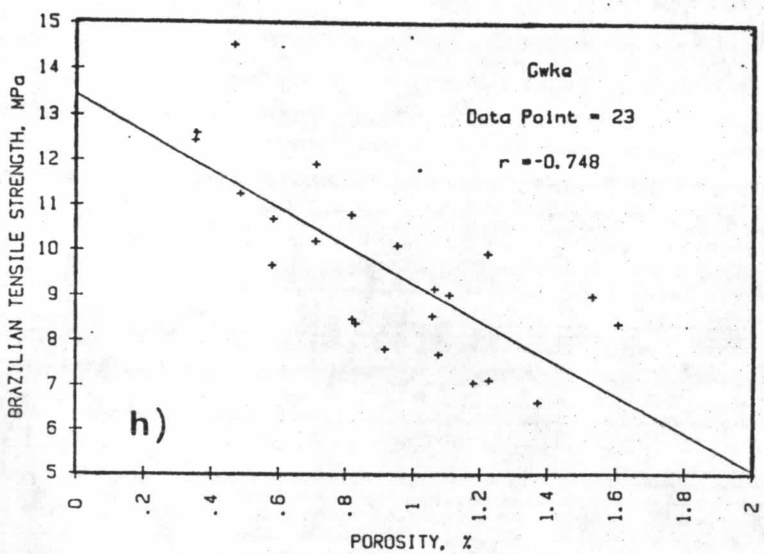

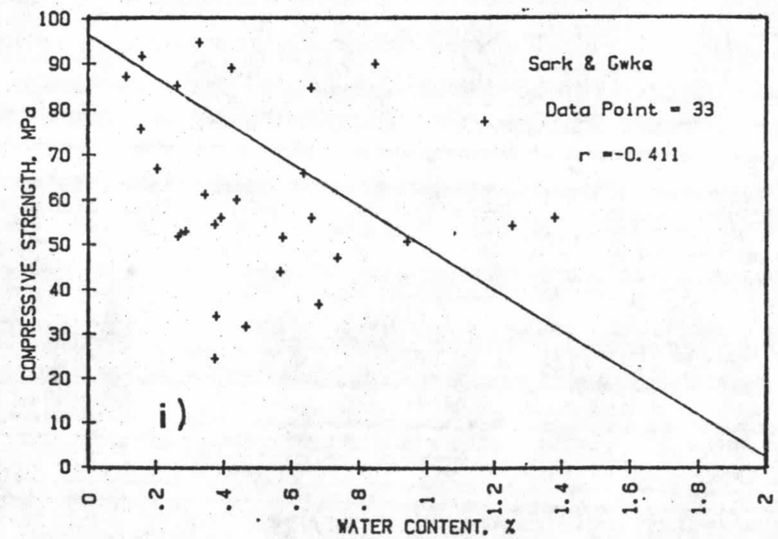

Figure 4.20 cont.

h) relationship between porosity and the Brazilian tensile strength.

i) effect of water content on compressive strength.

Table 4.26 Summary of engineering properties of the Chiew Larn graywackes

Properties Item		No. of Tests	Mean	S.D.	Min. Value	Max. Value
W	%	78	0.24	0.24	0.10	1.22
ρ_b	gm/cc	90	2.67	0.06	2.51	2.77
ρ_s	gm/cc	91	2.68	0.08	2.53	2.77
ρ_d	gm/cc	90	2.71	0.06	2.53	2.78
S_r	%	90	0.64	0.37	0.10	1.72
n	%	10	0.97	0.45	1.10	2.70
I_v	%	10	0.83	0.57	0.18	3.41
σ_c	MPa	37	64.51	24.00	24.45	150.03
$E_t x10^4$	MPa	37	5.48	2.86	1.18	14.58
$E_{sec} x10^4$	MPa	37	7.84	6.25	2.20	30.61
$E_{ave} x10^4$	MPa	37	6.51	4.79	1.68	27.08
ν_s	-	33	0.16	0.08	0.03	0.43
σ_t	MPa	96	10.43	2.95	3.86	17.34
c_a	MPa	23	15.33	3.23	7	17
$\emptyset_a$	degree	23	55.68	9.07	26	67
$\emptyset_{a_r}$	degree	23	34	12.17	18	55
I_{s_a}	MPa	230	4.26	1.50	1.23	9.91
I_{s_d}	Mpa	96	3.71	1.26	0.38	8.30
I_{s_i}	MPa	998	3.39	0.65	0.14	8.95
I_{d_2}	%	8	98.87	0.60	97.7	99.4
Sch	-	1041	43.20	5.40	25.73	54.29
$\varepsilon_v x10^{-6}$	-	28	693.75	646.79	53	2187
L.A.	%	6	28.04	11.76	19.01	50.78

Table 4.26 (cont.)

Properties	Item	No. of Tests	Mean	S.D.	Min. Value	Max. Value
U.F.	-	6	0.22	0.12	0.21	0.24
V_{p_a}	m/sec	36	4529	410	3427	5190
V_{p_d}	m/sec	37	4420	367	3675	5044
V_{p_s}	m/sec	37	4539	430	3315	5194
V_{s_a}	m/sec	36	2525	160	2133	2774
V_{s_d}	m/sec	37	2510	163	2075	2766
V_{s_s}	m/sec	37	2483	160	2213	2705
$E_a x10^4$	MPa	36	4.33	0.58	3.19	5.21
$E_d x10^4$	MPa	37	4.19	0.57	2.88	5.38
$E_s x10^4$	MPa	37	4.18	0.60	2.69	4.98
$Y_a x10^4$	MPa	36	5.55	0.95	3.15	7.11
$Y_d x10^4$	MPa	37	5.22	0.89	3.57	7.32
$Y_s x10^4$	MPa	37	5.49	1.02	2.91	7.17
$G_a x10^4$	MPa	36	1.71	0.21	1.22	2.04
$G_d x10^4$	MPa	37	1.66	0.22	1.13	2.19
$G_s x10^4$	MPa	37	1.64	0.21	1.29	1.94
$\lambda_a x10^4$	MPa	37	2.11	0.62	0.71	3.33
$\lambda_d x10^4$	MPa	37	1.85	0.54	0.78	3.17
$\lambda_s x10^4$	MPa	37	2.21	0.69	0.63	3.53
$K_a x10^4$	MPa	36	3.29	0.68	1.52	4.59
$K_d x10^4$	MPa	37	2.96	0.64	1.89	4.37
$K_s x10^4$	MPa	37	3.31	0.80	1.39	4.70
ν_a	-	36	0.27	0.03	0.18	0.31
ν_d	-	37	0.26	0.03	0.19	0.34
ν_s	-	37	0.28	0.03	0.21	0.36
c_s	MPa	18	14.00	3.88	7	17
ϕ_s	degree	18	52.17	6.59	42	60
ϕ_{s_r}	degree	18	40.83	13.63	24	59

Table 4.27 Summary of engineering properties of Chiew Larn subarkosic sandstones

Properties Item		No. of Tests	Mean	S.D.	Min. Value	Max. Value
W	%	4	0.33	0.23	0.11	0.61
ρ_b	gm/cc	5	2.61	0.37	2.35	2.72
ρ_d	gm/cc	5	2.68	0.07	2.59	2.73
ρ_s	gm/cc	5	2.63	0.07	2.56	2.72
S_r	%	5	1.02	0.61	0.34	1.92
n	%	5	1.40	0.80	0.60	2.20
σ_c	MPa	4	144.32	42.89	75.72	193.61
$E_t x10^4$	MPa	4	4.25	1.51	3.40	8.33
$E_{sec} x10^4$	MPa	4	6.79	1.78	4.21	8.64
$E_{ave} x10^4$	MPa	4	9.31	4.64	4.08	14.50
ν_s	-	4	0.16	0.02	0.14	0.18
σ_t	MPa	12	17.48	7.52	10.82	29.66
c_a	MPa	2	7	-	-	-
ϕ_a	degree	2	64	-	-	-
ϕ_{n_r}	degree	12	32	-	-	52
I_{s_i}	MPa	67	4.61	0.52	1.40	12.04
$\varepsilon_v x10^{-6}$		4	740.25	958.46	-334	1925
V_{P_a}	m/sec	2	4487	130	4395	4579
V_{P_d}	m/sec	2	4112	210	3965	4260
V_{P_s}	m/sec	2	4486	320	4260	4712
V_{S_a}	m/sec	2	5204	110	2429	2580
V_{S_d}	m/sec	2	2464	80	2408	2520
V_{S_s}	m/sec	2	2428	280	2233	2622
$E_a x10^4$	MPa	2	3.75	0.43	3.45	4.05

Table 4.27 (cont.)

Properties	Item	No. of Tests	Mean	S.D.	Min. Value	Max. Value
$E_d x10^4$	MPa	2	3.70	0.05	3.58	3.68
$E_s x10^4$	MPa	2	3.99	0.85	3.39	4.60
$Y_a x10^4$	MPa	2	5.51	0.47	5.18	5.84
$Y_d x10^4$	MPa	2	4.37	0.37	4.09	4.65
$Y_s x10^4$	MPa	2	3.99	0.85	3.39	4.60
$G_a x10^4$	MPa	2	1.72	0.19	1.58	1.85
$G_d x10^4$	MPa	2	1.57	0.12	1.49	1.56
$G_s x10^4$	MPa	2	1.55	0.36	1.29	1.80
$\lambda_a x10^4$	MPa	2	2.07	0.08	2.01	2.13
$\lambda_d x10^4$	MPa	2	1.23	0.36	0.79	1.68
$\lambda_s x10^4$	MPa	2	2.17	0.07	2.12	2.21
$K_a x10^4$	MPa	2	3.22	0.21	3.89	3.67
$K_d x10^4$	MPa	2	2.28	0.55	1.89	2.67
$K_s x10^4$	MPa	2	3.20	0.31	2.99	3.42
ν_a	-	2	0.27	0.01	0.27	0.28
ν_d	-	2	0.21	0.07	0.16	0.27
ν_s	-	2	0.28	0.03	0.21	0.36
ν_{ave}	-	4	0.71	0.03	0.22	0.22
ν_t	-	4	0.16	0.02	0.05	0.43